A&A 443, 143–156 (2005)
DOI: 10.1051/0004-6361:20053131

Astronomy & Astrophysics

Mira variables in the OGLE bulge fields⋆,⋆⋆

M. A. T. Groenewegen[1] and J. A. D. L. Blommaert[1,2]

[1] Instituut voor Sterrenkunde, KU Leuven, Celestijnenlaan 200B, 3001 Leuven, Belgium
e-mail: groen@ster.kuleuven.ac.be
[2] Sterrenkundig Observatorium, Universiteit Gent, Krijgslaan 281-S9, 9000 Gent, Belgium

Received 25 March 2005 / Accepted 9 June 2005

ABSTRACT

The 222 000 *I*-band light curves of variable stars detected by the OGLE-II survey in the direction of the Galactic Bulge have been fitted and also correlated with the DENIS and 2MASS *all-sky release* databases and with lists of known objects. Lightcurves and the results of the lightcurve fitting (periods and amplitudes) and DENIS and 2MASS data are presented for 2691 objects with *I*-band semi-amplitude larger than 0.45 mag, corresponding to classical Mira variables. That the Mira period distribution of 6 fields at similar longitude but spanning latitudes from −1.2 to −5.8 are statistically indistinguishable indicates similar populations with initial masses of 1.5−2 $M_{\odot}$, corresponding to ages of 1−3 Gyr. A field at similar longitude at $b = -0.05$ from Glass et al. (2001, MNRAS, 321, 77; erratum: 2002, MNRAS, 336, 1390) does show a significantly different period distribution, indicating the presence of a younger population of 2.5−3 $M_{\odot}$ and ages below 1 Gyr. The *K*-band period-luminosity relation is presented for the whole sample and for sub-fields. The zero point depends on Galactic longitude. Simulations are carried out to show that the observed dependence of the zero point with *l*, and the number of stars per field are naturally explained using the model of disk and bulge stars of Binney et al. (1997, MNRAS, 288, 365), for a viewing angle (major-axis Bar – axis perpendicular to the line-of-sight to the Galactic Centre) of 43 ± 17 degrees. The simulations also show that biases in the observed zero point are small, <0.02 mag. A comparison is made with similar objects in the Magellanic Clouds. The slope of the *PL*-relation in the Bulge and the MCs agree within the errorbars. Assuming the zero point does not depend on metallicity, a distance modulus difference of 3.72 between Bulge and LMC is derived. This implies a LMC DM of 18.21 for an assumed distance to the Galactic Centre (GC) of 7.9 kpc, or, assuming a LMC DM of 18.50, a distance to the GC of 9.0 kpc. From the results in Groenewegen (2004, A&A, 425, 595) it is found for carbon-rich Miras that the *PL*-relation implies a relative SMC-LMC DM of 0.38, assuming no metallicity dependence. This is somewhat smaller than the often quoted value near 0.50. Following theoretical work by Wood (1990, in From Miras to Planetary Nebulae, ed. M. O. Mennessier, & A. Omont (Gif-sur-Yvette: Éditions Frontières), 67) a metallicity term of the form $M_{\rm K} \sim \beta \log Z$ is introduced. If a relative SMC-LMC DM of 0.50 is imposed, $\beta = 0.4$ is required, and for that value the distance to the GC becomes 8.6 ± 0.7 kpc (for a LMC DM of 18.50), within the errorbar of the geometric determination of 7.9 ± 0.4 kpc. An independent estimate leads to a distance estimate to the GC of 8.8 ± 0.4 kpc.

Key words. stars: AGB and post-AGB – Galaxy: bulge – Galaxy: center

1. Introduction

In the course of the micro-lensing surveys in the 1990's the monitoring of the Small and Large Magellanic Clouds has revealed an amazing number and variety of variable stars. A big impact was felt and is being felt in all areas of variable star research, like Cepheids and RR Lyrae stars. Also in the area of variability in red variables (RVs) and AGB stars there has been remarkable progress. Wood et al. (1999) and Wood (2000) were the first to identify and label different sequences "ABC" thought to represent the classical Mira sequence ("C") and overtone pulsators ("A, B"), and sequence "D" which is not yet satisfactorily explained (Olivier & Wood 2003; Wood et al. 2004. Stars on this last sequence are referred to as having Long Secondary Periods – LSPs). This view has been subsequently confirmed and expanded upon by Noda et al. (2002), Lebzelter et al. (2002), Cioni et al. (2003), Ita et al. (2004), Kiss & Bedding (2003, 2004), and Fraser et al. (2005). These works differ in the source of the variability data (MACHO, OGLE, EROS, MOA), area (SMC or LMC), associated infrared data (Siding Spring 2.3 m, DENIS, 2MASS, SIRIUS), and selection on pulsation amplitude or infrared colours. In a recent paper, Groenewegen (2004, hereafter G04) analysed the OGLE data in the SMC and LMC, and correlated these sources with the DENIS and 2MASS surveys. The paper discussed the variability properties of three samples: about 2300 spectroscopically confirmed AGB stars, around 400 previously known LPV variables, and about 570 candidate dust-obscured AGB stars.

The present paper is an extension of the analysis in G04 to the OGLE data in the direction of the Galactic Bulge (GB). For this area of the sky, several papers also exist that use the results

⋆ Full Table 1 is available in electronic form at the CDS via anonymous ftp to cdsarc.u-strasbg.fr (130.79.128.5) or via http://cdsweb.u-strasbg.fr/cgi-bin/qcat?J/A+A/443/143
⋆⋆ Full Fig. 1, Full Table 2 and Appendices A–C are only available in electronic form at http://www.edpsciences.org

of the micro-lensing surveys and have extended previous classical works on Bulge variable stars, like those of Lloyd Evans (1976), Glass & Feast (1982), Whitelock et al. (1991), Glass et al. (1995, hereafter GWCF), Alard et al. (1996), and Glass et al. (2001).

Alard et al. (2001, hereafter ABC01) correlate ISOGAL sources within the NGC 6522 and Sgr I Baade windows with the MACHO database and present a list of 332 stars with complete 4-band *V*, *R*, and [7], [15] mag. Schultheis & Glass (2001) extended Alard et al. by also considering the DENIS and 2MASS data in those fields in general and for the variables in particular. Glass & Schultheis (2002, hereafter GS02) investigate a sample of 174 M-giants in the NGC 6522 Baade window and correlated them with DENIS ISOGAL and MACHO. Many stars of spectral type M 5 and all M 6 and later show variation, whereas subtypes M 1−M 4 do not (see also Glass et al. 1999).

Glass & Schultheis (2003, hereafter GS03) investigated the variable stars in the NGC 6522 Baade's window using MACHO data, and also used DENIS IR data. Of the 1661 selected stars 1085 were found to be variable. They present *K*-band *PL*-relations for sequences "ABCD". Wray et al. (2004) investigated small amplitude red giants variables in a sub-set of 33 OGLE fields. They identified two groups that seem to correspond to groups "A−" and "B−" in Ita et al. (2004; also see G04).

In our paper we describe results on Mira variables selected from OGLE Bulge fields. The paper is structured as follows. In Sect. 2 the OGLE, 2MASS and DENIS surveys are described. In Sect. 3 the model for the lightcurve analysis is briefly presented. In the rest of the paper, different results are described. The Period-Luminosity diagram is discussed in Sect. 5. A description of the Mira population with respect to the overall bulge population is given in Sect. 8. In Sect. 9 we show that the Miras are distributed in a bar-like structure and give the orientation. In the final section we give the distance to the Galactic Centre, based on the period-luminosity relation.

2. The data sets

The OGLE-II micro-lensing experiment observed forty-nine fields in the direction of the GB. Each field is $14.2' \times 57'$ and was observed in *BVI*, with an absolute photometric accuracy of 0.01−0.02 mag (Udalski et al. 2002). Table 4 lists the galactic coordinates of the field centers and the total number of sources detected in these fields.

Wozniak et al. (2002) present a catalog of about 222 000 variable objects based on the OGLE observations covering 1997−1999 and apply the difference image analysis (DIA) technique on the *I*-band data. The data files containing the *I*-band data of the candidate variable stars was downloaded from the OGLE homepage (`http://sirius.astrouw.edu.pl/~ogle/`). According to Wozniak et al., the level of contamination by spurious detections is about 10%, but we presume this level is much less at the brighter magnitudes of the LPVs considered here. Table 4 lists the number of detected variable stars per field (Wozniak et al. 2002).

The DENIS survey is a survey of the southern hemisphere in IJK_s (Epchtein et al. 1999). The second data release available through ViZier was used (The DENIS consortium, 2003). The 221 801 OGLE objects were correlated on position using a 3″ search radius and 59 894 matches were found.

The 2MASS survey is an all-sky survey in the JHK_s near-infrared bands. On March 25, 2003 the 2MASS team released the all-sky point source catalog (Cutri et al. 2003). The easiest way to check if a star is included in the 2MASS database is by uplinking a source table with coordinates to the 2MASS homepage. Such a table was prepared for the 221 801 OGLE objects and correlated on position using a 3″ radius. Data on 182 361 objects were returned.

3. Lightcurve analysis

The model to analyse the lightcurves is described in detail in Appendices A−C in G04.

Briefly, a first code (see for details Appendix A in G04) sequentially read in the *I*-band data for the 222 000 objects, determined periods through Fourier analysis, fit sine and cosine functions to the light curve through linear least-squares fitting, and made the final correlation with the pre-prepared DENIS and 2MASS source lists. All the relevant output quantities were written to file.

This file was read in by the second code (see for details Appendix B in G04). A further selection could be applied (typically on period, amplitude, and mean *I*-magnitude), multiple entries were filtered out (i.e. objects that appear in different OGLE fields), and a correlation made with pre-prepared lists of known non-LPVs and known LPVs or AGB stars. The output of the second code is a list with LPV candidates.

The third step (for details see Appendix C in G04) consisted of a visual inspection of the fits to the light curves of the candidate LPVs and a literature study through correlation with the SIMBAD database. Non-LPVs were removed, and sometimes the fitting was redone. The final list of LPV candidates was compiled.

Details on the small changes in the codes w.r.t. the implementation in G04 are given in Appendix A of the present paper.

4. Comparison of the datasets

4.1. Astrometry

As in G04, correlation between the OGLE objects and known LPVs and AGB stars, and known non-LPVs, was actually done in 2 steps. In the first step the correlation was made (for a 3″ search radius), and the differences and spread in ΔRA $\cos(\delta)$ and $\Delta\delta$ determined. These mean offsets were then applied in most cases to make the final cross-correlation, and this usually increased the number of matches. The results are listed in Table 3.

4.2. Photometry

As in G04, a comparison was made between the (mean) OGLE *I* and the (single-epoch) DENIS *I*, and between the (single-epoch)

Table 1. First entries in the electronically available table, which lists: OGLE-field and number, the three fitted periods with errors and amplitude (0.00 means no fit), mean $I_{\rm ogle}$, associated DENIS *IJK* photometry with errors, and associated 2MASS *JHK* photometry with errors (99.9 and 9.99 means no association, or no value).

OGLE-name	Period	Amp	Period	Amp	Period	Amp	$I_{\rm ogle}$	$I_{\rm denis}$	$J_{\rm denis}$	$K_{\rm denis}$	$J_{\rm 2MASS}$	$H_{\rm 2MASS}$	$K_{\rm 2MASS}$
bul_sc01_0098	124.1 ± 0.035	0.322	247.1 ± 0.038	1.520	0.0 ± 0.000	0.000	12.55	99.00 ± 9.99	99.00 ± 9.99	99.00 ± 9.99	9.06 ± 0.03	8.06 ± 0.04	7.56 ± 0.02
bul_sc01_0100	332.5 ± 1.306	0.856	0.0 ± 0.000	0.000	0.0 ± 0.000	0.000	19.31	99.00 ± 9.99	99.00 ± 9.99	99.00 ± 9.99	99.00 ± 9.99	99.00 ± 9.99	99.00 ± 9.99
bul_sc01_0103	224.2 ± 0.300	0.082	337.9 ± 0.055	0.904	0.0 ± 0.000	0.000	11.73	99.00 ± 9.99	99.00 ± 9.99	99.00 ± 9.99	8.86 ± 0.03	7.80 ± 0.03	7.11 ± 0.02
bul_sc01_0128	324.0 ± 2.263	0.708	0.0 ± 0.000	0.000	0.0 ± 0.000	0.000	19.56	99.00 ± 9.99	99.00 ± 9.99	99.00 ± 9.99	99.00 ± 9.99	99.00 ± 9.99	99.00 ± 9.99
bul_sc01_0177	332.3 ± 0.078	2.385	0.0 ± 0.000	0.000	0.0 ± 0.000	0.000	14.17	99.00 ± 9.99	99.00 ± 9.99	99.00 ± 9.99	8.82 ± 0.03	7.59 ± 0.03	6.90 ± 0.03
bul_sc01_0193	341.1 ± 0.110	0.769	267.1 ± 0.605	0.070	0.0 ± 0.000	0.000	12.60	99.00 ± 9.99	99.00 ± 9.99	99.00 ± 9.99	9.12 ± 0.02	7.93 ± 0.02	7.21 ± 0.02
bul_sc01_0235	98.4 ± 0.050	0.070	204.7 ± 0.615	0.114	261.8 ± 0.123	0.884	11.79	99.00 ± 9.99	99.00 ± 9.99	99.00 ± 9.99	9.17 ± 0.03	8.18 ± 0.05	7.58 ± 0.03
bul_sc01_0237	222.5 ± 2.146	0.345	275.0 ± 1.600	0.721	0.0 ± 0.000	0.000	18.66	99.00 ± 9.99	99.00 ± 9.99	99.00 ± 9.99	99.00 ± 9.99	99.00 ± 9.99	99.00 ± 9.99
bul_sc01_0388	107.2 ± 0.192	0.629	0.0 ± 0.000	0.000	0.0 ± 0.000	0.000	19.49	99.00 ± 9.99	99.00 ± 9.99	99.00 ± 9.99	99.00 ± 9.99	99.00 ± 9.99	99.00 ± 9.99
bul_sc01_0558	115.4 ± 0.030	0.167	232.2 ± 0.022	1.186	0.0 ± 0.000	0.000	13.66	99.00 ± 9.99	99.00 ± 9.99	99.00 ± 9.99	10.12 ± 0.02	8.92 ± 0.05	8.08 ± 0.02
bul_sc01_0602	105.6 ± 0.062	0.114	128.9 ± 0.102	0.106	315.7 ± 0.048	1.498	12.32	99.00 ± 9.99	99.00 ± 9.99	99.00 ± 9.99	8.48 ± 0.02	7.43 ± 0.05	6.86 ± 0.02
bul_sc01_0611	305.8 ± 1.143	0.915	0.0 ± 0.000	0.000	0.0 ± 0.000	0.000	19.37	99.00 ± 9.99	99.00 ± 9.99	99.00 ± 9.99	99.00 ± 9.99	99.00 ± 9.99	99.00 ± 9.99
bul_sc01_0878	129.1 ± 0.023	0.478	155.4 ± 0.204	0.072	471.0 ± 0.974	0.094	12.34	99.00 ± 9.99	99.00 ± 9.99	99.00 ± 9.99	10.06 ± 0.03	9.16 ± 0.03	8.73 ± 0.02
bul_sc01_0916	375.4 ± 0.057	0.686	0.0 ± 0.000	0.000	0.0 ± 0.000	0.000	11.41	99.00 ± 9.99	99.00 ± 9.99	99.00 ± 9.99	7.20 ± 0.02	5.97 ± 0.03	5.28 ± 0.02
bul_sc01_1241	280.1 ± 0.034	0.799	0.0 ± 0.000	0.000	0.0 ± 0.000	0.000	11.79	99.00 ± 9.99	99.00 ± 9.99	99.00 ± 9.99	8.94 ± 0.04	7.91 ± 0.05	7.31 ± 0.02
bul_sc01_1253	291.9 ± 1.259	0.746	0.0 ± 0.000	0.000	0.0 ± 0.000	0.000	19.03	99.00 ± 9.99	99.00 ± 9.99	99.00 ± 9.99	99.00 ± 9.99	99.00 ± 9.99	99.00 ± 9.99
bul_sc01_1254	295.2 ± 1.925	0.995	0.0 ± 0.000	0.000	0.0 ± 0.000	0.000	19.81	99.00 ± 9.99	99.00 ± 9.99	99.00 ± 9.99	99.00 ± 9.99	99.00 ± 9.99	99.00 ± 9.99
bul_sc01_1467	129.9 ± 0.042	0.205	167.1 ± 0.063	0.234	519.3 ± 0.106	1.125	12.34	99.00 ± 9.99	99.00 ± 9.99	99.00 ± 9.99	8.40 ± 0.02	7.29 ± 0.06	6.52 ± 0.02
bul_sc01_1533	116.2 ± 0.008	1.156	336.2 ± 0.360	0.181	505.8 ± 0.855	0.148	12.85	99.00 ± 9.99	99.00 ± 9.99	99.00 ± 9.99	10.39 ± 0.04	9.46 ± 0.05	8.97 ± 0.03
bul_sc01_1561	46.8 ± 0.056	0.558	0.0 ± 0.000	0.000	0.0 ± 0.000	0.000	18.22	99.00 ± 9.99	99.00 ± 9.99	99.00 ± 9.99	99.00 ± 9.99	99.00 ± 9.99	99.00 ± 9.99
bul_sc01_1616	457.7 ± 0.104	0.903	0.0 ± 0.000	0.000	0.0 ± 0.000	0.000	12.33	99.00 ± 9.99	99.00 ± 9.99	99.00 ± 9.99	8.81 ± 0.02	7.25 ± 0.04	6.38 ± 0.02
bul_sc01_1738	155.0 ± 0.055	0.153	458.0 ± 0.267	1.143	0.0 ± 0.000	0.000	13.27	99.00 ± 9.99	99.00 ± 9.99	99.00 ± 9.99	9.85 ± 0.02	8.31 ± 0.07	7.32 ± 0.02
bul_sc01_1818	279.3 ± 0.052	0.785	0.0 ± 0.000	0.000	0.0 ± 0.000	0.000	11.61	99.00 ± 9.99	99.00 ± 9.99	99.00 ± 9.99	9.22 ± 0.02	8.21 ± 0.05	7.56 ± 0.03

DENIS *JK* and the (single-epoch) 2MASS *JK* magnitudes. This was done by selecting those objects with an amplitude in the *I*-band of <0.05 mag.

Figure 2 shows the final results when offsets *I*(denis-ogle) = −0.03, *J*(denis-2mass) = −0.02, and *K*(denis-2mass) = −0.03 are applied. The latter values are consistent with those derived in OOS03 based on the 2MASS second incremental data release who found *J*(denis-2mass) = −0.02 ± 0.09, and *K*(denis-2mass) = −0.00 ± 0.07.

5. Period-luminosity relations

The full machinery outlined in Sect. 3 was performed. As in G04, all derived periods are given in Table 1 and are shown in Fig. 1. The present paper discusses only objects which have at least one period with an *I*-band amplitude larger than 0.45 mag[1], i.e. classical Mira variables (e.g. Hughes 1989). After visual inspection of the lightcurves, a sample of 2691 such objects remain. The number of objects per field is listed in the last column of Table 4.

Table 1 lists the stars in the sample, the fitted periods with errors and amplitudes, and the DENIS and 2MASS photometry of the associated sources. Table 2 lists alternative names and references from the literature. Figure 1 presents lightcurves and their fits.

Magnitudes are de-reddened using the $A_{\rm V}$ values that correspond to the respective OGLE field taken from Sumi (2004; and $A_{\rm V} = 6.0$ for the field 44 that they do not discuss), selective reddenings of $A_{\rm I}/A_{\rm V} = 0.49$, $A_{\rm J}/A_{\rm V} = 0.27$, $A_{\rm H}/A_{\rm V} = 0.20$, $A_{\rm K}/A_{\rm V} = 0.12$ (Draine 2003), and implicitly assuming that all objects suffer this reddening value (i.e. ignoring differential reddening within a field, and ignoring that foreground and background objects would suffer a different reddening). Sumi's method is based on the absolute magnitude of the Red Clump giants and is absolute calibrated using the $(V-K)$ colours of 20 RR Lyrae stars in Baade's window. Popowski et al. (2003) present an extinction map (over 9000 resolution elements of 4×4 arcmin size) towards the GB based on MACHO *V*, *R* photometry, under the assumption that colour–magnitude diagrams would look similar in the absence of extinction. For the centre of the OGLE fields it was checked if there was a tile in the Popowski et al. set within 0.05 degrees distance. For those, the value of the visual extinction has been listed next to the value in Sumi in Table 4. The rms difference $A_{\rm V}$ for the 21 field with values from both references is 0.18. Finally, Schultheis et al. (1999b) present a reddening map for the inner GB comparing DENIS *J*, *K* photometry to isochrones. Table 4 lists the values they find for two OGLE fields: SC44 which was not considered by Sumi (2004), and SC5 for which Sumi derive a larger $A_{\rm V}$ than Schultheis et al.: 5.73 versus 4.13.

In the further discussion we only use periods that fulfil the following conditions are used in the calculations (with ΔP the error in the period): $\Delta P/P < 0.01$ for $P < 500^{\rm d}$; $\Delta P < 5^{\rm d}$ for $500^{\rm d} < P < 800^{\rm d}$ and $\Delta P < 1.5^{\rm d}$ for $P > 800^{\rm d}$. The latter constraint was necessary because the long periods become comparable to the length of the dataset.

Figure 3 shows the *K*-band *PL*-relation for all periods which have an *I*-band amplitude larger than 0.45 mag and $(J-K)_0 < 2.0$ among the 2691 stars. The cut in $(J-K)$ colour is needed to prevent the *K*-magnitude being affected by circumstellar extinction, as shown in G04. Like G04, the *K*-magnitude is on the 2MASS system, and is the average of the DENIS and 2MASS photometry. In particular, if both DENIS and 2MASS *K*-band data are available, the DENIS data point is corrected as explained above (i.e. 0.03 mag added), and averaged with the 2MASS data point. This should take out some of the scatter in the *PL*-diagram, as the effect of the variability in the *K*-band is reduced. If only DENIS is available, the corrected value was used. In the left-hand panel the boundaries of the boxes "A−, A+, B−, B+, C, D" were taken from G04, but shifted by −4.0 to account for the approximate difference

[1] The amplitude, *A*, is used in the mathematical sense in the present paper, $y = A \sin x$. The peak-to-peak amplitude is 0.90 mag.

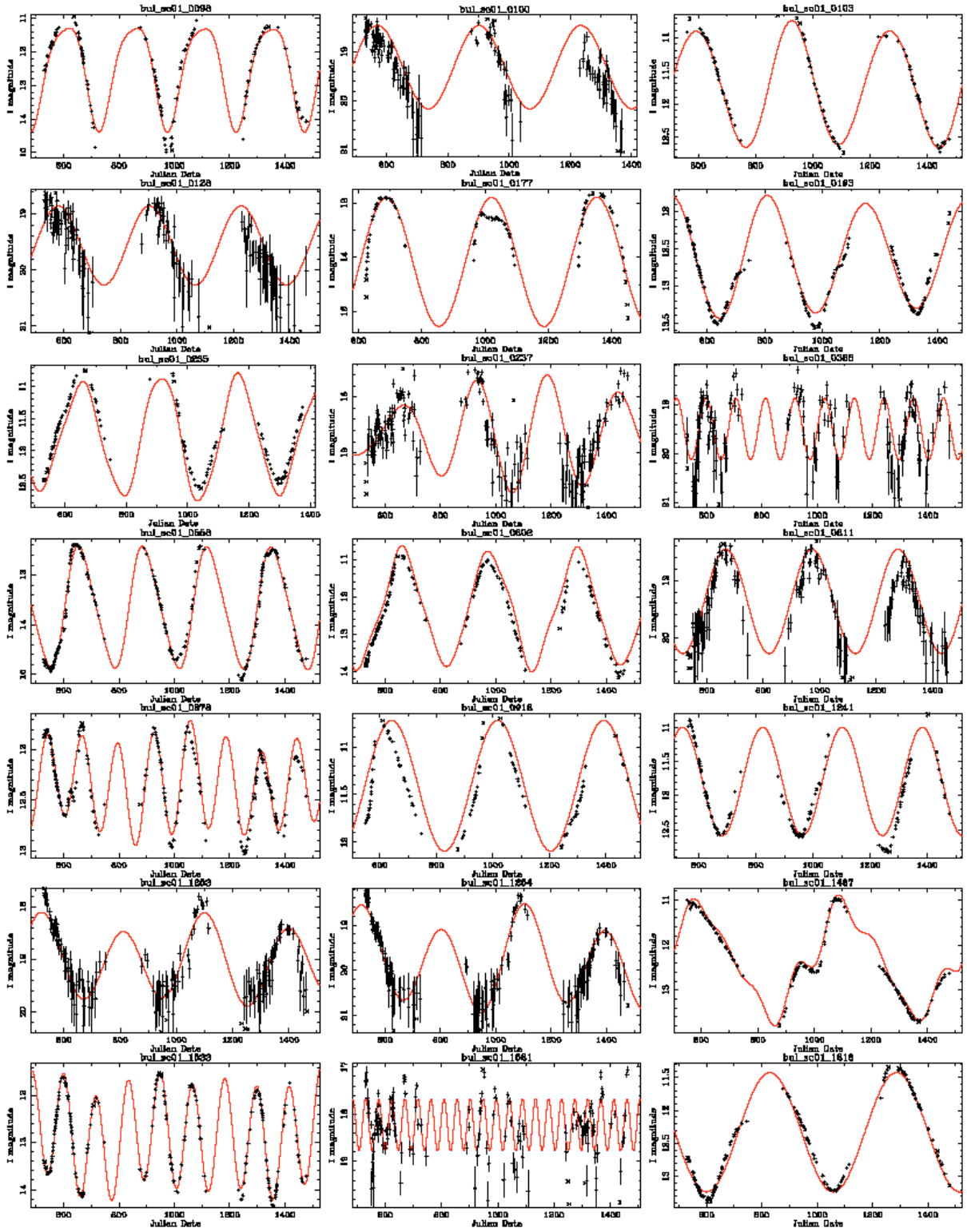

Fig. 1. First entries of electronically available figure with all lightcurves. The fit is indicated by the (red) solid line. Crosses indicate data points not included in the fit.

in distance modulus (DM), as, e.g., follows from the recent determination of 7.9 ± 0.4 kpc (Eisenhauer et al. 2003) for the distance to the GC, and 18.50 for the DM to the LMC (e.g. recent reviews by Walker 2003; Feast 2004a).

There is a reasonably well-defined sequence in Box "C", but when compared to the similar figure for the SMC and LMC in G04 (his Fig. 3) some differences can be noted as well. For the present Bulge sample there are a few objects located in Box "B+", and many in Box "D". In the SMC and LMC for this cut in amplitude, there are none in Box "B+" and few in "D". Several issues may play a role. Applying a certain cut in amplitude may sample slightly different variables in SMC, LMC,

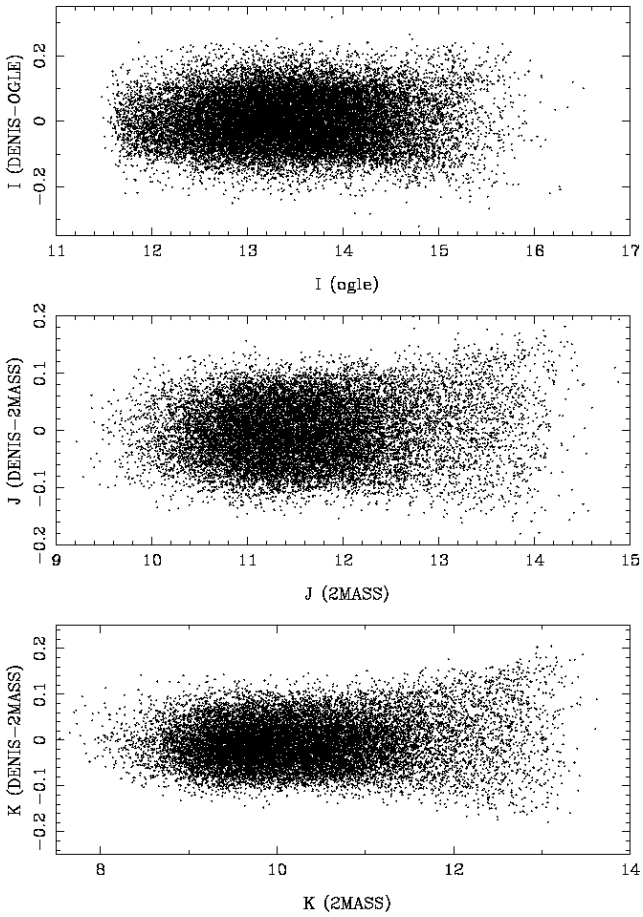

Fig. 2. Difference in photometry, *after* the following offsets were applied: I(denis-ogle) = −0.03, J(denis-2mass) = −0.02, K(denis-2mass) = −0.03.

and Bulge. Figure 3 in G04 clearly shows how lowering the cut in amplitude results in populating Box "B+" and then "A+", and increases the number of objects in "D". Another effect is the possible contribution of objects in the foreground and background of the Bulge, the depth of the Bulge, and finally, the orientation of the Bar, as the OGLE fields span 20 degrees in longitude (this last effect will be discussed later). Finally, the difference in DM may be different from the adopted value of 4.0.

To verify if the objects in Box "D" actually show LSP, they were all visually inspected. Few have a LSP, in agreement with the finding for LMC and SMC (for amplitudes >0.45 mag). This would call for enlargement of Box "C" to properly sample the *PL*-relation of the large amplitude (Mira) variables. To define this enlarged box, the *PL*-relation was inspected for each field independently. The right-hand panel in Fig. 3 shows the finally adopted boundaries of Box "C", which implies that Box "D" has contracted. Stars inside this redefined Box will be used to define the *PL*-relation. The *K*-band *PL*-relation is determined to be

$$m_{\rm K} = (-3.37 \pm 0.09)\ \log P + (15.44 \pm 0.21) \quad (1)$$

with an rms of 0.42 and based on 1292 stars, as shown in Fig. 3. The value of the slope is consistent with the median value when the *PL*-relation is determined for all fields individually. For reference, fitting all stars in Fig. 3, for a fixed slope of −3.37 results in a ZP of 15.47 ± 0.55.

Table 2. First entries in the electronically available table, which list: OGLE-field and number, other names, spectral type, and references. ISOGAL sources from the official catalog (OGA03) have the prefix "ISOGAL". ISOGAL sources studied in OOS03 have the prefix "OOS03". References in Col. 4 are given in the bibliography of the main text.

OGLE-name	Other name	Chemical type	Remarks
bul_sc01_0098	V 4713 Sgr		
bul_sc01_0100			
bul_sc01_0103			
bul_sc01_0128			
bul_sc01_0177			
bul_sc01_0193			
bul_sc01_0235			
bul_sc01_0237			
bul_sc01_0388			
bul_sc01_0558	BW6_V1_MISC		
bul_sc01_0602			
bul_sc01_0611			
bul_sc01_0878			
bul_sc01_0916			
bul_sc01_1241			
bul_sc01_1253			
bul_sc01_1254			
bul_sc01_1467	BW5_V1_MISC		
bul_sc01_1533			
bul_sc01_1561			
bul_sc01_1616			
bul_sc01_1738	BW5_V4_MISC		
bul_sc01_1818			

6. Historical versus current periods

Table 5 compares the period derived in the present paper (in case of multiple periods the one with the largest amplitude) with values derived in the literature. There are three cases where a previously determined period may be a harmonic of the present period, but overall there is good agreement between periods. In the 12 cases where there is a period available from LE76 (with the photographic plates taken between 1969 and 1971, hence 28 years of time difference with OGLE), there is no clear case for a star that has changed period. By comparison, G04 found that about 8% of LMC variables changed their period by more than 10% over about a 17-year timespan. To find 0 out of 12 in the present sample is consistent with this.

7. Colour–colour diagrams

The 2MASS and DENIS Colour–colour and colour–magnitude diagrams are shown in Fig. 4, together with that of spectroscopically confirmed M-stars in the LMC (see also Fig. 12 in G04). There appear to be more of the redder stars in the Bulge sample, but this is likely due to under representation in the LMC sample as this was restricted to spectroscopically known

Table 3. Comparison of coordinates and number of positional matches, before and after a correction was applied.

OGLE -(*other*)	ΔRA cos(δ)	$\Delta\delta$	N	ΔRA cos(δ)	$\Delta\delta$	N	Remark
IRAS	0.14 ± 0.94	0.50 ± 1.44	80				IRAS sources, not corrected
OGA03	−0.80 ± 0.85	−0.16 ± 0.89	1309	−0.11 ± 0.82	−0.02 ± 0.90	1319	ISOGAL sources from Omont et al. (2003; OGA03)
OOS03	−0.80 ± 0.88	−0.30 ± 0.95	800	−0.10 ± 0.86	−0.03 ± 0.99	817	ISOGAL sources from Ojha et al. (2003; OOS03)
GS02	−0.02 ± 0.58	0.30 ± 0.61	79	−0.04 ± 0.67	0.00 ± 0.61	80	MACHO sources from Glass & Schultheis (2002; GS02)
ABC01	−0.82 ± 0.98	−0.70 ± 0.96	293	−0.17 ± 1.08	−0.12 ± 1.01	320	ISOGAL sources from Alard et al. (2001; ABC01)
OGLE-I	−0.08 ± 0.70	−0.18 ± 0.44	728				OGLE-I sources, not corrected
BMB	−0.04 ± 0.70	−0.52 ± 0.90	282	+0.10 ± 0.79	−0.08 ± 0.91	286	sources from Blanco et al. (1984; BMB)
TLE	−0.08 ± 0.84	−0.25 ± 1.43	21				sources from Lloyd-Evans (1976), not corrected
B84	−0.46 ± 0.75	0.50 ± 0.97	61	−0.02 ± 0.76	0.08 ± 1.05	63	sources from Blanco (1984; B84)

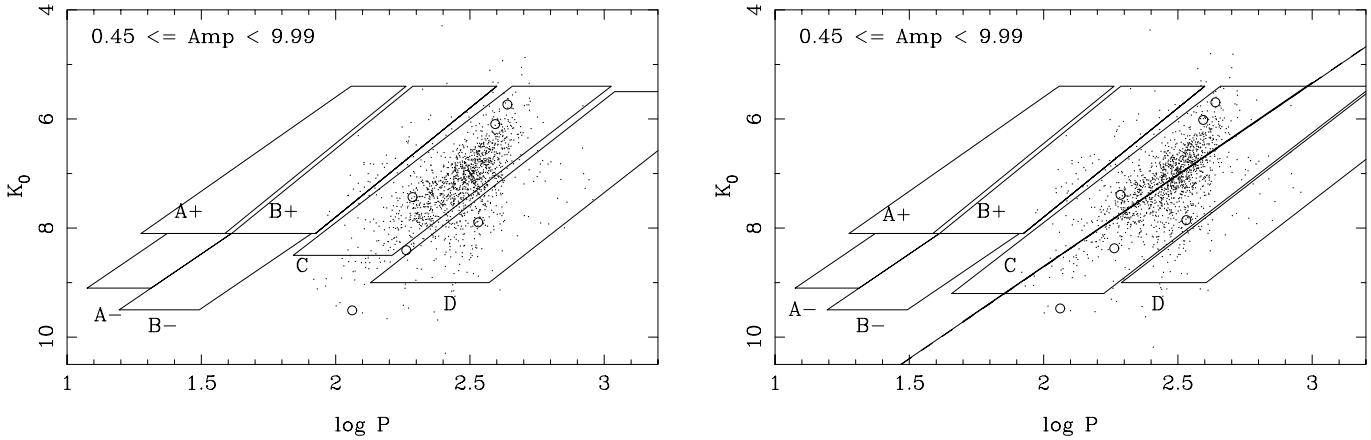

Fig. 3. *K*-band *PL*-relation for periods with an *I*-band amplitude larger than 0.45 mag and $(J-K)_0 < 2.0$. *Left panel*: sequences/Boxes "A+, A−, B+, B−, C, D" taken from G04 for the LMC and shifted by −4.0 in distance modulus. *Right panel*: enlarged Box "C" (and contracted Box "D",) to define the region for which the *PL*-relations will be computed. Only periods from Table 1 that fulfil $\Delta P/P < 0.01$ for $P < 500^{\rm d}$; $\Delta P < 5^{\rm d}$ for $500^{\rm d} < P < 800^{\rm d}$ and $\Delta P < 1.5^{\rm d}$ for $P > 800^{\rm d}$ are plotted and used in the analysis. Known M-stars are indicated by open circles. The line in the right-hand panel indicates the *PL*-relation of Eq. (1).

M-stars (i.e. in general optically selected). The sample of candidate infrared-selected AGB stars in the LMC (Fig. 12 in G04) does cover the $(I-K)$ and $(J-K)$ colour range observed in the Bulge).

The other main difference is that the Bulge stars are redder by ∼2 mag in $(I-J)_0$ than both LMC and SMC stars, as was also shown by Lebzelter et al. (2002) in a comparison of LMC and Bulge variable stars. As the diagrams involving J, H, K colours appear similar, it seems that this difference in $(I-J)$ must be due to a difference in I. The I-band measurements of M stars is strongly affected by the TiO and VO molecular absorption features (Lançon & Wood 2000). It is expected that for larger metallicities these lines will be stronger (Schultheis et al. 1999a), which will lead to redder $(I-J)$ colours.

The bullets connected by a line in the Bulge DENIS $(I-J)-(J-K)$ colour–colour diagram are the average colours of M 1, M 2, .., M 6, M 6.5, M 7, M 8 giants in the NGC 6522 Baade's window (Blanco 1986, GS02). There is a spread of typically 0.3–0.5 mag in $(I-J)$ and 0.2–0.3 mag in $(J-K)$ around these means, and there is only 1 M 8 giant in their sample. The colours of the Miras follow those of normal giants well until M 6.5, when the Miras become redder in $(I-J)$. There are also stars redder in $(J-K)$ than the single M 8 star in the sample of GS02, indicating either the presence of later spectral types or the onset of circumstellar reddening.

The conclusion of GS02 that "Many M 5 and all stars M 6 and later show variation, whereas subtypes (M 1–M 4) do not", is confirmed here, as there are essentially no objects located in the region of the DENIS $(I-J)-(J-K)$ colour–colour diagram occupied by spectral types of M 4 and earlier.

8. Mira bulge population as function of latitude

Figure 5 shows the period distribution of Miras in Box "C". A distinction is made between all Miras and those with $(J-K)_0 < 2.0$ (dashed histograms). The latter selection minimises any influence of circumstellar extinction. For comparison, the period distribution of LMC and SMC Miras is also shown[2]. The Kolmogorov-Smirnov (KS) test was performed to indicate that the probability that the period distributions of Bulge-LMC, Bulge-SMC, LMC-SMC are the same for all stars (those with $(J-K)_0 < 2$) is, respectively 0.36 (10^{-8}), 0.05 (0.31), and 0.05 (0.05).

[2] Derived following the implementation of the code and definition of the "boxes" as in G04, and applying the same selection criteria as in the present paper, i.e. I-amplitude larger than 0.45 mag.

Table 4. Properties of the OGLE-fields.

BUL_SC	l	b	Total[a]	Variable[b]	A_V[c]	LPV[d]
1	1.08	−3.62	730	4597	1.68/1.49	42
2	2.23	−3.46	803	5279	1.55/1.65	48
3	0.11	−1.93	806	8393	2.89	115
4	0.43	−2.01	774	9096	2.59/2.94	86
5	−0.23	−1.33	434	7257	5.73/–/4.13	118
6	−0.25	−5.70	514	3211	1.37	47
7	−0.14	−5.91	463	1618	1.33/1.28	21
8	10.48	−3.78	402	2331	2.14	8
9	10.59	−3.98	330	1847	2.08	21
10	9.64	−3.44	458	2499	2.23	16
11	9.74	−3.64	426	2256	2.27	18
12	7.80	−3.37	535	3476	2.29/2.20	33
13	7.91	−3.58	570	3084	2.06/1.82	21
14	5.23	2.81	619	4051	2.49	51
15	5.38	2.63	601	3853	2.77	71
16	5.10	−3.29	700	4802	2.15/2.23	45
17	5.28	−3.45	687	4690	1.94/2.29	167
18	3.97	−3.14	749	5805	1.83	55
19	4.08	−3.35	732	5255	2.74	51
20	1.68	−2.47	785	5910	1.94/2.02	64
21	1.80	−2.66	883	7449	1.83/1.78	60
22	−0.26	−2.95	715	5589	2.74	70
23	−0.50	−3.36	723	4815	2.70	60
24	−2.44	−3.36	612	4304	2.52	56
25	−2.32	−3.56	622	3046	2.34	61
26	−4.90	−3.37	728	4713	1.86	39
27	−4.92	−3.65	691	3691	1.69	46
28	−6.76	−4.43	406	1472	1.64	16
29	−6.64	−4.62	492	2398	1.53	36
30	1.94	−2.84	762	6893	1.91/1.78	50
31	2.23	−2.94	790	4789	1.81/1.74	59
32	2.34	−3.14	797	5007	1.61/1.82	54
33	2.35	−3.66	739	4590	1.70/1.82	105
34	1.35	−2.40	961	7953	2.52/2.32	60
35	3.05	−3.00	771	5169	1.84/2.20	39
36	3.16	−3.20	873	8805	1.62/1.52	38
37	0.00	−1.74	664	8367	3.77	108
38	0.97	−3.42	710	5072	1.83/1.94	57
39	0.53	−2.21	784	7338	2.63/2.70	99
40	−2.99	−3.14	631	4079	2.94	55
41	−2.78	−3.27	603	4035	2.65	49
42	4.48	−3.38	601	4360	2.29	32
43	0.37	2.95	474	3351	3.67	112
44	−0.43	−1.19	319	7836	6.0/–/6.00	132
45	0.98	−3.94	627	2262	1.64/1.53	32
46	1.09	−4.14	552	2057	1.71/1.65	26
47	−11.19	−2.60	301	1152	2.60	12
48	−11.07	−2.78	287	973	2.35	12
49	−11.36	−3.25	251	826	2.09	18
Total			30 490	221 701		2691

[a] Total number of objects detected in the field. From Udalski et al. (2002), in units of 10^3 objects. [b] Total number of candidate variable stars. From Wozniak et al. (2002). [c] Visual extinction. From Sumi (2004), except for SC44, where $A_V = 6.0$ has been adopted based on the proximity to SC5. The second value – when listed – comes from Popowski et al. (2003). The third value – when listed – comes from Schultheis et al. (1999b). [d] Total number of LPVs.

Any difference, in particular between Bulge and LMC period distribution, is difficult to quantify further as this depends in a complicated way on the Star Formation History and evolutionary tracks ($T_{\rm eff}$ – Luminosity – Mass – metallicity). Regarding the period distribution of Bulge Miras as such, previous studies are limited to selected small fields (e.g. TLE, GWCF, Glass et al. 2001). Whitelock et al. (1991) present the period distribution of about 140 IRAS sources, but no direct comparison is possible because of the difference in the selection criteria of the samples.

Figure 6 shows the period distribution of selected fields with very similar longitudes that cover a range in latitudes (the stars with $(J-K)_0 < 2.0$ are again shown as dashed histogram). To add a field even closer to the GC than surveyed by OGLE the data in Glass et al. (2001, 2002) is considered on a field centred on $l = -0.05, b = -0.05$. They present the results of a K-band survey of 24×24 arcmin^2 for LPVs down to $K \sim 12.0$. From the list of 409 stars, 14 were removed because of double entries, quality index of zero, uncertain or no listed period or amplitude. The coordinates were uploaded to the IPAC webserver, and 2MASS data within 2.5″ was retrieved for these 395 stars to get information on the $(J - K)$ colour. As an additional check and to eliminate multiple stars within the search circle, it was verified that the single-epoch 2MASS K magnitude is consistent with the mean K-magnitude and amplitude listed in Glass et al. For 345 stars 2MASS data is available. The magnitudes were corrected for interstellar reddening using the extinction map of the inner GB at 2′ resolution by Schultheis et al. (1999b). The extinction value of the nearest available grid point in this map was taken. The extinction values range between 18.5 and 30.4 with a mean of 24.7. The top panel in Fig. 6 lists 333 stars with $K > 7$ (to eliminate 3 likely foreground objects) and K-band amplitude larger than 0.35 (to correspond roughly to the cut in I-band amplitude of 0.45 mag), and 88 (the histogram with slanted hatching), or 236 (dashed histogram) stars which also have $(J - K)_0 < 2.0$. The last sample is the one that results when the reddening values from Schultheis et al. are multiplied by 1.35. They mention that the reddening may be underestimated in the direction of the GC because of J-band non-detections. For the one field in common, their value is a factor 1.3−1.4 smaller than derived by Sumi (2004). In addition, for their default reddening (the histogram with slanted hatching in Fig. 6) there would be many stars even at periods shorter than about 250 days that still would have $(J-K)_0 > 2.0$ which is not observed in the other fields. This could of course be real, but it is generally believed (e.g. Launhardt et al. 2002) that the population of low- and intermediate mass stars in the Nuclear Bulge (the inner about 30 pc from the GC) and GB are similar, but that in the former there is an overabundance of 10^7–10^8 year old stars. In this picture one would expect the period distributions to be similar at shorter periods, essentially independent of latitude. Therefore the period distribution of stars with $(J - K)_0 < 2.0$ for the increased reddening is adopted.

The KS test was performed on consecutive fields in latitude for the distributions based on the stars with $(J - K)_0 < 2.0$. It was found that the probability that the distributions are the same is 10^{-10} for the $b = -0.05/-1.21$ fields, 0.50 for the $b = -1.21/-1.39$ fields, 0.80 for the $b = -1.39/-1.81$, and >0.99

Table 5. Current period compared to values listed in the literature.

OGLE-name	Periods	Remark
bul_sc01_0558	232.2 (OGLE-II), 217.0, Mira (OGLE-I)	
bul_sc01_1467	519.3 (OGLE-II), 265.0, Mira (OGLE-I)	harmonic?
bul_sc01_1738	458.0 (OGLE-II), 227.5, Mira (OGLE-I)	harmonic?
bul_sc01_2079	524.7 (OGLE-II), 520.0, Mira (OGLE-I)	
bul_sc20_0832	245.9 (OGLE-II), 254.1: (ABC01), 235 (LE76), 336 (GWCF)	
bul_sc20_0975	167.7 (OGLE-II), 145.8 (ABC01)	
bul_sc20_1189	220.0 (OGLE-II), 121.3 (ABC01)	harmonic?
bul_sc20_1292	87.7 (OGLE-II), 88.1 (ABC01)	
bul_sc20_1761	231.6 (OGLE-II), 107.9 (ABC01), 240 (LE76), 235 (GWCF)	
bul_sc20_1826	331.7 (OGLE-II), 330: (LE76)	
bul_sc20_1928	297.6 (OGLE-II), 300 (LE76), 293 (GWCF)	
bul_sc20_2013	453.3 (OGLE-II), 474.2: (ABC01), 500:: (LE76), 480 (GWCF)	
bul_sc20_2269	409.3 (OGLE-II), 400: (LE76), 383 (GWCF)	
bul_sc20_2291	311.2 (OGLE-II), 306.9: (ABC01), 315 (LE76), 308 (GWCF)	
bul_sc34_3759	289.8 (OGLE-II), 293.8 (ABC01), 265 (LE76), 237 (GWCF)	
bul_sc45_0704	405.3 (OGLE-II), 430 (LE76), 467, Mira (OGLE-I), 413 (GS03)	
bul_sc45_1068	115.2 (OGLE-II), 115 (LE76), 116 (GCVS), 116 (GS03)	
bul_sc45_1586	193.3 (OGLE-II), 190 (LE76), 195 (GS03)	
bul_sc46_0866	322.1 (OGLE-II), 305 (LE76), 320 (GS03)	
bul_sc46_1163	343.7 (OGLE-II), 329.0, Mira (OGLE-I)	

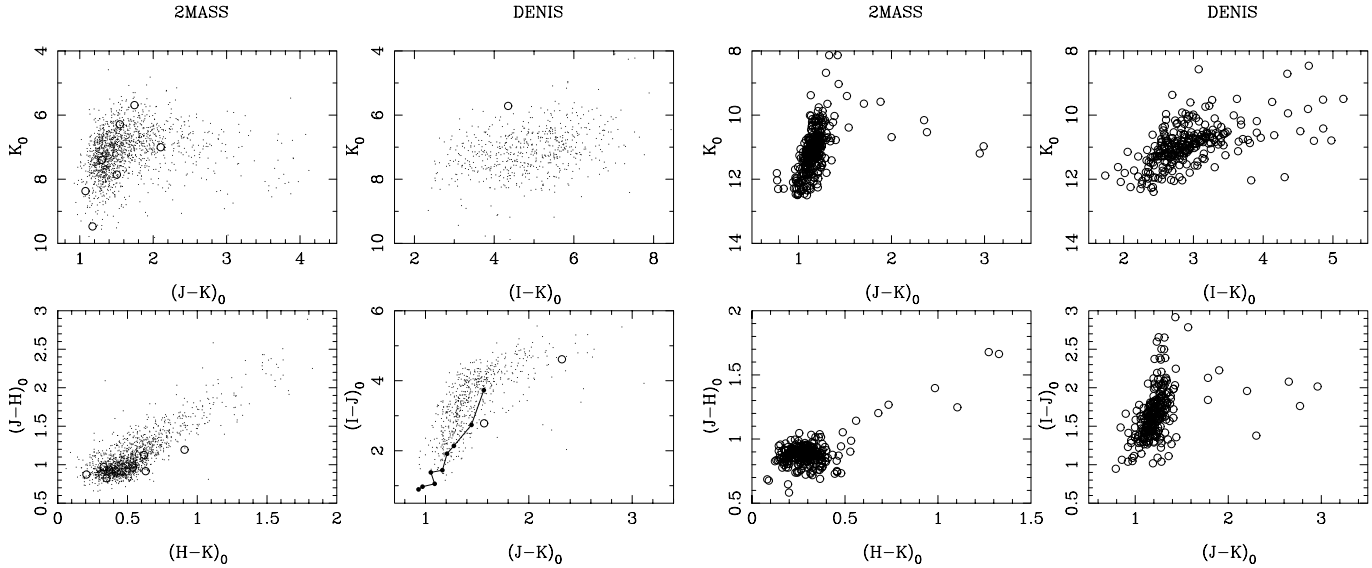

Fig. 4. Colour–magnitude and colour–colour diagrams using 2MASS and DENIS photometry for the Bulge stars (*left*), and spectroscopically confirmed M-stars in the LMC (*right*, from G04). The bullets connected by a line in the Bulge DENIS $(I-J)-(J-K)$ diagram are the average colours of M 1, M 2, .., M 6, M 6.5, M 7, M 8 giants in the NGC 6522 Baade's window (Blanco 1986; Glass & Schultheis 2002).

for the fields at more negative latitudes. The conclusion is that the period distributions of the fields at and below −1.2 degree are statistically indistinguishable, but that the field at −0.05 latitude has a significantly different period distribution; the probability that this distribution is the same as the distribution of the combined 6 OGLE fields is 10^{-22}. This conclusion is independent of the assumed reddening of the inner Bulge field, which influences how many stars will have $(J-K)_0 < 2.0$. For the default reddening of Schultheis et al., the probability that the distributions are the same for the $b = -0.05/-1.21$ fields is still only 0.0033. The difference in the period distributions is especially clear at longer periods. Of the 236 stars in the inner field with $(J-K)_0 < 2.0$ 61 have $P > 500$ days, while in the other fields this is 3 out of 367.

The difference in period distribution might be due to an under representation of short period stars in the inner field. However, Fig. 4 in Glass et al. illustrates that the expected K-magnitudes at short periods are not fainter than the completeness limit of their survey. In fact, Glass et al. mention that they expect that the number of short-period Miras ($P <$ 250 days) is at least 75% complete. As a test, one-third of those stars with $P < 250$ days were randomly duplicated and added

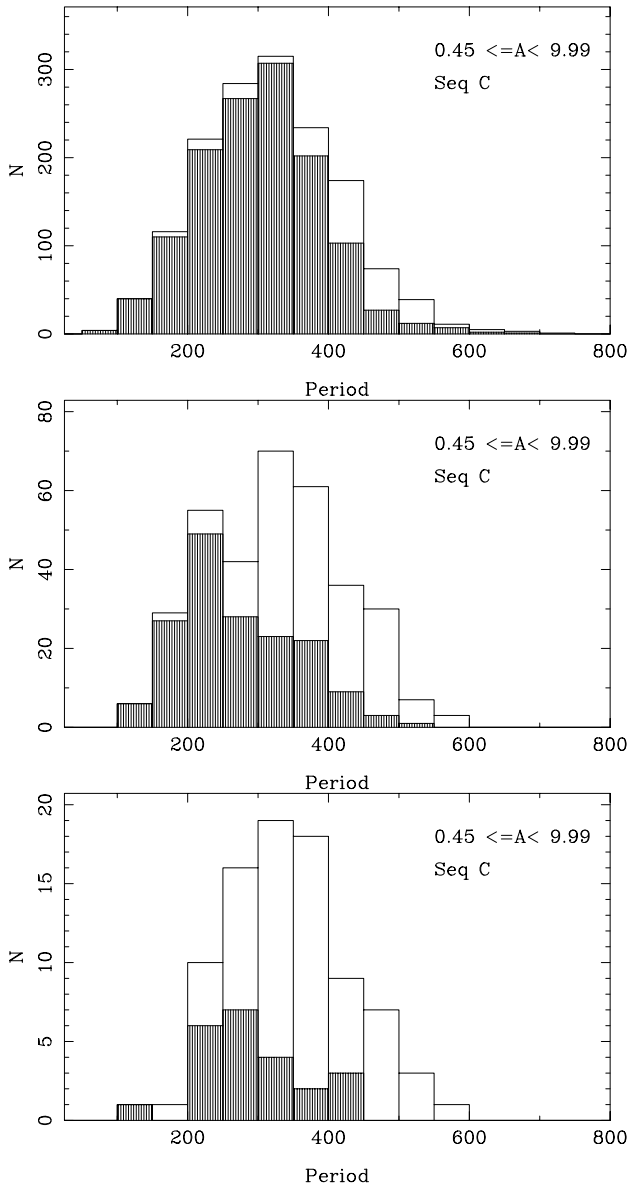

Fig. 5. Period distribution of large amplitude variables in box "C", for Bulge (*top*), LMC (*middle*), and SMC (*bottom*). For the shaded histogram only stars with $(J-K)_0 < 2.0$ have been included.

to the sample, and the KS test was repeated to find again a large difference between the period distribution of the field at −0.05 degrees and the other fields.

This difference is emphasised in Fig. 7 where the scaled period distribution of stars which have $(J-K)_0 < 2.0$ in the 5 fields between $b = -1.39°$ and $b = -5.8°$ has been subtracted from the inner field. The scaling was done in such a way that at shorter periods the two distributions would cancel at a level of 1σ (based on Poisson errors). Even if the scaling is done in a slightly different way, the result is always very similar, in the sense that there is a significant ($>4\sigma$) overabundance of LPVs in the inner field between about 350 and 600 days.

The conclusion is that there is a significant population of LPVs with period $\gtrsim$500 days present in the inner field, which remains barely present at latitude −1.2° and is absent for $b \lesssim -1.4°$. This was indirectly noted by Glass et al., who noticed that the average period of the stars in this field at $b = -0.05°$ is 427 d (and that of the known OH/IR stars 524 d), while the average period in the Sgr I window ($b = -2.6°$) is 333 d, with no known OH/IR stars (GWCF).

To quantify the nature of the Mira Bulge population, synthetic AGB evolutionary models were calculated, which are described in detail in Appendix C.

In brief, the synthetic AGB code of Wagenhuber & Groenewegen (1998) was fine-tuned to reproduce the models of Vassiliadis & Wood (1993) and then extended to more initial masses, including mass loss on the RGB. For several initial masses the fundamental mode period distribution was calculated for stars inside the observed instability strip for which the mass loss was below a critical value to simulate the fact that they should be optically visible. Vassiliadis & Wood (1993) provide calculations for 4 different metal abundances: $Z = 0.016, 0.008, 0.004$, and 0.001. We used the models for $Z = 0.016$, representing a solar mix, which is most appropriate for our Bulge sample (e.g. Rich 1998). We also show that our results are essentially unchanged if $Z = 0.01$ or 0.02 are adopted. From the comparison of the observed period distribution for fields more than 1.2° away from the galactic centre with the theoretical ones, we deduced that the periods can be explained with a population of stars with Main Sequence masses in the range of 1.5 to 2.0 $M_\odot$. A possible extension to smaller masses is possible, but not necessary to explain the periods below 200 days. To explain the excess periods in the range of 350−600 days observed closer to the centre, we need initial masses in the range 2.5−3 $M_\odot$. The presence of more massive stars in the inner field at $b = -0.05°$ cannot be excluded, as it turns out that for more massive stars, the optically visible Mira phase is essentially absent. Sevenster (1999) analyses OH/IR stars (which are LPVs with longer periods and higher mass loss rates than the Miras) in the inner Galaxy and come to the conclusion that OH/IR stars in the bulge have a minimum intial mass of about 1.3 $M_\odot$, based on an analysis of infrared colours, compatible with our results. We briefly mention here the result from Olivier et al. (2001) who studied a sample of LPVs in the solar neighbourhood with periods in the 300 to 800 days range. They conclude that a majority of these stars had initial masses in the range of 1−2 $M_\odot$, with an average value of 1.3 $M_\odot$, lower than what we find for the 300 to 600 day range sample. This difference may be explained by the fact that our conclusions are only valid for a sample with no, or only low, mass loss rates ($\lesssim 5 \times 10^{-6}$ $M_\odot$/yr), contrary to their sample which was selected to contain stars with significant mass loss ($\sim 10^{-5}$ $M_\odot$/yr). As can be seen in the Vassiliadis & Wood (1993) models, the period increases considerably when the stellar mass is reduced by the mass loss process.

We did not see a variation in the period distributions for the higher latitude fields (beyond 1° latitude) and can consider this as a homogeneous "bulge" population, which according to the Vassiliadis & Wood (1993) model, has ages in the range of 1 to about 3 Gyr. The excess population closer to the Galactic Centre is younger than 1 Gyr. According to Launhardt et al. (2002), the Nuclear Bulge (approximately the central degree) contains, besides the bulge population seen at higher latitudes, an additional population due to recent star formation closer to

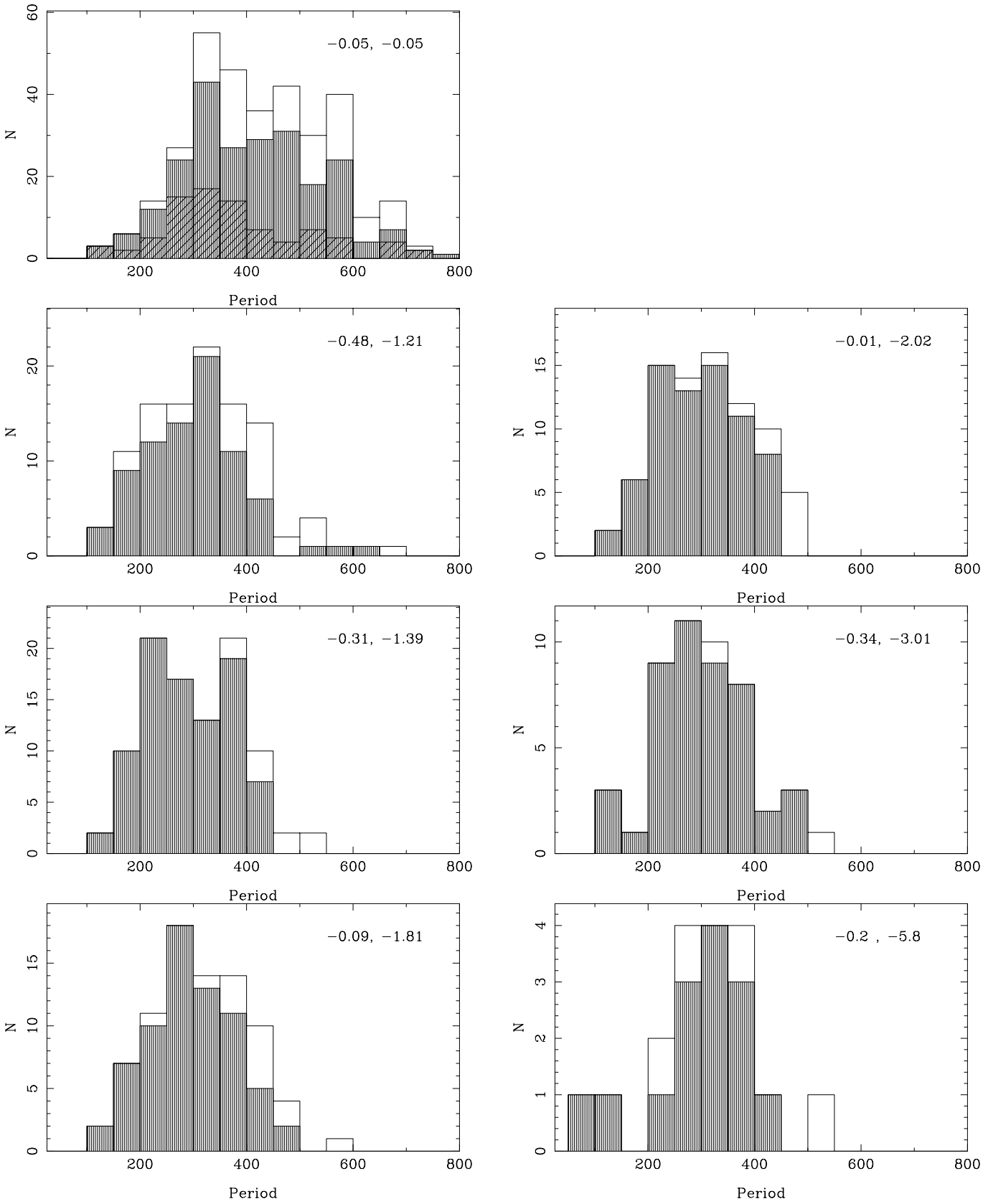

Fig. 6. Mira period distribution for 7 fields with similar longitudes but a range in latitudes (as indicated in the top right corner). For the field at $b \sim -5.8°$, OGLE fields 6 and 7 have been combined. For the shaded histograms only stars with $(J-K)_0 < 2.0$ have been included. The field at $(-0.05, -0.05)$ is based on Glass et al. (2001); see main text for details. The histogram with slanted hatching is for the reddening by Schultheis et al. (1999b) for stars in this field, the shaded histogram for the adopted reddening which is 1.35 times larger.

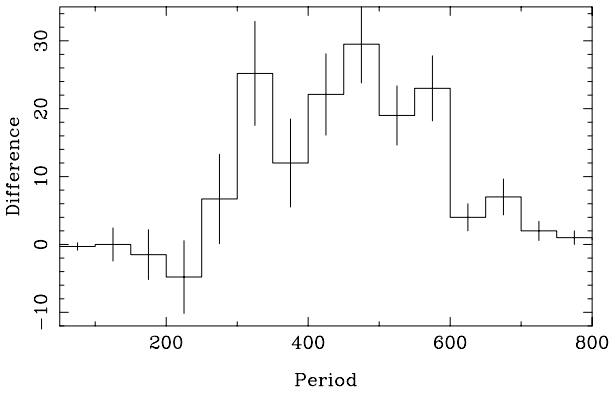

Fig. 7. Period distribution of the stars in the $b = -0.05°$ field with $(J-K)_0 < 2.0$ minus the suitably scaled period distribution of the stars in the $b = -1.39$ to $-5.8°$ fields with $(J-K)_0 < 2.0$. The scaling is such that below $\lesssim$300 days the two distributions cancel at the 1σ level.

the galactic centre. Blommaert et al. (1998) find that the extrapolation of the number density of bulge OH/IR stars towards the galactic centre would explain half of the galactic centre OH/IR population, but that an additional population, intrinsic to the galactic centre, exists, which agrees with what we see in the distribution here.

The formation history of the Bulge is still a matter of debate. In several works such as Kuijken & Rich (2002) and recently in Zoccali et al. (2004), the bulge is considered to be old (>10 Gyr) and formed on a relatively short timescale (<1 Gyr) (e.g. Ferreras et al. 2003). On the basis of the modelling of colour–magnitude diagrams, Zoccali et al. claim that no trace has been found of any younger stellar population than 10 Gyr. The bulge Miras do not fit in this picture as they are considerably younger, according to our analysis. The field studied by Zoccali et al. is centred at $(l, b) = (0.277, -6.167)$ so at a slighter higher latitude than our extreme fields ($b \approx -5.8°$). Although we were limited by the small number of Miras detected at the highest latitude fields, we did not see a change in period distribution for those fields. Zoccali et al. (2004) acknowledge the presence of Miras, but consider them as part of the old population. It is true that Miras are also detected in globular clusters and thus can be associated with old ages, as is the case for a 1 $M_\odot$ star in the Vassiliadis & Wood (1993) model, but these stars produce periods shorter than 200 days (Fig. C.1), insufficient to explain the period distribution seen in the bulge. The periods of Miras in Globular Clusters range from 150 to 300 days (Frogel & Whitelock 1998) and so only overlap with the shorter periods of the bulge Miras.

Our results agree more with the analysis of the infrared ISOGAL survey discussed in van Loon et al. (2003). They conclude that the bulk of the bulge population is old (more than 7 Gyr) but that a fraction of the stars is of intermediate age (1 to several Gyr). The Miras in our study can thus be considered as the intermediate age population seen in their analysis. van Loon et al. also see evidence of an even younger population (<200 Myr), but according to our findings, this would be restricted to the area close to the Galactic Centre.

Our discussion of the ages of the Mira stars is based on the assumption that they have evolved from single stars. An alternative scenario suggested by Renzini & Greggio (1990) would be that the brighter (longer period) Miras could evolve from close binaries where the components coalesced to form one single star. This could lead to an underestimation of the age as the Mira essentially is the product of lower mass and thus older stars. This scenario may seem in better agreement with the idea that the bulge consists of an old stellar population. It does however, suffer from the same problem as the intermediate age population, in the sense that no clear evidence for Blue Stragglers (which would be the Main Sequence counterpart of the Miras) is found (Kuijken & Rich 2002).

If indeed the bulk of the bulge population is old and formed quickly and if the Miras are of intermediate age, then our Miras must be representatives of a population which was added at a later stage, and it is unclear how it relates to the overall bulge. An interesting scenario suggested in Kormendy & Kennicutt (2004) is the one in which a secondary bulge, also called pseudo-bulge, forms within an old bulge. Such a process would be connected to the presence of a "bar" which would add "disky" material into the old classical bulge. The Miras are indeed situated in a bar-structure, as discussed in the following section.

9. The orientation of the bar

Table 6 lists the zero points (ZPs) of the the K-band PL-relation (for a fixed slope of −3.37) for the individual OGLE fields. To increase the statistics, some neighbouring fields have been added together, as indicated in the first column of the table. The galactic coordinates listed are the mean values of all individual objects, rather than the mean of the field centres. Figure 9 plots these ZPs (with error bars) as a function of Galactic longitude. There is a clear correlation as the formal weighted fit has a slope of -0.023 ± 0.005 (magnitude/degree). Restricting the fields to those with longitudes $-5 < l < +5$ (reducing the contamination by disk stars, see Appendix B) the fit becomes:

$$m_{\rm K} = (-0.0192 \pm 0.0087)\ l\ +\ (15.484 \pm 0.019) \qquad (2)$$

with an rms of 0.10 and based on 32 fields.

The interpretation of this correlation is that the Bulge Miras are located in the Galactic Bar that has a certain orientation towards the observer. A similar correlation was found by Wray (2004), who concluded that an appropriately chosen ZP in I for the small amplitude OGLE variables in their sample (which they identify as corresponding to in Box "A−") correlated with Galactic longitude. No estimate for the orientation of the Bar was given however.

In Appendix B Monte Carlo simulations were carried out in order to quantify two issues: can these observations be used to constrain the orientation of the Galactic Bar, and, second, given the specific location of the OGLE fields, if there is any bias in the derived zero point compared to a fiducial ZP, when all Miras would be located exactly in the Galactic Centre (GC). As described in Appendix B, for a spatial distribution of Bulge and Disk stars following Binney et al. (1997), viewing angles ϕ of 43 and 79 degrees (see the orientation in Fig. 8) result in slopes (magnitude versus l, Eq. (2)) in agreement with observations. However, the model with $\phi = 43°$ gives a much better fit to

Table 6. Zero point of the *K*-band *PL*-relation.

Fields	$l^{(a)}$ (deg)	$b^{(a)}$ (deg)	ZP$^{(b)}$ (mag)	N$^{(c)}$
8, 9, 10, 11	9.98	−3.75	15.58 ± 0.59	23
12, 13	7.74	−3.50	15.43 ± 0.44	27
15	5.34	+2.59	15.38 ± 0.48	22
17	5.21	−3.50	15.36 ± 0.47	24
14	5.14	+2.73	15.36 ± 0.38	29
16	5.04	−3.37	15.41 ± 0.62	17
42	4.29	−3.52	15.46 ± 0.45	13
19	3.98	−3.41	15.35 ± 0.28	20
18	3.90	−3.19	15.37 ± 0.45	20
35, 36	3.04	−3.18	15.42 ± 0.39	29
33	2.24	−3.72	15.55 ± 0.37	22
32	2.26	−3.22	15.57 ± 0.37	24
31	2.15	−3.01	15.52 ± 0.41	32
2	2.08	−3.59	15.49 ± 0.39	19
30	1.90	−2.90	15.56 ± 0.41	25
21	1.77	−2.70	15.50 ± 0.44	33
20	1.64	−2.52	15.42 ± 0.43	41
34	1.33	−2.43	15.29 ± 0.33	35
46	1.08	−4.14	15.46 ± 0.32	18
1	0.94	−3.69	15.51 ± 0.34	22
45	1.00	−3.96	15.44 ± 0.51	15
38	0.88	−3.49	15.44 ± 0.36	25
39	0.48	−2.26	15.30 ± 0.39	69
4	0.30	−2.10	15.48 ± 0.46	54
43	0.21	+2.84	15.42 ± 0.35	47
3	−0.01	−2.02	15.43 ± 0.40	70
37	−0.09	−1.81	15.34 ± 0.38	68
7	−0.09	−5.86	15.67 ± 0.36	6
5	−0.31	−1.39	15.38 ± 0.42	90
6	−0.28	−5.70	15.80 ± 0.46	8
22	−0.34	−3.01	15.50 ± 0.42	46
44	−0.48	−1.26	15.36 ± 0.36	79
23	−0.63	−3.44	15.53 ± 0.40	30
25	−2.41	−3.64	15.44 ± 0.31	33
24	−2.56	−3.46	15.62 ± 0.34	29
41	−2.86	−3.35	15.63 ± 0.38	24
40	−3.16	−3.27	15.50 ± 0.37	34
26, 27	−4.99	−3.58	15.63 ± 0.42	39
28, 29	−6.75	−4.55	15.55 ± 0.42	13
47, 48, 49	−11.19	−2.78	15.95 ± 0.35	18

$^{(a)}$ Mean values of individual objects. $^{(b)}$ Zero point of the *K*-band *PL*-relation for a slope of −3.37. $^{(c)}$ Number of objects in Box "C" used to calculate the *PL*-relation.

the number of stars per field. The bias in the ZPs is essentially independent of viewing angles, and for the best fitting model the observed ZP derived for all stars (Eq. (1)) is too bright by 0.018 mag (±0.013), while the ZP in Eq. (2) is too bright by 0.002 (±0.021) mag.

The preferred value of $\phi = 43°$ is in agreement with the values of about 45° by Whitelock (1992), based on 104 IRAS detected Mira variables, and the preferred value of 46° by Sevenster et al. (1999), based on an analysis of OH/IR stars in the inner Galaxy.

Other values in the literature are usually much larger, between 60 and 80 degrees: Dwek et al. (1995) and

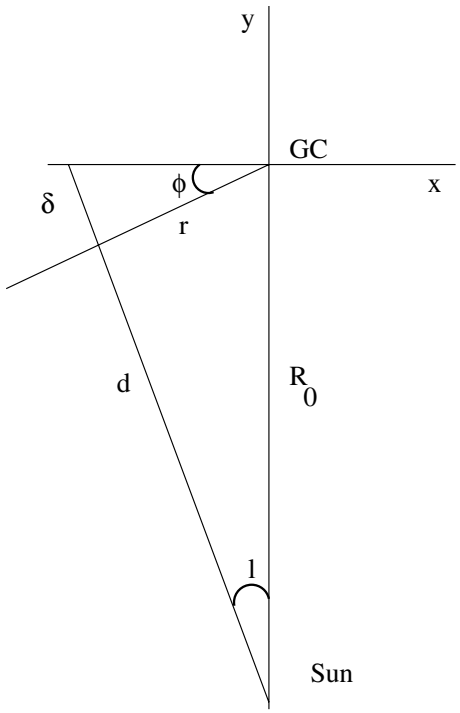

Fig. 8. Schematic drawing of the orientation of the major-axis of the Galactic Bar w.r.t. the Sun and the Galactic Centre. The *z*-axis is directed towards the reader. See Appendix B.

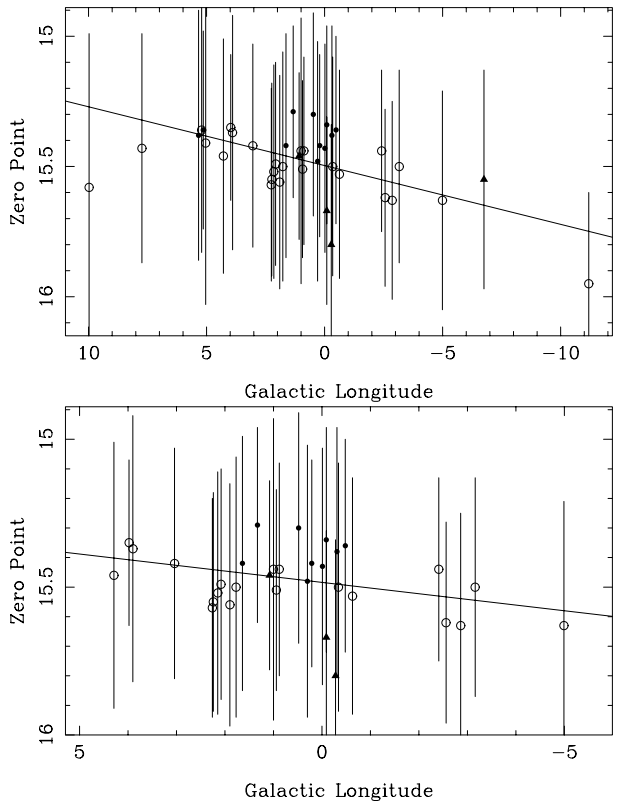

Fig. 9. Zero point of the *K*-band *PL*-relation as a function of Galactic longitude. Galactic latitudes below −4.0 are indicated by filled triangles, those larger than −2.6 by filled circles, and the remaining by open circles. Error bars are also plotted. The lines represent linear least-squares fits to all fields (*top panel*), and those with $|l| < 5°$ (*bottom panel*).

Binney et al. (1997), based on COBE-DIRBE data; Stanek et al. (1997), based on bulge red clump stars; Robin et al. (2003) and Picaud & Robin, based on colour–magnitude fitting. Sevenster et al. (1999), however, argue that these values are commonly found when no velocity data is available, the longitude range is too narrow, or when low latitudes are excluded. It is also possible that these studies are tracing other populations, which may be distributed differently than the Miras. Whitelock et al. and Sevenster et al. do use populations closely related to the Mira stars and find an angle of the bar close to the one we derive.

10. The distance to the galactic centre

A slope of the K-band PL-relation of -3.37 ± 0.09 was derived, a quantity which has seldom been determined before. GS03 derived a PL-relation in NGC 6522 based on 34 MACHO variables with r-amplitude >1.5 and DENIS K photometry: $m_{\rm K} = -4.6\ \log P + 18.1$. No errors or rms were given, as – by their own account – this fit was made by eye. Much better agreement is found with GWCF. Based on multi-epoch data of 55 stars they found $m_{\rm K} = (-3.47 \pm 0.35)\ \log P + (15.64 \pm 0.86)$ (rms = 0.35) in the Sgr I field.

Zero points for the K-band PL-relation were derived in two ways. First, a direct fit to all stars resulting in (15.44 ± 0.21), and secondly, determining ZPs per (sub)-field, and fitting this as a function of l, resulting in (15.484 ± 0.019). Applying the small bias corrections discussed at the end of Sect. 9 and averaging over the two estimates, the adopted K-band PL-relation for Miras at the GC is:

$$m_{\rm K} = -3.37 \log P + (15.47 \pm 0.03). \quad (3)$$

The derived PL-relation can be compared to the one derived for 83 O-rich LPVs in the LMC derived in G04: $m_{\rm K} = (-3.52 \pm 0.16)\ \log P + (19.56 \pm 0.38)$, with an rms of 0.26. Since the slopes are not exactly the same, the magnitudes were compared at the approximate mean period of $\log P = 2.45$. The difference in magnitude is 3.72. Adopting the LMC based slope of −3.52 for the GB Miras and re-fitting the ZP, the bias corrected ZP would become 15.85, resulting in a GB-LMC DM difference of 3.71, essentially the same value. If the distance to the GC is assumed to be 7.94 kpc (Eisenhauer et al. 2003; in a recent preprint this was even lowered to 7.62 ± 0.32 kpc, Eisenhauer et al. 2005), then the LMC would be at a DM = 18.21; or if the DM to the LMC is assumed to be 18.50 (Walker 2003; Feast 2004a), then the GC would be at 9.0 kpc. A similar result was found by GWCF, who derived a distance to the GC of 8.9 ± 0.7 kpc, assuming 18.55 for the LMC DM and $\phi = 45°$. The analysis so far has assumed no metallicity dependence of the Mira PL-relation. Wood (1990) present linear non-adiabatic pulsation calculations that suggest a dependence of the form $\log P \sim 0.46 \log Z + 1.59 \log L$, but he notes that in the K-band the dependence is expected to be weaker, and following the example he presents, one infers a dependence of $0.25 \log Z$ in the K-band. In G04, K-band PL-relations were derived for carbon-miras in the SMC and LMC. At a characteristic period of $\log P = 2.45$, one infers a relative difference in DM of 0.38, which is smaller than the commonly quoted value of near 0.50 (0.48−0.53 ± 0.11, FO cepheids, Bono et al. 2002; 0.46−0.51±0.15, FU cepheids, Groenewegen 2000; 0.44±0.05, TRGB, Cioni et al. 2000). This may hint at a metallicity dependence of the Mira K-band PL-relation. To test this hypothesis, a correction to the K-magnitude of $+\beta \log Z$ was assumed[3] (for both O- and C-rich LPVs), and the Bulge, LMC, and SMC was assumed to have solar, solar/2, and solar/4 metallicity, respectively. For a value $\beta = 0.25$ the relative SMC-LMC DM based on the C-Miras was increased from 0.38 to 0.46, while the relative DM LMC-GC was increased from 3.72 to 3.80. If the relative SMC-LMC DM is fixed at 0.50, then $\beta = 0.40$ is required, and the relative DM LMC-GC becomes 3.84 for that value. For an LMC DM of 18.50, the distance to the GC then becomes 8.6 kpc. The error in this value is somewhat difficult to estimate, as the PL-relations derived in G04 and here are from – at best – the average of two K values. Work by Feast et al. (1989) indicates that in the case of multi-epoch data (and for the small depth effect in the LMC), the intrinsic dispersion in the PL-relation is about 0.13 mag. Therefore we assign an error of 0.18 to the difference in DM, which implies an error of 0.7 kpc. Based on this large sample of Mira variables in the direction of the GB, the conclusion is that the distance to the GC is between 8.6 and 9.0 (±0.7) kpc, depending on the metallicity dependence of the K-band PL-relation. Feast (2004b) discusses the zeropoint of the Mira K-band PL-relation and, adopting the slope observed in the LMC (−3.47), derives a zeropoint of 1.00 ± 0.08, averaging over independently derived ZPs from trigonometric parallaxes, OH VLBI expansion parallaxes and Galactic Globular Clusters. Adopting a slope of −3.47 and re-fitting the ZP of the Bulge sample, the bias corrected value becomes 15.73 ± 0.03 and, without metallicity correction (consistent with the assumption above about the metallicities in Bulge, LMC, SMC), leads to a distance to the GC of 8.8 ± 0.4 kpc. This independent distance estimate is in between the values derived using no or a strong metallicity dependent zero point.

Acknowledgements. This research made use of the SIMBAD database, operated at the CDS, Strasbourg, France. This publication makes use of data products from the Two Micron All Sky Survey, which is a joint project of the University of Massachusetts and the Infrared Processing and Analysis Center/California Institute of Technology, funded by the National Aeronautics and Space Administration and the National Science Foundation.

References

Alard, C., Terzan, A., & Guibert, J. 1996, A&AS, 120, 275
Alard, C., Blommaert, J. A. D. L., Cesarsky, C., et al. 2001, ApJ, 552, 289 (ABC01)
Binney, J., Gerhard, O., & Spergel, D. 1997, MNRAS, 288, 365
Blanco, B. M. 1984, AJ, 89, 1836 (B84)
Blanco, B. M. 1986, AJ, 91, 290
Blanco, V. M., McCarthy, M. F., & Blanco, B. M. 1984, AJ, 89, 636 (BMB)
Blommaert, J. A. D. L., van der Veen, W. E. C. J., van Langevelde, H. J., Habing, H. J., & Sjouwerman, L. O. 1998, A&A, 329, 991

[3] That is, $M_{\rm K} = M_{\rm K}({\rm ref}) + \beta \log (Z/Z_{\rm ref})$, where $M_{\rm K}({\rm ref})$ is the known magnitude in a galaxy with metallicity $Z_{\rm ref}$, and $M_{\rm K}$ the magnitude it would have in a galaxy with metallicity Z.

Bono, G., Groenewegen, M. A. T., Marconi, M., & Caputo, F. 2002, ApJ, 574, L33
Catchpole, R. M. 1982, MNRAS, 200, 33p
Cieslinski, D. 2003, PASP, 115, 193
Cioni, M.-R. L., Blommaert, J. A. D. L., Groenewegen, M. A. T., et al. 2003, A&A, 406, 51
Cioni, M.-R. L., van der Marel, R. P., Loup, C., & Habing, H. J. 2000, A&A, 359, 601
Cutri, R. M., Skrutskie, M. F., Van Dyk, S., et al. 2003, Explanatory Supplement to the 2MASS All-Sky Data Release
DENIS consortium 2003, http://vizier.u-strasbg.fr/viz-bin/VizieR?-source=DENIS2
Dominici, T. P., Horvath, J. E., Medina Tanco, G. A., Teixeira, R., & Benevides-Soares, P. 1999, A&AS, 139, 321 (DHM99)
Draine, B. T. 2003, ARA&A, 41, 241
Dutra, C. M., & Bica, E. 2000, A & A 359, L9
Dwek, E., Arendi, R. G., Hauser, M. G., et al. 1995, ApJ, 445, 716
Eisenhauer, F., Schödel, R., Genzel, R., et al. 2003, ApJ, 597, L12
Eisenhauer, F., Genzel, R., Alexander, T., et al. 2005, ApJ, 628, 24
Epchtein, N., Deul, E., Derriere, S., et al. 1999, A&A, 349, 236
Feast, M. W. 2004a, in Nearby Large-Scale Structures and the Zone of Avoidance, ed. A. P. Fairall, & P. Woudt, ASP Conf. Ser, in press [arXiv:astro-ph/0405440]
Feast, M. W. 2004b, in Variable Stars in the Local Group, ed. D. W. Kurtz, & Karen Pollard, IAU Coll., 193, ASP Conf. Ser., 310, 304
Feast, M. W., Glass, I. S., Whitelock, P. A., & Catchpole, R. M. 1989, MNRAS, 241, 375
Felli, M., Testi, L., Schuller, F., & Omont, A. 2002, A&A, 392, 971
Ferreras, I., Wyse, R. F. G., & Silk, J. 2003, MNRAS, 355, 64
Fluks, M. A., Plez, B., Thé, P. S., et al. 1994, A&AS, 105, 311
Fraser, O. J., Hawley, S. L., Cook, K. H., & Keller, S. C. 2005, AJ, 129, 768
Frogel, J. A., & Whitelock, P. A. 1998, AJ, 116, 754
Frogel, J. A., & Whitford, A. E. 1987, ApJ, 320, 199 (FW87)
Glass, I. S. 1986, MNRAS, 221, 879 (G86)
Glass, I. S., & Feast, M. W. 1982, MNRAS, 198, 199 (GF82)
Glass, I. S., & Schultheis, M. 2002, MNRAS, 337, 519 (GS02)
Glass, I. S., & Schultheis, M. 2003, MNRAS, 345, 39 (GS03)
Glass, I. S., Whitelock, P. A., Catchpole, R. M., & Feast, M. W. 1995, MNRAS, 273, 383 (GWCF)
Glass, I. S., Ganesh, S., Alard, C., et al. 1999, MNRAS, 308, 127
Glass, I. S., Matsumoto, S., Carter, B. S., & Sekiguchi, K. 2001, MNRAS, 321, 77; erratum: 2002, MNRAS, 336, 1390
Groenewegen, M. A. T. 1993, Ph.D. Thesis, Chap. 5, University of Amsterdam
Groenewegen, M. A. T. 2000, A&A, 363, 901
Groenewegen, M. A. T. 2004, A&A, 425, 595 (G04)
Hughes, S. M. G. 1989, AJ, 97, 1634
Ita, Y., Tanabé, T., Matsunaga, N., et al. 2004, MNRAS, 347, 720
Izumiura, H., Deguchi, S., Hashimoto, O., et al. 1995, ApJ, 453, 837
Kiss, L. L., & Bedding, T. 2003, MNRAS, 343, L79
Kiss, L. L., & Bedding, T. 2004, MNRAS, 347, L83
Kormendy, J., & Kennicutt, C., Jr. 2004, ARAA, 42, 603
Kohoutek, L. 2002, AN 323, 57
Kuijken, K., & Rich, R. M. 2002, AJ, 124, 2054
Kwok, S., Volk, K., & Bidelman, W. P. 1997, ApJS, 112, 557
Lançon, A., & Wood, P. 2000, A&AS, 146, 217
Launhardt, R., Zylka, R., & Mezger, P. G. 2002, A&A, 384, 112
Lebzelter, T., Schulteis, M., & Melchior, A. L. 2002, A&A, 393, 573
Lloyd-Evans, T. 1976, MNRAS, 174, 169 (LE76)
Maíz-Apellániz, J. 2001, AJ, 121, 2737
McWilliam, A., & Rich, R. R. 1994, ApJS, 91, 749
Medina Tanco, G. A., & Steiner, J. E. 1995, AJ, 109, 1770
Messineo, M., Habing, H. J., Sjouwerman, L. O., Omont, A., & Menten, K. M. 2002, A&A, 393, 115
Munari, U., & Zwitter, T. 2002, A&A, 383, 188
Noda, S., Takeuti, M., Abe, F., et al. 2002, MNRAS, 330, 137
Ojha, D. K., Omont, A., Schuller, F., et al. 2003, A&A, 403, 141 (OOS03)
Olivier, E. A., & Wood, P. R. 2003, ApJ, 584, 1035
Omont, A., Ganesh, S., Alard, C., et al. 1999, A&A, 348, 755
Paunzen, E., Maitzen, H. M., Rakos, K. D., & Sschombert, J. 2003, A&A, 403, 937
Picaud, S., & Robin, A. C. 2004, A&A, 428, 891
Popowski, P., Cook, K. H., & Becker, A. C. 2003, AJ, 126, 2910
Raharto, M., Hamajima, K., Ichikawa, T., Ishida, K., & Hidayat, B. 1984, AnTok 19, 46
Renzini, A., & Greggio, L. 1990, in Bulges of Galaxies, ESO-CTIO workshop No. 35, ed. B. J. Jarvis, & D. M. Terndrup, 47
Rich, R. M. 1998, in The Central Regions of the Galaxy and Galaxies (Dordrecht: Kluwer), ed. Sofue Y., IAU Symp., 184, 11
Robin, A. C., Reylé, C., Derrière, & Picaud, S. 2003, A&A, 409, 523; erratum: 2004, A&A, 416, 157
Sevenster, M. N. 1999, MNRAS, 310, 629
Sevenster, M. N., Chapman, J. M., Habing, H. J., Killeen, N. E. B., & Lindqvist, M. 1997, A&AS, 122, 79
Sevenster, M. N., Saha, P., Valls-Gabaud, D., & Fux, R. 1999, MNRAS, 307, 584
Schultheis, M., & Glass, I. S. 2001, MNRAS, 327, 1193
Schultheis, M., Aringer, B., Jorgensen, U. G., Lebzelter, T., & Plez, B. 1999a, in Abstract of the 2nd Austrian ISO workshop Atmospheres of M, S and C giants, Vienna, Austria, ed. J. Hron, & S. Höfner, 93
Schultheis, M., Ganesh, S., Simin, G., et al. 1999b, A&A, 349, L69
Sivagnnanam, P., Braz, M. A., Le Squeren, A. M., & Tran Minh, F. 1990, A&A, 233, 112
Stanek, K. Z., Udalski, A., Szymański, M., et al. 1997, ApJ, 477, 163
Sumi, T. 2004, MNRAS, 349, 193
Sumi, T., Wu, X., Udalski, A., et al. 2004, MNRAS, 348, 1439
te Lintel Hekkert, P., Caswell, J. L., Habing, H. J., Haynes, R. F., & Norris, R. P. 1991, A&AS, 90, 327
Terzan, A., & Gosset, E. 1991, A&AS, 90, 451 (TG91)
Terzan, A., & Ounnas, C. 1988, A&AS, 76, 205 (TO88)
Udalski, A., Kubiak, M., Szymański, M., et al. 1994, AcA, 44, 317
Udalski, A., Szymański, M., Kaluzny, J., et al. 1995a, AcA, 45, 1
Udalski, A., Olech, A., Szymański, M., et al. 1995b, AcA, 45, 433
Udalski, A., Olech, A., Szymański, M., et al. 1996, AcA, 46, 51
Udalski, A., Olech, A., Szymański, M., et al. 1997, AcA, 47, 1
Udalski, A., Szymański, M., Kubiak, M. et al. 2002, AcA, 52, 217
Vassiliadis, E., & Wood, P. R. 1993, ApJ, 413, 641
Wagenhuber, J., & Groenewegen, M. A. T. 1998, A&A, 340, 183
Walker, A. R. 2003, in Stellar candles for the extragalactic distance scale, Lect. Notes Phys., 635, 265
Whitelock, P. A. 1992, in Variable stars and galaxies, ASPC Ser., 30, 11
Whitelock, P. A., Feast, M. W., & Catchpole, R. M. 1991, MNRAS, 248, 276
Wood, P. R. 1990, in From Miras to Planetary Nebulae, ed. M. O. Mennessier, & A. Omont (Gif-sur-Yvette: Éditions Frontières), 67
Wood, P. R. 2000, PASA 17, 18
Wood, P. R., Alcock, C., Allsman, R. A., et al. 1999, in AGB stars, ed. T. Le Bertre, A. Lèbre, & C. Waelkens (Kluwer Academic Publishers, ASP), IAU Symp., 191, 151
Wood, P. R., Olivier, E. A., & Kawaler, S. D. 2004, ApJ, 604, 800
Wozniak, P. R., Udalski, A., Szymanski, M., et al. 2002 AcA, 52, 129
Wray, J. J., Eyer, L., & Paczynski, B. 2004, MNRAS, 349, 1059
Zoccali, M., Renzini, A., Ortolani, S., et al. 2003, A&A, 399, 931

Online Material

Appendix A: The light curve analysis model

Some small changes w.r.t. the implementation of the lightcurve analysise model in G04 are described.

The only change in the first part of the code is the level at which a period is accepted as significant. This level was set at *significance* = 1.0×10^{-16}, compared to 5.5×10^{-11} in G04. This was possible as – contrary to G04 – only objects with large amplitudes were searched for. The resulting increase in the number of spurious periods was then caught in the process of visual inspection.

As in G04 a list of known objects (both known non-LPVs, and known AGB giants and LPVs) was compiled to ease automatic association. The list comprises:

(1) 14 833 IRAS sources within 10 deg. radius of the centre of the 49 OGLE fields at RA = 268.87, Dec = −31.03[4];
(2) 51 141 ISOGAL sources from Omont et al. (2003, hereafter OGA03; those within the extreme values of the OGLE field boundaries 261.612 <= RA <= 276.133, −40.726 <= Dec <= −21.328);
(3) 268 pulsating variable stars, 1650 Eclipsing Binaries, and 943 Miscellaneous variable stars from OGLE-I (Udalski et al. 1994, 1995a,b, 1996, 1997);
(4) 332 objects from Alard et al. (2001, hereafter ABC01), who correlated ISOGAL sources within the NGC 6522 and Sgr I Baade windows with the MACHO database;
(5) 2353 objects from Ojha et al. (2003, hereafter OOS03), who studied sources in 9 ISOGAL fields;
(6) 174 M-giants later than spectral type M0 in the NGC 6522 Baade's window from Glass & Schultheis (2002, hereafter GS02);
(7) 421 objects from Glass et al. (2001, and erratum), who monitored in K over four years an 24×24 arcmin area near the Galactic Centre;
(8) 122 objects from Alard et al. (1996, identified as Ter-[number]), who identified LPV using red photographic plates;
(9) 494 objects from Lloyd-Evans (1976, hereafter Lloyd-Evans (1976), who identified Mira variables in the three Baade windows, identified as TLE-[field]-[number] in Table 2), Blanco et al. (1984, hereafter BMB, who identified M giants in Baade's window), and Blanco (1984, hereafter B84, who identified RR Lyrae variables) with coordinates listed in the SIMBAD database to 1″ or better;
(10) 33 Nova related objects from Cieslinski (2003). The total number of sources used in the automatic correlation is 72 764.

Appendix B: Simulations of the Galactic bulge and foreground disk stars

This appendix describes the calculations to model a population in the direction of the Galactic Bulge.

The basic model is essentially the one proposed by Binney et al. (1997) to model the dust-corrected near-infrared COBE/DIRBE surface brightness map of the inner galaxy. The number density of bulge stars is assumed to be:

$$f_{\rm b} = f_0 \exp(-a^2/a_{\rm m}^2) \;/\; (1 + a/a_0)^{\beta} \tag{B.1}$$

with $f_0 = 624$, $a_{\rm m} = 1.9$ kpc, $a_0 = 0.10$ kpc, $\beta = 1.8$. Binney et al. assume a tri-axial bulge with axial ratios 1:0.6:0.4. For numerical convenience a prolate ellipsoid is assumed here: $a = \sqrt{x^2 + (y/\eta)^2 + (z/\eta)^2}$ with the value of $\eta = 0.5$ taken from Binney et al.

The number of Bulge objects up to a radius r from the centre, which defines the probability density function in the simulation, is approximated as

$$N_{\rm b}(r) = \int_0^r 4\pi a^2 f_{\rm b}(a)\, {\rm d}a \tag{B.2}$$

up to a maximum radius that is taken to be the co-rotation radius, with a default value of $R_{\rm cr} = 2.4$ kpc, following Dwek et al. (1995).

The number density of disk stars is assumed to be:

$$\begin{aligned} f_{\rm d} \;=\; & (\exp(-|z|/z_0) + \alpha \exp(-|z|/z_1)) \\ & \times R_{\rm d}\, (\exp(-r/R_{\rm d}) - f_{\rm h}\, \exp(-r/R_{\rm h})) \end{aligned} \tag{B.3}$$

with $z_0 = 0.210$ kpc, $z_1 = 0.042$ kpc, $\alpha = 0.27$, $R_{\rm d} = 2.5$ kpc (Binney et al.) and $R_{\rm h} = 1.3$ kpc (Picaud & Robin 2004). This functional form follows Binney et al., but also allows for a "hole" in the inner disk (the scaling parameter is $0 \le f_{\rm h} \le 1$ and identical to zero in Binney et al.). The total number of disk stars and the probability density functions are defined as:

$$N_{\rm d} \equiv N_{{\rm d},z}(z) \times N_{{\rm d},r}(r)$$

given by,

$$\begin{aligned} N_{\rm d} \;=\; & \left[2 \int_0^z \exp(-z/z_0) + \alpha\, \exp(-z/z_1)\, {\rm d}z\right] \\ & \times \left[\int_0^r 2\pi r R_{\rm d} (\exp(-r/R_{\rm d}) - f_{\rm h}\, \exp(-r/R_{\rm h}))\, {\rm d}r\right] \end{aligned} \tag{B.4}$$

up to maximum values $z_{\rm max} = (R_{\rm cr}\ \eta)$, and $R_{\rm max} = 8.0$ kpc, respectively.

A disk or bulge star is generated according to the ratio $N_{\rm b}/(N_{\rm b} + N_{{\rm d},z} \times N_{{\rm d},r})$. In the case of a disk star, its height above the plane z, distance to the GC r, and a random angle between 0 and 2π in the Galactic plane are drawn according to the probability functions $N_{{\rm d},z}(z)$ and $N_{{\rm d},r}(r)$. Its coordinates x, y, z are then known.

In the case of a bulge star, the distance a to the GC is drawn according to the probability function $N_{\rm b}$, and then a star is randomly placed on the surface of the appropriate ellipsoid, to find x, y, z. These values are then rotated by an angle ϕ in the Galactic plane (see Fig. 8). The Galactic coordinates are then derived assuming a distance from the Sun to the GC of $R_0 = 8.5$ kpc, and height above the plane of $z_0 = +24$ pc (Maíz-Apellániz 2001)

In a second step the known distance to the Sun is used to calculate every stars appararent magnitude, assuming an arbitrary $M_{\rm K}$ of −7.5 mag with a Gaussian dispersion of $\sigma_{\rm K} = 0.15$ mag. This is close to the dispersion observed in the

[4] Retrieved from the infrared science archive at IPAC, http://irsa.ipac.caltech.edu/

PL-relation in LMC Miras when multi-epoch photometry is available to accurately determine mean-light magnitudes (Feast et al. 1989).

In a third step it is verified for every simulated star if it is located within one of the 40 lines-of-sight considered, listed in Table 6. The field sizes of $14.2' \times 57'$ are approximated by a circle of radius 0.27 degrees. If so, it is assumed the star would have been "detected". Given the relative brightness of the LPVs it is assumed that completeness is not an issue.

The number of stars drawn was such that a total of about 1200 objects were "detected", similar to the actual number. At the end of the simulation, the average magnitude and dispersion per line-of-sight was determined, and a weighted least-square fit was made of the mean magnitude versus longitude for all fields and for those with $|l| < 5^\circ$, as for the observations. In addition, the mean magnitude and dispersion for all "detected" stars was determined.

Such a simulation was repeated 1000 times. Then, distribution functions and from that median and 1-sigma values of the following parameters were determined: the number of stars (total, disk, bulge), mean magnitude and sigma (for every line-of-sight), mean magnitude and sigma for all stars, and slope and error in the slope both when fitted over all longitudes, and for those fields with $|l| < 5^\circ$.

For the standard model of Binney et al. described above (i.e. $f_{\rm h} = 0$), it turns out that for two values of ϕ a slope (because of the contamination by disk stars in the outer fields, the slope fitted over $|l| < 5^\circ$ is considered from now on) in agreement with observations is found: $\phi = 43$ and 79 degrees (with values between 25 and 85 degrees resulting in predicted slopes within 1-σ of the observed one.)

Figures B.1–B.3 show the results for these two cases. Figure B.1 shows the distribution on the Galactic Plane for a random sub-sample of all stars simulated, and illustrates a fundamental difference between the two cases. For large viewing angles, the outer fields $|l| \gtrsim 10^\circ$ will be dominated by disk stars. Figure B.2 shows for the same random sub-sample the observed magnitude as a function of l. In Fig. B.3 the simulated mean magnitude and error for each field are compared to the observations in the top panel, while in the bottom panel the observed and predicted number of objects are compared. It is from this plot that one may conclude that the model with $\phi = 43^\circ$ is to be preferred over the one with $\phi = 79^\circ$ as the latter model predicts too few stars, especially in the outer fields, compared to the observations. Comparing only the observed and predicted number of stars (in an χ^2 sense) a best fit is found for $\phi = 35^\circ$ (with values between 0 and 60 degrees resulting in a reduced χ^2 within 1 unit of the minimum χ^2). Combining the constraints from the slope and the number of stars a viewing angle of $\phi = 43 \pm 17$ degrees is the preferred value.

One may consider the ratio of Bulge to Disk stars as uncertain, and therefore, a model was considered with $\phi = 79^\circ$ and $f_0 = 350$. The latter value was set so that the model predicted the observed number of stars in the $l = -11^\circ$ field. Such a model would still underestimate the number of stars in the outer fields at positive l, and would give a slope no longer in agreement with observations.

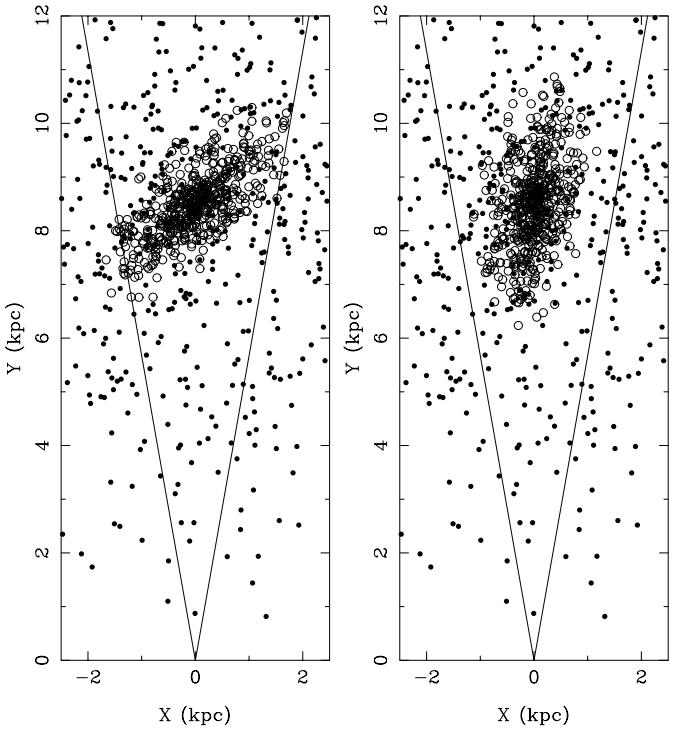

Fig. B.1. For angles of ϕ of 43 and 79 degrees (*left and right panel*), the projection (drawn to scale) on the Galactic Plane of 1300 randomly drawn stars. Disk stars are represented by filled circles, Bulge stars by open circles. The Sun is at $X = 0$, $Y = 0$. The Galactic Centre is at $X = 0$, $Y = 8.5$. The lines illustrate Galactic longitudes of ±10 degrees.

Finally, a model including a hole in the inner disk was considered (i.e. $f_{\rm h} = 1$). To have the same ratio of bulge to disk stars, f_0 was set to 425. The results are very similar and the best fitting angle is now 40 degrees.

For reference, the predicted number of disk and bulge stars for the viewing angles of 43 and 79 degrees and for the model with $\phi = 40^\circ$ and the central hole in the disk are listed in Table B.1. As they are quite different, these predictions may be useful when additional data (proper motion[5], radial velocities) become available to constrain the ratio of disk to bulge objects as a function of galactic coordinates.

Appendix C: Comparing stellar evolution codes

The models described in Vassiliadis & Wood (1993, VW) were downloaded from P. Wood's webpage (`http://www.mso.anu.edu.au/~wood/`). These files list the relevant stellar quantities (remaining stellar mass, luminosity, and effective temperature amongst other quantities), and the evolutionary time, for the individual calculated models on the AGB. They are available for $Z = 0.016$ (1.0, 1.5, 2.0, 2.5, 3.5, 5.0 $M_\odot$), $Z = 0.008$ (0.945, 1.0, 1.5, 2.0, 2.5, 3.5, 5.0 $M_\odot$), $Z = 0.004$ (0.89, 1.0, 1.5, 2.0, 2.5, 3.5, 5.0 $M_\odot$), and $Z = 0.001$ (1.0, 1.5 $M_\odot$).

[5] Sumi et al. (2004) present proper motions for 5 million objects in the OGLE fields, centred on the expected I_0 magnitude and $(V-I)_0$ colour of red clump giants but also including some red giants. Of the 2691 LPVs in the present study, 1612 are listed in Sumi et al.

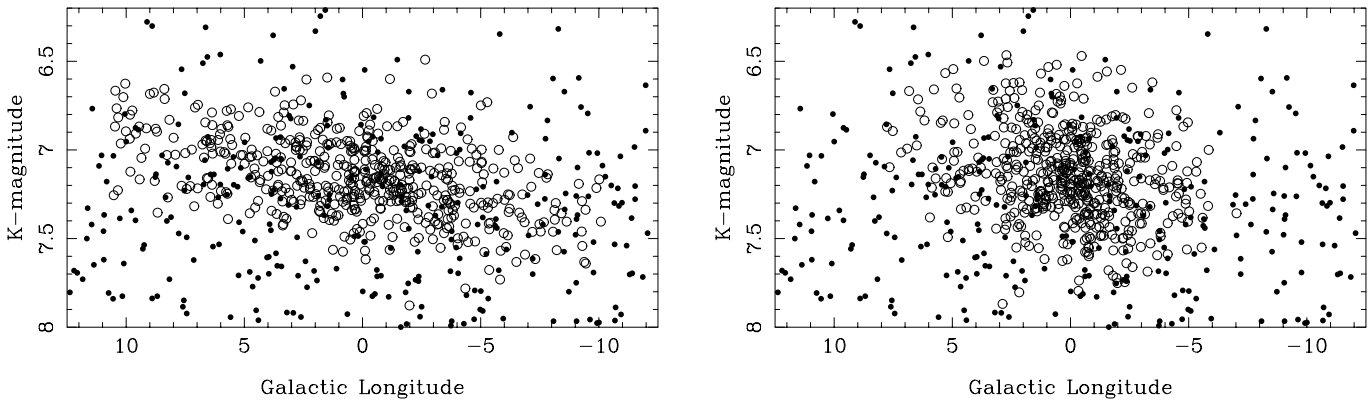

Fig. B.2. For angles of ϕ of 43 and 79 degrees (*left and right panel*), the distribution of K-magnitudes as a function of Galactic longitude for the stars shown in Fig. B.1. Disk stars are represented by filled circles, Bulge stars by open circles.

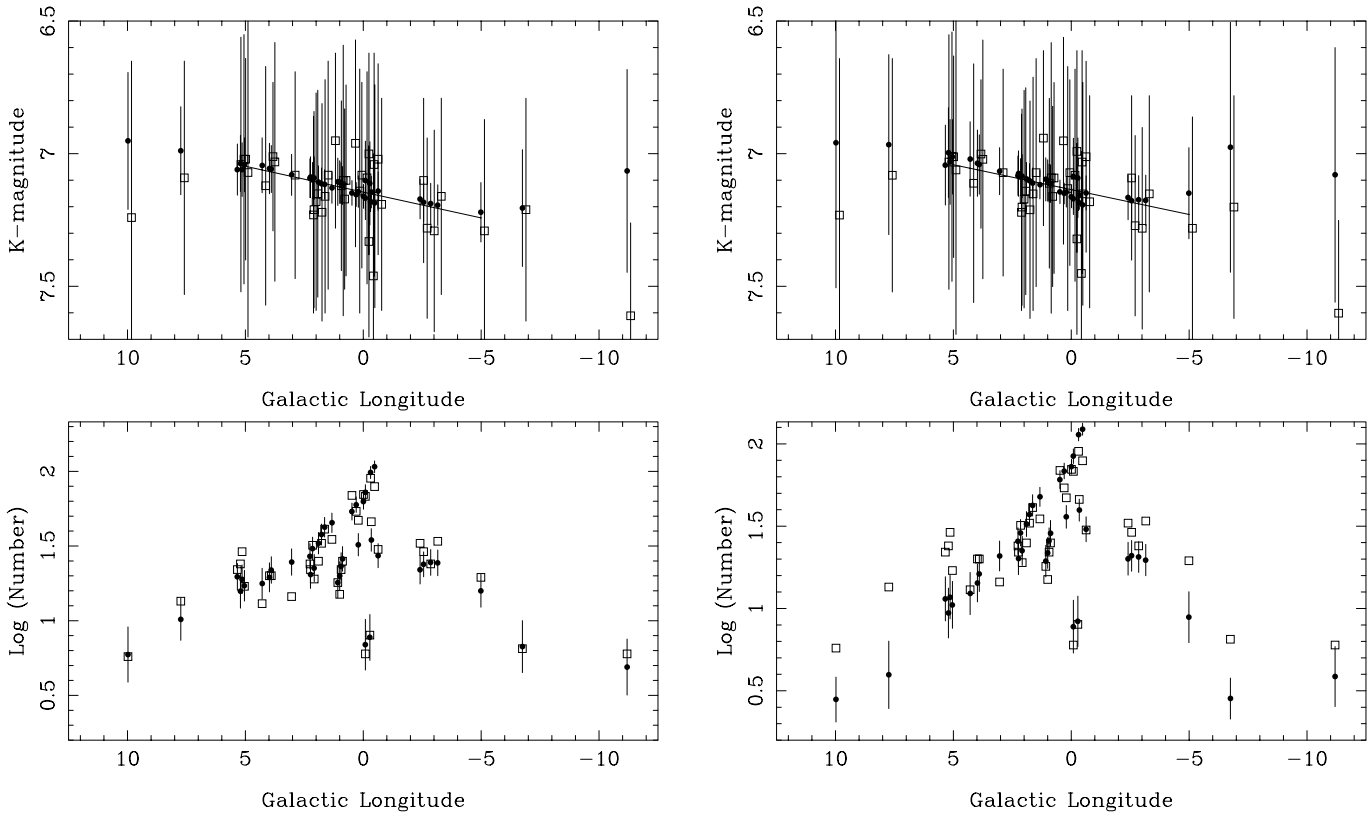

Fig. B.3. For angles of ϕ of 43 and 79 degrees (*left and right panel*), *the top panel* compares the observed (open squares) and modelled (filled circles) mean magnitudes and errors for the 40 fields listed in Table 6, with the line indicating the best fit over the range $|l| < 5°$. For clarity the observed and modelled points are slightly off-set in longitude. *The bottom panel* compares the observed (open squares) and modelled (filled circles) number of stars per field. For both angles the observed slope over the range $|l| < 5°$ is reproduced, but the distribution of stars is fitted much better for $\phi = 43°$.

For our comparison with the simulations, we used the solar metallicity models, which are expected to be the most representative for our Bulge sample. However, different studies indicate that the Bulge may have quite a broad metallicity distribution, peaking at about −0.25 dex with dispersion of 0.3 dex (see e.g. McWilliam & Rich 1994; Ramirez et al. 2000). The AGB lifetime, LPV lifetime, and LPV period distribution was determined. The AGB lifetime is defined as the time between the first model in the file (the start of the AGB) up to the point where the remaining envelope mass becomes less than 0.04 $M_{\odot}$, or $T_{\rm eff} > 4500$ K, which is taken as the start of the post-AGB evolution.

For each timestep, the fundamental period is calculated following VW. The star is assumed to be in the Mira instability strip when the bolometric magnitude is within 0.20 mag (the assumed width of the instability strip at a given period) of the *PL*-relation (Feast et al. 1989)

$$M_{\rm bol} = -3.00\ \log P + 2.85 \qquad \text{(C.1)}$$

Table B.1. Observed total, and predicted number of disk and bulge stars per field.

			$\phi = 43°$		$\phi = 79°$		$\phi = 40°$, $f_h = 1$	
l	b	N_{obs}	N_{disk}	N_{bulge}	N_{disk}	N_{bulge}	N_{disk}	N_{bulge}
9.98	−3.75	5.75	2.1 ± 1.5	3.1 ± 2.0	2.8 ± 0.9	0.0 ± 0.0	2.0 ± 1.5	3.9 ± 1.9
7.74	−3.50	13.5	3.1 ± 1.6	6.8 ± 2.6	2.8 ± 1.6	1.8 ± 1.2	3.0 ± 1.7	7.5 ± 2.8
5.34	+2.59	22	5.6 ± 2.4	14.0 ± 3.5	4.0 ± 1.9	7.4 ± 2.6	4.2 ± 2.2	15.4 ± 3.9
5.21	−3.50	24	3.8 ± 1.7	12.0 ± 3.6	2.9 ± 1.7	6.6 ± 2.5	2.9 ± 1.7	12.9 ± 3.6
5.14	+2.73	29	5.0 ± 2.3	13.9 ± 3.4	3.8 ± 1.8	7.9 ± 2.8	3.9 ± 2.0	15.3 ± 4.0
5.04	−3.37	17	3.9 ± 2.0	13.0 ± 3.5	2.9 ± 1.7	7.4 ± 2.7	3.0 ± 2.0	13.9 ± 3.5
4.29	−3.52	13	3.8 ± 1.8	14.0 ± 3.6	2.8 ± 1.7	9.5 ± 3.0	2.9 ± 1.5	15.2 ± 3.7
3.98	−3.41	20	3.9 ± 2.0	15.5 ± 4.1	2.9 ± 1.8	11.2 ± 3.4	3.0 ± 1.8	16.6 ± 4.0
3.90	−3.19	20	4.8 ± 2.2	17.2 ± 4.0	3.7 ± 1.7	12.7 ± 3.4	3.7 ± 1.8	18.7 ± 4.1
3.04	−3.18	14.5	4.9 ± 2.2	19.9 ± 4.4	3.8 ± 1.7	17.1 ± 4.1	3.8 ± 1.7	21.1 ± 4.7
2.24	−3.72	22	3.0 ± 1.9	16.9 ± 4.1	2.1 ± 1.5	17.4 ± 4.1	2.0 ± 1.5	18.3 ± 3.9
2.26	−3.22	24	4.9 ± 2.3	21.7 ± 4.5	3.8 ± 2.0	21.8 ± 4.4	3.1 ± 1.9	23.5 ± 4.7
2.15	−3.01	32	5.7 ± 2.2	24.9 ± 5.0	4.0 ± 1.9	24.5 ± 4.8	3.9 ± 1.8	26.5 ± 4.8
2.08	−3.59	19	3.9 ± 1.9	18.5 ± 4.3	2.9 ± 1.7	19.4 ± 4.3	2.8 ± 1.5	19.9 ± 4.5
1.90	−2.90	25	6.1 ± 2.5	26.7 ± 5.0	4.7 ± 2.1	27.9 ± 5.1	4.1 ± 2.0	28.7 ± 5.0
1.77	−2.70	33	7.1 ± 2.6	30.4 ± 5.4	5.2 ± 2.1	31.6 ± 5.4	5.0 ± 2.3	32.2 ± 5.4
1.64	−2.52	41	8.3 ± 2.9	33.8 ± 5.6	6.0 ± 2.4	36.1 ± 6.0	5.8 ± 2.2	35.9 ± 6.0
1.33	−2.43	35	8.8 ± 2.8	36.6 ± 6.1	6.6 ± 2.5	41.0 ± 6.3	5.9 ± 2.5	39.1 ± 5.9
1.08	−4.14	18	2.2 ± 1.5	15.3 ± 3.8	1.9 ± 1.3	17.4 ± 4.0	1.9 ± 1.3	16.5 ± 3.9
0.94	−3.69	22	3.7 ± 1.9	19.6 ± 4.4	2.8 ± 1.6	22.9 ± 4.6	2.0 ± 1.5	21.0 ± 4.2
1.00	−3.96	15	2.9 ± 1.7	17.0 ± 4.0	2.0 ± 1.4	19.6 ± 4.3	2.0 ± 1.3	18.1 ± 4.1
0.88	−3.49	25	4.0 ± 1.9	21.7 ± 4.6	3.0 ± 1.7	25.4 ± 4.8	2.9 ± 1.7	23.4 ± 4.5
0.48	−2.26	69	10.1 ± 3.0	43.3 ± 6.4	7.5 ± 2.6	53.2 ± 7.2	6.9 ± 2.6	46.0 ± 6.7
0.30	−2.10	54	11.6 ± 3.1	48.1 ± 6.3	8.6 ± 2.8	59.6 ± 7.2	7.9 ± 2.7	51.0 ± 6.6
0.21	+2.84	47	5.0 ± 2.4	26.9 ± 5.0	3.9 ± 2.1	31.8 ± 5.2	3.7 ± 1.7	28.2 ± 5.1
-0.01	−2.02	70	12.0 ± 3.5	50.6 ± 6.4	9.0 ± 2.9	63.6 ± 7.0	8.5 ± 2.7	53.6 ± 6.8
-0.09	−1.81	68	14.2 ± 3.6	57.8 ± 7.4	10.7 ± 3.0	73.3 ± 8.1	10.1 ± 3.1	61.6 ± 7.5
-0.09	−5.86	6	1.0 ± 0.8	6.0 ± 2.4	0.9 ± 0.7	7.0 ± 2.5	0.0 ± 0.5	6.3 ± 2.6
-0.31	−1.39	90	20.7 ± 4.4	77.4 ± 8.5	15.2 ± 3.8	98.4 ± 9.7	14.8 ± 3.8	81.9 ± 8.6
-0.28	−5.70	8	1.0 ± 0.8	6.9 ± 2.6	0.9 ± 0.7	7.7 ± 2.8	0.0 ± 0.7	7.1 ± 2.6
-0.34	−3.01	46	5.8 ± 2.2	29.1 ± 5.4	4.2 ± 2.0	35.0 ± 5.5	3.9 ± 1.8	30.4 ± 5.6
-0.48	−1.26	79	23.3 ± 4.7	83.5 ± 8.8	17.4 ± 4.1	105.5 ± 9.9	16.7 ± 4.0	88.6 ± 9.0
-0.63	−3.44	30	4.0 ± 1.9	22.9 ± 4.5	3.0 ± 1.8	27.1 ± 5.0	2.9 ± 1.6	24.4 ± 4.9
-2.41	−3.64	33	3.1 ± 1.7	18.3 ± 4.2	2.1 ± 1.5	17.5 ± 3.9	2.1 ± 1.5	19.8 ± 4.4
-2.56	−3.46	29	3.9 ± 2.1	19.9 ± 4.1	2.9 ± 1.7	17.9 ± 4.1	2.9 ± 1.7	21.2 ± 4.6
-2.86	−3.35	24	4.1 ± 2.1	20.1 ± 4.2	3.0 ± 1.9	17.1 ± 4.2	3.0 ± 1.8	21.2 ± 4.5
-3.16	−3.27	34	4.3 ± 2.0	19.8 ± 4.3	3.1 ± 1.7	16.1 ± 4.1	3.0 ± 1.8	21.4 ± 4.5
-4.99	−3.58	19.5	3.1 ± 1.7	12.2 ± 3.5	2.8 ± 1.6	6.1 ± 2.6	2.9 ± 1.6	13.5 ± 3.5
-6.75	−4.55	6.5	1.9 ± 1.2	4.9 ± 2.2	2.0 ± 1.0	0.9 ± 0.7	1.0 ± 1.0	5.2 ± 2.1
-11.19	−2.78	6.0	4.9 ± 2.0	0.0 ± 0.0	3.9 ± 1.5	0.0 ± 0.0	5.0 ± 2.0	0.0 ± 0.5

when assuming a LMC distance of 18.50 *and when the mass loss rate is below a critical value*, as this *PL*-relation was derived for optically visible objects and the LPV samples studied in G04 and in the present paper have been culled by only considering objects with $(J-K)_0 < 2.0$. In such a way the lifetime and the period distribution of optically visible LPVs can be determined.

The critical mass loss rate is determined by taking typical values of luminosity and effective temperature inside the instability strip for each mass in the grid of solar metallicities and then using a radiative transfer program (Groenewegen 1993) with the appropriate model atmosphere for M-stars (Fluks et al. 1994), and typical dust properties (silicate dust, condensation temperature of 1500 K, dust-to-gas ratio 0.005, expansion velocity 10 km s^{-1}) to determine the critical mass loss rate at which the star would become redder in $(J-K)$ than 2.0. The critical mass loss rates found were between 4 and 20×10^{-6} $M_\odot$ yr^{-1} depending on the initial mass of the model. In fact, the critical mass loss rate was observed to scale with $\sqrt{L}$, as expected as the dust optical depth predominantly determines the infrared colours; hence, the mass loss rate is proportional to the stellar radius, all other things being equal. For the 1.0 and 1.5 $M_\odot$ initial mass models, the mass loss rate inside the instability strip always remains below the critical mass loss rate. The adopted critical mass loss rate is 1.0×10^{-5} $\sqrt{L/13000}$ $M_\odot$ yr^{-1} . The results for the solar metallicty models are summarised in Table C.1.

We now consider the synthetic AGB models of Wagenhuber & Groenewegen (1998; WG), first because the VW models exist only for a limited number of initial

Table C.1. AGB lifetime and optically visible LPV lifetimes for two sets of models.

		Vassiliadis & Wood			Wagenhuber & Groenewegen		
Z	Mass ($M_\odot$)	MS lifetime (10^9 years)	AGB lifetime (10^3 years)	LPV lifetime (10^3 years)	AGB lifetime (10^3 years)	LPV lifetime (10^3 years)	Remark
0.016	1.0	11.25	595	101	487	49	$\eta_{\rm RGB} = 0$, $\alpha = 1.9$
					560	93	$\eta_{\rm RGB} = 0$, $\alpha = 2.0$
					595	129	$\eta_{\rm RGB} = 0$, $\alpha = 2.1$
0.016	1.5	2.742	929	272	873	303	$\eta_{\rm RGB} = 0$, $\alpha = 1.9$
					942	284	$\eta_{\rm RGB} = 0$, $\alpha = 2.0$
					1019	282	$\eta_{\rm RGB} = 0$, $\alpha = 2.1$
0.016	2.0	1.236	1168	153	1596	253	$\eta_{\rm RGB} = 0$, $\alpha = 2.0$
					1684	222	$\eta_{\rm RGB} = 0$, $\alpha = 2.1$
0.016	2.5	0.619	2291	8	2284	84	$\eta_{\rm RGB} = 0$, $\alpha = 2.0$
					2354	50	$\eta_{\rm RGB} = 0$, $\alpha = 2.1$
0.016	3.5	0.231	543	0	497	0	$\eta_{\rm RGB} = 0$, $\alpha = 2.0$
					542	0	$\eta_{\rm RGB} = 0$, $\alpha = 2.1$
0.016	5.0	0.096	673	0	175	0	$\eta_{\rm RGB} = 0$, $\alpha = 2.0$
					174	0	$\eta_{\rm RGB} = 0$, $\alpha = 2.1$

masses and second because mass loss on the RGB was only included for initial masses *below* 1 $M_\odot$, while it is well known that the effect of mass loss on the RGB is substantial also at and above 1 $M_\odot$. The VW mass loss rate recipe was implemented; and to mimic the VW tracks as closely as possible, the mixing length parameter α (basically setting the effective temperature scale) in the WG models was tuned to give similar AGB and LPV lifetimes. The results are summarised in Table C.1. It turns out that with $\alpha = 2.0$ the lifetimes match very well especially at low initial mass.

Mass loss on the RGB is described by a Reimers law with a scaling factor $\eta_{\rm RGB} = 0.35$. This gives the required mass loss (0.13, 0.16, 0.17 $M_\odot$ for a star of 1.0 $M_\odot$ initial mass at $Z = 0.004$, 0.008, 0.019, respectively; M. Salaris, private communication) to give the observed mean colour of Horizontal Branch stars in Galactic Globular Clusters. Table C.2 summarises the AGB and LPV lifetime for a set of WG models with $\eta_{\rm RGB} = 0.35$ and $\alpha = 2.0$, and Fig. C.1 displays the period distribution of optically visible stars inside the instability strip (normalised to one each time) for a few initial masses.

Table C.2 also includes the results for a few initial masses if slightly different metallicities of $Z = 0.01$ and 0.02 are adopted, and Fig. C.2 shows the corresponding Period distribution. These results indicate that the effect of metallicity on the pulsation properties for the typical metallicities in the Bulge is small.

Table C.2. AGB lifetime and optically visible LPV lifetimes for the final set of synthetic models, with $\eta_{\rm RGB} = 0.35$ and $\alpha = 2.0$.

Z	Mass ($M_\odot$)	AGB lifetime (10^3 years)	LPV lifetime (10^3 years)
0.016	0.85	240	1.6
0.016	0.9	288	1.0
0.016	1.0	305	1.5
0.016	1.1	445	41.
0.010	1.2	644	132.
0.016	1.2	552	108.
0.020	1.2	528	95.
0.016	1.3	648	161.
0.016	1.4	770	247.
0.016	1.5	858	296.
0.016	1.6	965	293.
0.016	1.7	1103	282.
0.016	1.8	1211	296.
0.016	1.9	1362	289.
0.010	2.0	1610	234.
0.016	2.0	1522	269.
0.020	2.0	1527	283.
0.016	2.1	1711	250.
0.016	2.2	1898	220.
0.016	2.3	2071	182.
0.016	2.4	2182	131.
0.016	2.5	2269	90.
0.016	2.6	2300	59.
0.016	2.7	2260	40.
0.016	2.8	2125	26.
0.016	2.9	1903	14.
0.010	3.0	1435	3.
0.016	3.0	1643	10.
0.020	3.0	1748	10.
0.016	3.1	1355	3.
0.016	3.4	641	0.

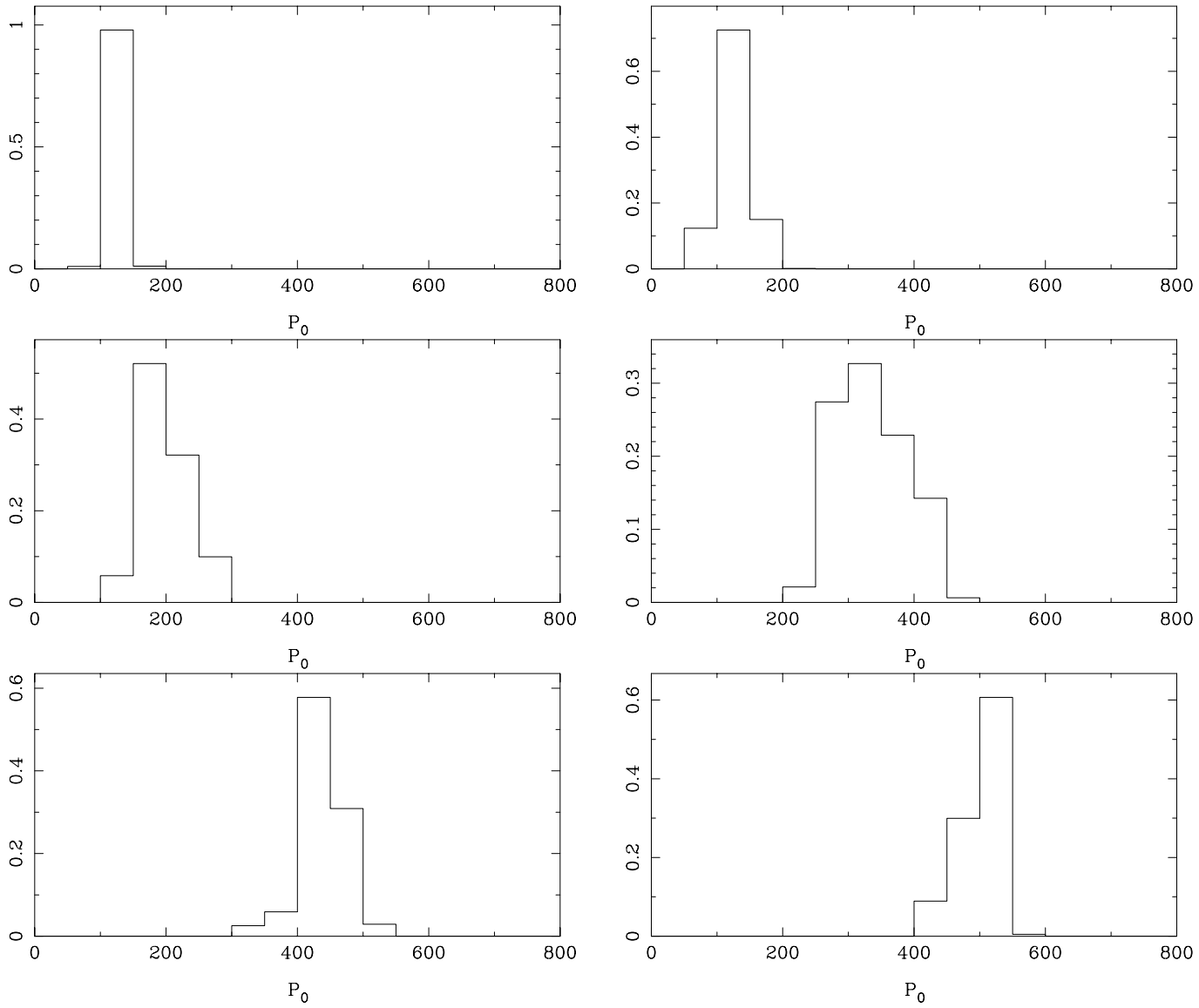

Fig. C.1. Theoretical period distribution of optically visible stars inside the observed instability strip for masses 1.1, 1.2, 1.5, 2.0, 2.5, 3.0 $M_{\odot}$ (*left to right, top to bottom*).

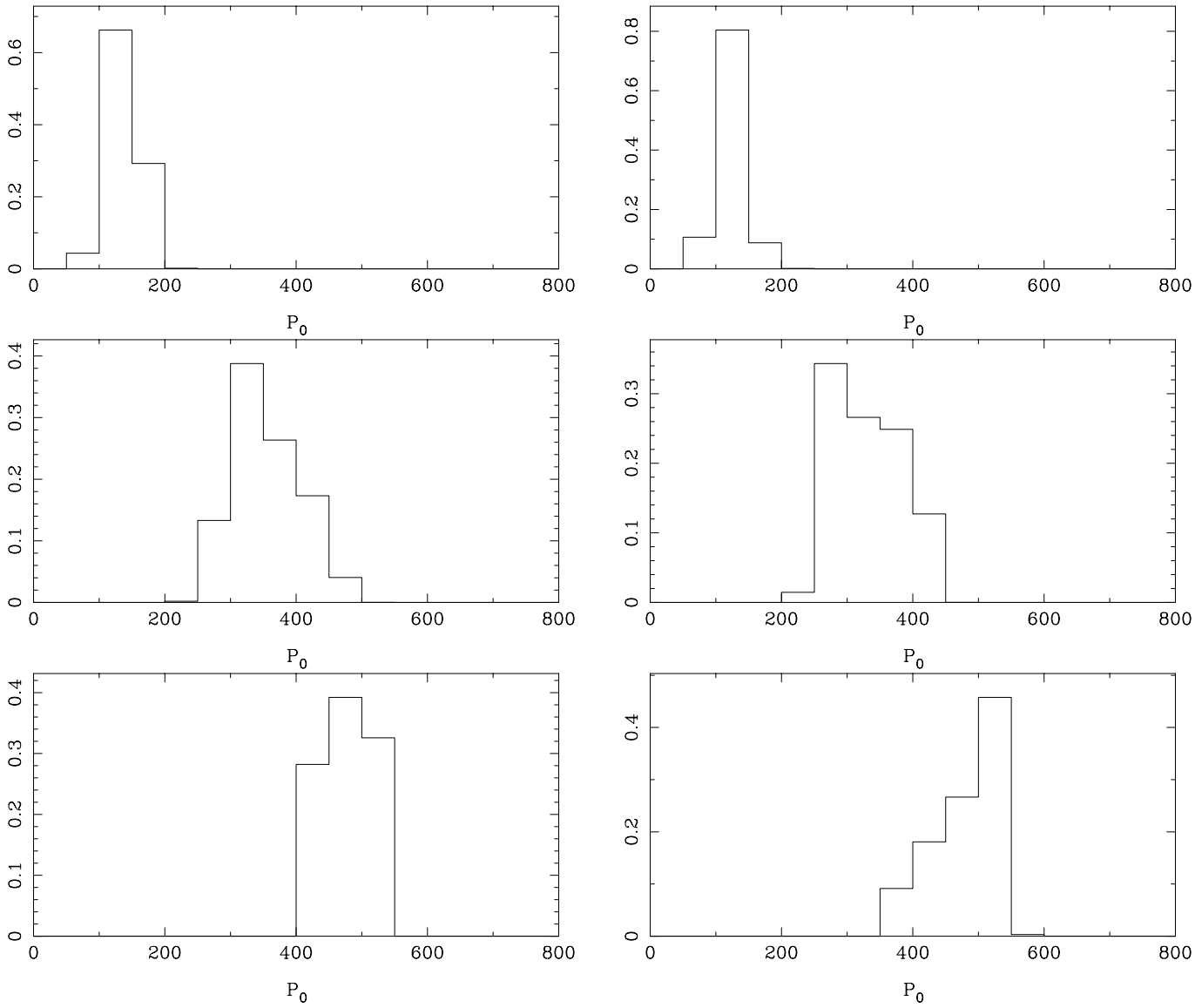

Fig. C.2. Like Fig. C.1 illustrating the influence of metallicity on the theoretical distribution. In the left hand panels for $Z = 0.010$ and on the right for $Z = 0.020$, for stars with inital masses 1.2 (*top*), 2.0 (*middle*) and 3.0 (*bottom*) $M_{\odot}$.

Table 2. First entries in the electronically available table, which list: OGLE-field and number, other names, spectral type, and references. ISOGAL sources from the official catalog (OGA03) have the prefix "ISOGAL". ISOGAL sources studied in OOS03 have the prefix "OOS03". References in Col. 4 are given in the bibliography of the main text.

OGLE-name	Other name	Chemical type	Remarks
bul_sc01_0098	V 4713 Sgr		
bul_sc01_0100			
bul_sc01_0103			
bul_sc01_0128			
bul_sc01_0177			
bul_sc01_0193			
bul_sc01_0235			
bul_sc01_0237			
bul_sc01_0388			
bul_sc01_0558	BW6_V1_MISC		
bul_sc01_0602			
bul_sc01_0611			
bul_sc01_0878			
bul_sc01_0916			
bul_sc01_1241			
bul_sc01_1253			
bul_sc01_1254			
bul_sc01_1467	BW5_V1_MISC		
bul_sc01_1533			
bul_sc01_1561			
bul_sc01_1616			
bul_sc01_1738	BW5_V4_MISC		
bul_sc01_1818			
bul_sc01_1821			
bul_sc01_1944			
bul_sc01_2079	BW5_V2_MISC, V 3999 Sgr		
bul_sc01_2222			
bul_sc01_2231			
bul_sc01_2303			
bul_sc01_2447			
bul_sc01_2542	TLE_NGC_6522_181, V 1371 Sgr, MACHO 119.19833.209	M7	GS03, Glass & Feast (1982; GF82), Lloyd-Evans (1976; hereafter LE76)
bul_sc01_3024			
bul_sc01_3202			
bul_sc01_3212			
bul_sc01_3916			
bul_sc01_3955			
bul_sc01_4032			
bul_sc01_4178			
bul_sc01_4185			
bul_sc01_4194			
bul_sc01_4200			
bul_sc01_4350			
bul_sc02_0002			
bul_sc02_0033			
bul_sc02_0061			
bul_sc02_0080			
bul_sc02_0098			
bul_sc02_0136			
bul_sc02_0206			
bul_sc02_0341			
bul_sc02_0369			
bul_sc02_0409			
bul_sc02_0420			

Table 2. continued.

OGLE-name	Other name	Chemical type	Remarks
bul_sc02_0529			
bul_sc02_0564			
bul_sc02_0574			
bul_sc02_0654			
bul_sc02_0748			
bul_sc02_1136			
bul_sc02_1214			
bul_sc02_1220			
bul_sc02_1331	IRAS_18017-2907		
bul_sc02_1492			
bul_sc02_1555			
bul_sc02_1561			
bul_sc02_1733			
bul_sc02_1985			
bul_sc02_2007			
bul_sc02_2276			
bul_sc02_2604			
bul_sc02_2755			
bul_sc02_2834			
bul_sc02_2842			
bul_sc02_2861			
bul_sc02_3055			
bul_sc02_3184			
bul_sc02_3258			
bul_sc02_3358			
bul_sc02_3360			
bul_sc02_3580			
bul_sc02_3721			
bul_sc02_3738			
bul_sc02_3778			
bul_sc02_3933			
bul_sc02_4290			
bul_sc02_4321			
bul_sc02_4772			
bul_sc02_4926			
bul_sc02_5217			
bul_sc02_5236			
bul_sc03_0047			
bul_sc03_0048			
bul_sc03_0057			
bul_sc03_0078			
bul_sc03_0114			
bul_sc03_0135			
bul_sc03_0191			
bul_sc03_0307			
bul_sc03_0318			
bul_sc03_0375			
bul_sc03_0689			
bul_sc03_0756			
bul_sc03_0773			
bul_sc03_0878			
bul_sc03_0897			
bul_sc03_0921			
bul_sc03_0926			
bul_sc03_1072			
bul_sc03_1082			
bul_sc03_1098			
bul_sc03_1105			
bul_sc03_1109			

Table 2. continued.

OGLE-name	Other name	Chemical type	Remarks
bul_sc03_1272			
bul_sc03_1288			
bul_sc03_1393			
bul_sc03_1707			
bul_sc03_1788			
bul_sc03_1810			
bul_sc03_1833			
bul_sc03_1890			
bul_sc03_1952			
bul_sc03_2188			
bul_sc03_2334			
bul_sc03_2339	ISOGAL-PJ175332.8-300746		
bul_sc03_2487	ISOGAL-PJ175336.4-300655		
bul_sc03_2495	ISOGAL-PJ175345.6-300709		
bul_sc03_2532	ISOGAL-PJ175358.1-300652		
bul_sc03_2553			
bul_sc03_2695			
bul_sc03_2750	ISOGAL-PJ175328.9-300529		
bul_sc03_2751	ISOGAL-PJ175330.7-300517		
bul_sc03_2767			
bul_sc03_2806	ISOGAL-PJ175358.6-300546		
bul_sc03_2855			
bul_sc03_2862	ISOGAL-PJ175319.0-300407		
bul_sc03_2878	ISOGAL-PJ175327.8-300410		
bul_sc03_3023	ISOGAL-PJ175331.3-300330		
bul_sc03_3086	ISOGAL-PJ175403.2-300321		
bul_sc03_3177	ISOGAL-PJ175335.7-300255		
bul_sc03_3205	ISOGAL-PJ175355.6-300231		
bul_sc03_3346	ISOGAL-PJ175306.1-300103		
bul_sc03_3351	ISOGAL-PJ175310.0-300037		
bul_sc03_3552			
bul_sc03_3686	ISOGAL-PJ175336.6-295916		
bul_sc03_3710			
bul_sc03_3712			
bul_sc03_3714			
bul_sc03_3870			
bul_sc03_3941	ISOGAL-PJ175332.6-295712		
bul_sc03_3951			
bul_sc03_4046	ISOGAL-PJ175327.1-295643		
bul_sc03_4235			
bul_sc03_4419			
bul_sc03_4426	IRAS_17502-2953		
bul_sc03_4494			
bul_sc03_4522			
bul_sc03_4551			
bul_sc03_4588			
bul_sc03_4629			
bul_sc03_4644			
bul_sc03_4774			
bul_sc03_4784			
bul_sc03_4865			
bul_sc03_5306			
bul_sc03_5364			
bul_sc03_5383			
bul_sc03_5408			
bul_sc03_5414			
bul_sc03_5426			
bul_sc03_5703			
bul_sc03_5877			

Table 2. continued.

OGLE-name	Other name	Chemical type	Remarks
bul_sc03_5929			
bul_sc03_6083			
bul_sc03_6107			
bul_sc03_6205			
bul_sc03_6207			
bul_sc03_6208			
bul_sc03_6508			
bul_sc03_6587			
bul_sc03_6668			
bul_sc03_6711			
bul_sc03_6756			
bul_sc03_6997			
bul_sc03_7010			
bul_sc03_7068			
bul_sc03_7129			
bul_sc03_7147			
bul_sc03_7270			
bul_sc03_7348			
bul_sc03_7487			
bul_sc03_7491			
bul_sc03_7505			
bul_sc03_7572			
bul_sc03_7614			
bul_sc03_7694			
bul_sc03_7733			
bul_sc03_7775			
bul_sc03_8032			
bul_sc03_8070			
bul_sc03_8185			
bul_sc03_8195	IRAS_17507-2931		
bul_sc03_8201	[DB2000] 16		Dutra & Bica (2000)
bul_sc03_8207			
bul_sc03_8374			
bul_sc03_8429			
bul_sc04_0040			
bul_sc04_0047			
bul_sc04_0197			
bul_sc04_0352			
bul_sc04_0375	ISOGAL-PJ175405.7-300902		
bul_sc04_0408			
bul_sc04_0429			
bul_sc04_0456			
bul_sc04_0478			
bul_sc04_0585			
bul_sc04_0678			
bul_sc04_1100			
bul_sc04_1490			
bul_sc04_1491			
bul_sc04_1616			
bul_sc04_1688			
bul_sc04_1709			
bul_sc04_1817			
bul_sc04_1841			
bul_sc04_1842			
bul_sc04_1895			
bul_sc04_1972			
bul_sc04_1992			
bul_sc04_2209			
bul_sc04_2303			

Table 2. continued.

OGLE-name	Other name	Chemical type	Remarks
bul_sc04_2833	OOS03-PJ175432.0-295326, ISOGAL-PJ175432.0-295326		
bul_sc04_2839	OOS03-PJ175435.0-295341, ISOGAL-PJ175435.0-295341		
bul_sc04_2865			
bul_sc04_2874	OOS03-PJ175439.8-295341, ISOGAL-PJ175439.8-295341		
bul_sc04_2999	OOS03-PJ175427.9-295233, ISOGAL-PJ175427.9-295233		
bul_sc04_3039	OOS03-PJ175443.4-295247, ISOGAL-PJ175443.4-295247		
bul_sc04_3043	OOS03-PJ175446.1-295315, ISOGAL-PJ175446.1-295315		
bul_sc04_3286			
bul_sc04_3919			
bul_sc04_3921			
bul_sc04_3922			
bul_sc04_3965			
bul_sc04_4078	OOS03-PJ175505.4-294715, ISOGAL-PJ175505.4-294715		
bul_sc04_4120			
bul_sc04_4147			
bul_sc04_4179	OOS03-PJ175442.9-294649, ISOGAL-PJ175442.9-294649		
bul_sc04_4215	OOS03-PJ175459.0-294701, ISOGAL-PJ175459.0-294701, IRAS_17517-2946		Messineo et al. (2002), Felli et al. (2002)
bul_sc04_4252			
bul_sc04_4277			
bul_sc04_4281			
bul_sc04_4434			
bul_sc04_4626			
bul_sc04_4628			
bul_sc04_4662	OOS03-PJ175450.8-294406, ISOGAL-PJ175450.8-294406		
bul_sc04_4722			
bul_sc04_4750			
bul_sc04_4926			
bul_sc04_5344	OOS03-PJ175506.7-294013, ISOGAL-PJ175506.7-294013		
bul_sc04_5559			
bul_sc04_5579			
bul_sc04_5649	OOS03-PJ175500.7-293908, ISOGAL-PJ175500.7-293908		
bul_sc04_5704			
bul_sc04_5917			
bul_sc04_5951			
bul_sc04_6066			
bul_sc04_6265			
bul_sc04_6371			
bul_sc04_6468			
bul_sc04_6592			
bul_sc04_6896			
bul_sc04_6912			
bul_sc04_6944			
bul_sc04_6993			
bul_sc04_7164			
bul_sc04_7206			
bul_sc04_7290			

Table 2. continued.

OGLE-name	Other name	Chemical type	Remarks
bul_sc04_7534			
bul_sc04_7541			
bul_sc04_7691			
bul_sc04_8070			
bul_sc04_8241			
bul_sc04_8585			
bul_sc04_8592			
bul_sc04_8667			
bul_sc04_8749			
bul_sc04_8786			
bul_sc04_8831			
bul_sc04_8886			
bul_sc04_8891			
bul_sc04_9008			
bul_sc04_9056			
bul_sc05_0084			
bul_sc05_0108			
bul_sc05_0118			
bul_sc05_0126			
bul_sc05_0260	V 2187		Terzan & Ounnas (1988; TO88)
bul_sc05_0277			
bul_sc05_0347			
bul_sc05_0363			
bul_sc05_0364			
bul_sc05_0367			
bul_sc05_0373			
bul_sc05_0479			
bul_sc05_0513			
bul_sc05_0519			
bul_sc05_0638			
bul_sc05_0903			
bul_sc05_0918			
bul_sc05_0939			
bul_sc05_1006			
bul_sc05_1072			
bul_sc05_1133			
bul_sc05_1185			
bul_sc05_1304			
bul_sc05_1419			
bul_sc05_1533			
bul_sc05_1534			
bul_sc05_1584			
bul_sc05_1708	V 2155		TO88
bul_sc05_1795			
bul_sc05_1843			
bul_sc05_1845			
bul_sc05_1894	NGC 6451 PMR 775		Paunzen et al (2003)
bul_sc05_1907			
bul_sc05_2051			
bul_sc05_2107			
bul_sc05_2132			
bul_sc05_2136			
bul_sc05_2152			
bul_sc05_2241	V 2186		TO88
bul_sc05_2367			
bul_sc05_2524	V 2162		TO88
bul_sc05_2556			
bul_sc05_2659			
bul_sc05_2677			

Table 2. continued.

OGLE-name	Other name	Chemical type	Remarks
bul_sc05_2790			
bul_sc05_3021			
bul_sc05_3027			
bul_sc05_3050			
bul_sc05_3125			
bul_sc05_3330			
bul_sc05_3346			
bul_sc05_3414			
bul_sc05_3416			
bul_sc05_3431			
bul_sc05_3451			
bul_sc05_3601			
bul_sc05_3893			
bul_sc05_3894			
bul_sc05_3902			
bul_sc05_3949			
bul_sc05_4084			
bul_sc05_4093			
bul_sc05_4104			
bul_sc05_4161			
bul_sc05_4196			
bul_sc05_4269			
bul_sc05_4342			
bul_sc05_4354			
bul_sc05_4447			
bul_sc05_4498			
bul_sc05_4511			
bul_sc05_4531			
bul_sc05_4543			
bul_sc05_4598			
bul_sc05_4660			
bul_sc05_4765			
bul_sc05_4880			
bul_sc05_4911			
bul_sc05_4916			
bul_sc05_4968			
bul_sc05_5001			
bul_sc05_5003			
bul_sc05_5082			
bul_sc05_5088			
bul_sc05_5118			
bul_sc05_5226			
bul_sc05_5246			
bul_sc05_5247			
bul_sc05_5366			
bul_sc05_5391			
bul_sc05_5464			
bul_sc05_5473			
bul_sc05_5635			
bul_sc05_5748			
bul_sc05_5823			
bul_sc05_6058			
bul_sc05_6075			
bul_sc05_6188			
bul_sc05_6232			
bul_sc05_6393			
bul_sc05_6467			
bul_sc05_6478			
bul_sc05_6479			

Table 2. continued.

OGLE-name	Other name	Chemical type	Remarks
bul_sc05_6569			
bul_sc05_6596			
bul_sc05_6605			
bul_sc05_6617			
bul_sc05_6622			
bul_sc05_6729			
bul_sc05_6788			
bul_sc05_6805			
bul_sc05_6919			
bul_sc05_6922			
bul_sc05_7023			
bul_sc05_7079			
bul_sc05_7150			
bul_sc05_7226			
bul_sc05_7232			
bul_sc06_0003			
bul_sc06_0007			
bul_sc06_0221			
bul_sc06_0246			
bul_sc06_0265			
bul_sc06_0288			
bul_sc06_0289			
bul_sc06_0430			
bul_sc06_0432			
bul_sc06_0434			
bul_sc06_0435			
bul_sc06_0558			
bul_sc06_0825			
bul_sc06_0828			
bul_sc06_0839			
bul_sc06_0895			
bul_sc06_1026			
bul_sc06_1074			
bul_sc06_1799			
bul_sc06_1806			
bul_sc06_1807			
bul_sc06_1809			
bul_sc06_1812			
bul_sc06_1813			
bul_sc06_1816			
bul_sc06_1967			
bul_sc06_1971			
bul_sc06_1973			
bul_sc06_1974			
bul_sc06_2084			
bul_sc06_2230			
bul_sc06_2240			
bul_sc06_2505			
bul_sc06_2516			
bul_sc06_2525			
bul_sc06_2552			
bul_sc06_2818			
bul_sc06_2834			
bul_sc06_2927			
bul_sc06_2997			
bul_sc06_3091			
bul_sc06_3092			
bul_sc06_3093			
bul_sc06_3098			

Table 2. continued.

OGLE-name	Other name	Chemical type	Remarks
bul_sc06_3099			
bul_sc06_3103			
bul_sc06_3195			
bul_sc07_0078			
bul_sc07_0081			
bul_sc07_0082			
bul_sc07_0083			
bul_sc07_0085			
bul_sc07_0175			
bul_sc07_0193			
bul_sc07_0202			
bul_sc07_0203			
bul_sc07_0413			
bul_sc07_0425	IRAS_18059-3218		
bul_sc07_0749			
bul_sc07_0750			
bul_sc07_1162			
bul_sc07_1267			
bul_sc07_1282			
bul_sc07_1464	[DHM99] BE582		DMH99
bul_sc07_1469			
bul_sc07_1487			
bul_sc07_1491			
bul_sc07_1607	IRAS_18061-3140		Kwok et al. (1997), te Lintel Hekkert et al. (1991), Sivagnanam et al. (1990)
bul_sc08_0190			
bul_sc08_0616			
bul_sc08_1081			
bul_sc08_1622			
bul_sc08_1687			
bul_sc08_1693			
bul_sc08_2299			
bul_sc08_2311			
bul_sc09_0078			
bul_sc09_0210			
bul_sc09_0286			
bul_sc09_0320			
bul_sc09_0321			
bul_sc09_0322			
bul_sc09_0414			
bul_sc09_0536			
bul_sc09_0539			
bul_sc09_0660			
bul_sc09_0689			
bul_sc09_1074			
bul_sc09_1113			
bul_sc09_1115			
bul_sc09_1177			
bul_sc09_1180			
bul_sc09_1233			
bul_sc09_1610			
bul_sc09_1767			
bul_sc09_1769			
bul_sc09_1771			
bul_sc10_0079			
bul_sc10_0256			
bul_sc10_0268			
bul_sc10_0318			
bul_sc10_0406			

Table 2. continued.

OGLE-name	Other name	Chemical type	Remarks
bul_sc10_0792			
bul_sc10_0937			
bul_sc10_1238			
bul_sc10_1411			
bul_sc10_1456			
bul_sc10_1690			
bul_sc10_1979			
bul_sc10_2017			
bul_sc10_2048			
bul_sc10_2052			
bul_sc10_2383			
bul_sc11_0274			
bul_sc11_0416			
bul_sc11_0709			
bul_sc11_0795	IRAS_18177-2233		
bul_sc11_0850			
bul_sc11_0857			
bul_sc11_1132	IRAS_18180-2225		
bul_sc11_1432			
bul_sc11_1448			
bul_sc11_1528			
bul_sc11_1531			
bul_sc11_1532			
bul_sc11_1540			
bul_sc11_1743			
bul_sc11_1916			
bul_sc11_1930			
bul_sc11_2001			
bul_sc11_2049			
bul_sc12_0116			
bul_sc12_0124			
bul_sc12_0353			
bul_sc12_0412			
bul_sc12_0508			
bul_sc12_0509			
bul_sc12_0573			
bul_sc12_0700			
bul_sc12_0804	IRAS_18131-2413		
bul_sc12_0809			
bul_sc12_0827			
bul_sc12_0995			
bul_sc12_0999			
bul_sc12_1066			
bul_sc12_1428			
bul_sc12_2084			
bul_sc12_2115			
bul_sc12_2149			
bul_sc12_2267			
bul_sc12_2346			
bul_sc12_2375			
bul_sc12_2395			
bul_sc12_2403			
bul_sc12_2435			
bul_sc12_2454			
bul_sc12_2487			
bul_sc12_2502			
bul_sc12_2599	IRAS_18125-2345		
bul_sc12_2905			
bul_sc12_3025	IRAS_18131-2338		

Table 2. continued.

OGLE-name	Other name	Chemical type	Remarks
bul_sc12_3370			
bul_sc12_3386			
bul_sc12_3387			
bul_sc13_0045			
bul_sc13_0151			
bul_sc13_0324			
bul_sc13_0605			
bul_sc13_0689			
bul_sc13_0909			
bul_sc13_1016			
bul_sc13_1142			
bul_sc13_1286			
bul_sc13_1542			
bul_sc13_1563			
bul_sc13_1581			
bul_sc13_1867			
bul_sc13_1986			
bul_sc13_2194			
bul_sc13_2245			
bul_sc13_2413			
bul_sc13_2662			
bul_sc13_2868			
bul_sc13_2987			
bul_sc13_3002			
bul_sc14_0057			
bul_sc14_0061			
bul_sc14_0104			
bul_sc14_0106			
bul_sc14_0189			
bul_sc14_0212			
bul_sc14_0359			
bul_sc14_0378			
bul_sc14_0582			
bul_sc14_0636			
bul_sc14_0650			
bul_sc14_0894			
bul_sc14_0900			
bul_sc14_0969			
bul_sc14_1172			
bul_sc14_1275			
bul_sc14_1349			
bul_sc14_1361			
bul_sc14_1616			
bul_sc14_1671			
bul_sc14_1673			
bul_sc14_1685			
bul_sc14_1810			
bul_sc14_1854			
bul_sc14_2081			
bul_sc14_2456			
bul_sc14_2459			
bul_sc14_2466			
bul_sc14_2527			
bul_sc14_2579			
bul_sc14_2664			
bul_sc14_2733			
bul_sc14_2913			
bul_sc14_2914			
bul_sc14_2921			

Table 2. continued.

OGLE-name	Other name	Chemical type	Remarks
bul_sc14_2930			
bul_sc14_3181			
bul_sc14_3189			
bul_sc14_3214			
bul_sc14_3362			
bul_sc14_3365			
bul_sc14_3386			
bul_sc14_3503			
bul_sc14_3580			
bul_sc14_3669			
bul_sc14_3738			
bul_sc14_3848			
bul_sc14_3849			
bul_sc14_3853			
bul_sc14_3876			
bul_sc14_3890			
bul_sc15_0397			
bul_sc15_0433			
bul_sc15_0571			
bul_sc15_0587			
bul_sc15_0704			
bul_sc15_0857			
bul_sc15_0877			
bul_sc15_0902			
bul_sc15_0915			
bul_sc15_0917			
bul_sc15_1099			
bul_sc15_1120			
bul_sc15_1136			
bul_sc15_1137			
bul_sc15_1141			
bul_sc15_1194			
bul_sc15_1222			
bul_sc15_1223			
bul_sc15_1357			
bul_sc15_1379			
bul_sc15_1391			
bul_sc15_1392			
bul_sc15_1394			
bul_sc15_1601			
bul_sc15_1638			
bul_sc15_1656			
bul_sc15_1698			
bul_sc15_1702			
bul_sc15_1710			
bul_sc15_1788			
bul_sc15_1793			
bul_sc15_1794			
bul_sc15_1796			
bul_sc15_1797			
bul_sc15_1798			
bul_sc15_1801			
bul_sc15_1802			
bul_sc15_1804			
bul_sc15_1896			
bul_sc15_1897			
bul_sc15_1914			
bul_sc15_1965			
bul_sc15_2106			

Table 2. continued.

OGLE-name	Other name	Chemical type	Remarks
bul_sc15_2111			
bul_sc15_2135			
bul_sc15_2170			
bul_sc15_2182			
bul_sc15_2304			
bul_sc15_2314			
bul_sc15_2360			
bul_sc15_2511			
bul_sc15_2722			
bul_sc15_2794			
bul_sc15_2869			
bul_sc15_3075			
bul_sc15_3171			
bul_sc15_3189			
bul_sc15_3190			
bul_sc15_3244			
bul_sc15_3254			
bul_sc15_3360			
bul_sc15_3401			
bul_sc15_3445			
bul_sc15_3452			
bul_sc15_3530			
bul_sc15_3539			
bul_sc15_3540			
bul_sc15_3599			
bul_sc15_3611			
bul_sc15_3760			
bul_sc15_3771			
bul_sc16_0211			
bul_sc16_0280			
bul_sc16_0645			
bul_sc16_0653			
bul_sc16_0663			
bul_sc16_0804			
bul_sc16_0926			
bul_sc16_0968			
bul_sc16_1060			
bul_sc16_1428			
bul_sc16_1777			
bul_sc16_1822			
bul_sc16_2046			
bul_sc16_2164			
bul_sc16_2494			
bul_sc16_2496			
bul_sc16_2841			
bul_sc16_3224			
bul_sc16_3270			
bul_sc16_3572			
bul_sc16_3608			
bul_sc16_3667			
bul_sc16_3693			
bul_sc16_3699			
bul_sc16_3700			
bul_sc16_3701			
bul_sc16_3819			
bul_sc16_3857	IRAS_18065-2601		
bul_sc16_3861			
bul_sc16_4025			
bul_sc16_4082			

Table 2. continued.

OGLE-name	Other name	Chemical type	Remarks
bul_sc16_4100			
bul_sc16_4223			
bul_sc16_4224			
bul_sc16_4238			
bul_sc16_4495			
bul_sc16_4552			
bul_sc16_4567			
bul_sc16_4577			
bul_sc16_4709			
bul_sc16_4710			
bul_sc16_4712			
bul_sc16_4713			
bul_sc16_4714			
bul_sc16_4716			
bul_sc17_0146			
bul_sc17_0275			
bul_sc17_0283			
bul_sc17_0284			
bul_sc17_0336			
bul_sc17_0389			
bul_sc17_0392			
bul_sc17_0403			
bul_sc17_0638			
bul_sc17_0639			
bul_sc17_0655			
bul_sc17_0657			
bul_sc17_0658			
bul_sc17_0661			
bul_sc17_0665			
bul_sc17_0667			
bul_sc17_0668			
bul_sc17_0670			
bul_sc17_0671			
bul_sc17_0675			
bul_sc17_0676			
bul_sc17_0677			
bul_sc17_0708			
bul_sc17_0709			
bul_sc17_0710			
bul_sc17_0713			
bul_sc17_0719			
bul_sc17_0725			
bul_sc17_0726			
bul_sc17_0728			
bul_sc17_0732			
bul_sc17_0751			
bul_sc17_0983			
bul_sc17_0987			
bul_sc17_1021			
bul_sc17_1049			
bul_sc17_1052			
bul_sc17_1054			
bul_sc17_1055			
bul_sc17_1056			
bul_sc17_1065			
bul_sc17_1067			
bul_sc17_1070			
bul_sc17_1094			
bul_sc17_1095			

Table 2. continued.

OGLE-name	Other name	Chemical type	Remarks
bul_sc17_1101			
bul_sc17_1157			
bul_sc17_1353			
bul_sc17_1366			
bul_sc17_1368			
bul_sc17_1369			
bul_sc17_1372			
bul_sc17_1378			
bul_sc17_1504	IRAS_18079-2623		
bul_sc17_1583			
bul_sc17_1595			
bul_sc17_1601			
bul_sc17_1602			
bul_sc17_1607			
bul_sc17_1608			
bul_sc17_1612			
bul_sc17_1613			
bul_sc17_1614			
bul_sc17_1616			
bul_sc17_1633			
bul_sc17_1644			
bul_sc17_1659			
bul_sc17_1699			
bul_sc17_1783			
bul_sc17_1795			
bul_sc17_1797			
bul_sc17_1803			
bul_sc17_1953			
bul_sc17_1964			
bul_sc17_2116			
bul_sc17_2129			
bul_sc17_2292			
bul_sc17_2296			
bul_sc17_2297			
bul_sc17_2298			
bul_sc17_2301			
bul_sc17_2302			
bul_sc17_2303			
bul_sc17_2304			
bul_sc17_2305			
bul_sc17_2306			
bul_sc17_2308			
bul_sc17_2309			
bul_sc17_2311			
bul_sc17_2312			
bul_sc17_2314			
bul_sc17_2316			
bul_sc17_2317			
bul_sc17_2318			
bul_sc17_2319			
bul_sc17_2320			
bul_sc17_2321			
bul_sc17_2322			
bul_sc17_2323			
bul_sc17_2324			
bul_sc17_2493			
bul_sc17_2552			
bul_sc17_2565			
bul_sc17_2566			

Table 2. continued.

OGLE-name	Other name	Chemical type	Remarks
bul_sc17_2568			
bul_sc17_2578			
bul_sc17_2579			
bul_sc17_2580			
bul_sc17_2704			
bul_sc17_2867			
bul_sc17_2949			
bul_sc17_2953			
bul_sc17_2957			
bul_sc17_2958			
bul_sc17_2960			
bul_sc17_2961			
bul_sc17_2964			
bul_sc17_2966			
bul_sc17_2967			
bul_sc17_2969			
bul_sc17_3009			
bul_sc17_3019			
bul_sc17_3191			
bul_sc17_3199			
bul_sc17_3200			
bul_sc17_3210			
bul_sc17_3216			
bul_sc17_3218			
bul_sc17_3219			
bul_sc17_3253			
bul_sc17_3266			
bul_sc17_3269			
bul_sc17_3277	MM7-B_V98_EB		
bul_sc17_3280			
bul_sc17_3281			
bul_sc17_3350			
bul_sc17_3434			
bul_sc17_3437			
bul_sc17_3492	IRAS_18075-2558		
bul_sc17_4011			
bul_sc17_4016			
bul_sc17_4017			
bul_sc17_4019			
bul_sc17_4020			
bul_sc17_4021			
bul_sc17_4062			
bul_sc17_4063			
bul_sc17_4065			
bul_sc17_4067			
bul_sc17_4068			
bul_sc17_4092			
bul_sc17_4100			
bul_sc17_4116			
bul_sc17_4127			
bul_sc17_4131			
bul_sc17_4133			
bul_sc17_4163			
bul_sc17_4166			
bul_sc17_4168			
bul_sc17_4217			
bul_sc17_4221			
bul_sc17_4222			

Table 2. continued.

OGLE-name	Other name	Chemical type	Remarks
bul_sc17_4226			
bul_sc17_4271			
bul_sc17_4282			
bul_sc17_4358			
bul_sc17_4516			
bul_sc18_0202			
bul_sc18_0471			
bul_sc18_0472			
bul_sc18_0698			
bul_sc18_0779			
bul_sc18_0788			
bul_sc18_0835			
bul_sc18_0883			
bul_sc18_0884			
bul_sc18_0900			
bul_sc18_0903			
bul_sc18_0905			
bul_sc18_0910			
bul_sc18_0981			
bul_sc18_0995			
bul_sc18_1050			
bul_sc18_1065			
bul_sc18_1066			
bul_sc18_1140			
bul_sc18_1381			
bul_sc18_1485			
bul_sc18_1486			
bul_sc18_1588			
bul_sc18_1597			
bul_sc18_1600			
bul_sc18_1617			
bul_sc18_1821			
bul_sc18_1832			
bul_sc18_1925			
bul_sc18_2067			
bul_sc18_2240			
bul_sc18_2631			
bul_sc18_2652			
bul_sc18_2665			
bul_sc18_3398			
bul_sc18_3509			
bul_sc18_3592			
bul_sc18_3630			
bul_sc18_3654			
bul_sc18_3951			
bul_sc18_4066			
bul_sc18_4202			
bul_sc18_4640			
bul_sc18_4666			
bul_sc18_4688			
bul_sc18_4703			
bul_sc18_4794			
bul_sc18_4809			
bul_sc18_4914			
bul_sc18_4923			
bul_sc18_5001			
bul_sc18_5342			
bul_sc18_5361			
bul_sc18_5379	IRAS_18039-2649		

Table 2. continued.

OGLE-name	Other name	Chemical type	Remarks
bul_sc18_5569			
bul_sc19_0505			
bul_sc19_0506			
bul_sc19_0608			
bul_sc19_0655			
bul_sc19_0664			
bul_sc19_0734			
bul_sc19_0747			
bul_sc19_0760			
bul_sc19_0867			
bul_sc19_0890			
bul_sc19_0891			
bul_sc19_0892			
bul_sc19_0961	IRAS_18046-2730		
bul_sc19_1373			
bul_sc19_1394			
bul_sc19_1402			
bul_sc19_1436			
bul_sc19_1587			
bul_sc19_1614			
bul_sc19_1621			
bul_sc19_2131			
bul_sc19_2139			
bul_sc19_2302			
bul_sc19_2330			
bul_sc19_2332	V 4720 Sgr		
bul_sc19_2449			
bul_sc19_2462			
bul_sc19_2486			
bul_sc19_2948			
bul_sc19_2950			
bul_sc19_3196			
bul_sc19_3310			
bul_sc19_3334			
bul_sc19_3335			
bul_sc19_3487			
bul_sc19_3581			
bul_sc19_3641			
bul_sc19_3787			
bul_sc19_3797			
bul_sc19_3831	IRAS_18050-2659		Kwok et al. (1997), Izumiura et al. (1995), te Lintel Hekkert (1991)
bul_sc19_4048			
bul_sc19_4066			
bul_sc19_4132			
bul_sc19_4344			
bul_sc19_4423			
bul_sc19_4430			
bul_sc19_4649			
bul_sc19_4777			
bul_sc19_4831			
bul_sc19_4879			
bul_sc19_4898			
bul_sc20_0147			
bul_sc20_0150			
bul_sc20_0170			
bul_sc20_0190			
bul_sc20_0197			

Table 2. continued.

OGLE-name	Other name	Chemical type	Remarks
bul_sc20_0500			
bul_sc20_0537			
bul_sc20_0661			
bul_sc20_0674			
bul_sc20_0832	ABC01_113.18413.1776, OOS03-PJ175923.7-291236, ISOGAL-PJ175923.7-291236, TLE_Sgr_I_39, V 3978 Sgr		Glass et al. (1999), GWCF, LE76
bul_sc20_0975	ABC01_113.18284.59, ISOGAL-PJ175900.2-291111		
bul_sc20_1189	ABC01_113.18414.98, OOS03-PJ175908.3-290855, ISOGAL-PJ175908.3-290855		Glass et al. (1999)
bul_sc20_1292	ABC01_113.18414.290, OOS03-PJ175918.0-290806, ISOGAL-PJ175918.0-290806		
bul_sc20_1761	ABC01_113.18675.1135, OOS03-PJ175947.9-290349, ISOGAL-PJ175947.9-290349, TLE_Sgr_I_56, V 2467 Sgr		Glass et al. (1999), GWCF, GWCF, Catchpole (1982), LE76
bul_sc20_1826	OOS03-PJ175929.7-290319, ISOGAL-PJ175929.7-290319, TLE_Sgr_I_55, V 3979 Sgr		Glass et al. (1999), GWCF, LE76
bul_sc20_1837			
bul_sc20_1928	ABC01_113.18416.290, OOS03-PJ175923.3-290214, ISOGAL-PJ175923.3-290214, TLE_Sgr_I_54, V 2446 Sgr		Glass et al. (1999), GWCF, LE76
bul_sc20_2013	ABC01_113.18416.198, OOS03-PJ175910.4-290129, ISOGAL-PJ175910.4-290129, TLE_Sgr_I_53, V 3976 Sgr		Messineo et al. (2002), Glass et al. (1999), GWCF, Glass et al. (1986; G86), LE76
bul_sc20_2210			
bul_sc20_2269	ABC01_113.18287.2391, OOS03-PJ175901.2-285822, ISOGAL-PJ175901.2-285822, TLE_Sgr_I_79, V 3975 Sgr, IRAS_17558-2858		Glass et al. (1999), GWCF, G86, LE76
bul_sc20_2291	ABC01_113.18417.1965, OOS03-PJ175913.7-285852, ISOGAL-PJ175913.7-285852, TLE_Sgr_I_87, V 3977 Sgr		Glass et al. (1999), GWCF, LE76
bul_sc20_2309			
bul_sc20_2312			
bul_sc20_2335			
bul_sc20_2448			
bul_sc20_2958			
bul_sc20_3055			
bul_sc20_3098			
bul_sc20_3146			
bul_sc20_3170			
bul_sc20_3256			
bul_sc20_3406			
bul_sc20_3519			
bul_sc20_3530			
bul_sc20_3568			
bul_sc20_3715			
bul_sc20_3815			
bul_sc20_3818			

Table 2. continued.

OGLE-name	Other name	Chemical type	Remarks
bul_sc20_3886			
bul_sc20_3891			
bul_sc20_4367			
bul_sc20_4404			
bul_sc20_4413			
bul_sc20_4621			
bul_sc20_4675			
bul_sc20_4763			
bul_sc20_4768			
bul_sc20_4790			
bul_sc20_4874			
bul_sc20_4939			
bul_sc20_4954			
bul_sc20_5108			
bul_sc20_5141			
bul_sc20_5147			
bul_sc20_5152			
bul_sc20_5158			
bul_sc20_5159			
bul_sc20_5171			
bul_sc20_5315			
bul_sc20_5369			
bul_sc20_5657			
bul_sc20_5736			
bul_sc20_5781			
bul_sc20_5840			
bul_sc21_0035			
bul_sc21_0055			
bul_sc21_0209			
bul_sc21_0531			
bul_sc21_0635			
bul_sc21_0740			
bul_sc21_1228			
bul_sc21_1235			
bul_sc21_1258			
bul_sc21_1415			
bul_sc21_1433			
bul_sc21_1459			
bul_sc21_1463			
bul_sc21_1615			
bul_sc21_1745			
bul_sc21_1954			
bul_sc21_1982			
bul_sc21_2008			
bul_sc21_2679			
bul_sc21_2895			
bul_sc21_2919			
bul_sc21_3198			
bul_sc21_3216			
bul_sc21_3239			
bul_sc21_3519			
bul_sc21_3541			
bul_sc21_3611			
bul_sc21_3629			
bul_sc21_3954			
bul_sc21_4176			
bul_sc21_4627			
bul_sc21_4690			
bul_sc21_4849			

Table 2. continued.

OGLE-name	Other name	Chemical type	Remarks
bul_sc21_4940			
bul_sc21_5109			
bul_sc21_5112			
bul_sc21_5129			
bul_sc21_5301			
bul_sc21_5358			
bul_sc21_5569			
bul_sc21_5635			
bul_sc21_5654			
bul_sc21_5727			
bul_sc21_6155			
bul_sc21_6187			
bul_sc21_6221			
bul_sc21_6291			
bul_sc21_6346			
bul_sc21_6427			
bul_sc21_6462			
bul_sc21_6542			
bul_sc21_6564			
bul_sc21_6647			
bul_sc21_6683			
bul_sc21_6792			
bul_sc21_7104			
bul_sc21_7140			
bul_sc21_7167			
bul_sc21_7392			
bul_sc21_7403			
bul_sc22_0158			
bul_sc22_0372	IRAS_17531-3110		
bul_sc22_0384			
bul_sc22_0434			
bul_sc22_0689			
bul_sc22_0693			
bul_sc22_0698			
bul_sc22_0711			
bul_sc22_0771			
bul_sc22_0986			
bul_sc22_1083			
bul_sc22_1086			
bul_sc22_1150			
bul_sc22_1230			
bul_sc22_1319			
bul_sc22_1382			
bul_sc22_1395			
bul_sc22_1579			
bul_sc22_1599			
bul_sc22_1726			
bul_sc22_1841			
bul_sc22_1984			
bul_sc22_1997			
bul_sc22_2093			
bul_sc22_2269			
bul_sc22_2331	IRAS_17540-3053		
bul_sc22_2351			
bul_sc22_2354			
bul_sc22_2395			
bul_sc22_2403			
bul_sc22_2407			
bul_sc22_2471			

Table 2. continued.

OGLE-name	Other name	Chemical type	Remarks
bul_sc22_2678			
bul_sc22_2790			
bul_sc22_2989			
bul_sc22_3006			
bul_sc22_3025			
bul_sc22_3036			
bul_sc22_3143			
bul_sc22_3184			
bul_sc22_3293			
bul_sc22_3304			
bul_sc22_3440			
bul_sc22_3512			
bul_sc22_3535			
bul_sc22_3810			
bul_sc22_4005			
bul_sc22_4177			
bul_sc22_4224			
bul_sc22_4288			
bul_sc22_4296			
bul_sc22_4414			
bul_sc22_4618			
bul_sc22_4619			
bul_sc22_4621			
bul_sc22_4717			
bul_sc22_4731			
bul_sc22_4744			
bul_sc22_4765			
bul_sc22_4866			
bul_sc22_4905			
bul_sc22_4908			
bul_sc22_4993			
bul_sc22_5238			
bul_sc22_5239			
bul_sc22_5309			
bul_sc22_5512			
bul_sc22_5515			
bul_sc22_5562			
bul_sc22_5571			
bul_sc23_0073			
bul_sc23_0133			
bul_sc23_0134			
bul_sc23_0189			
bul_sc23_0200			
bul_sc23_0414			
bul_sc23_0432			
bul_sc23_0661	IRAS_17545-3132		
bul_sc23_0723			
bul_sc23_0933			
bul_sc23_0963			
bul_sc23_0965			
bul_sc23_1037			
bul_sc23_1095			
bul_sc23_1114			
bul_sc23_1148			
bul_sc23_1188			
bul_sc23_1362			
bul_sc23_1372			
bul_sc23_1376			
bul_sc23_1612			

Table 2. continued.

OGLE-name	Other name	Chemical type	Remarks
bul_sc23_1821			
bul_sc23_1875			
bul_sc23_1944			
bul_sc23_2209			
bul_sc23_2324			
bul_sc23_2351			
bul_sc23_2512			
bul_sc23_2513			
bul_sc23_2542			
bul_sc23_2545			
bul_sc23_2549			
bul_sc23_2641			
bul_sc23_2808			
bul_sc23_2837			
bul_sc23_2927			
bul_sc23_2952			
bul_sc23_3001			
bul_sc23_3145			
bul_sc23_3367			
bul_sc23_3368			
bul_sc23_3449			
bul_sc23_3467			
bul_sc23_3518			
bul_sc23_3598			
bul_sc23_3616			
bul_sc23_3628			
bul_sc23_3641			
bul_sc23_3678			
bul_sc23_3695			
bul_sc23_3711			
bul_sc23_3824			
bul_sc23_3870			
bul_sc23_3873			
bul_sc23_3916			
bul_sc23_4423			
bul_sc23_4585			
bul_sc23_4647			
bul_sc23_4766			
bul_sc23_4772			
bul_sc24_0090			
bul_sc24_0226			
bul_sc24_0296	IRAS_17503-3315		
bul_sc24_0311			
bul_sc24_0323			
bul_sc24_0324			
bul_sc24_0352			
bul_sc24_0394			
bul_sc24_0399			
bul_sc24_0412			
bul_sc24_0565			
bul_sc24_0668			
bul_sc24_0773			
bul_sc24_0835			
bul_sc24_0849			
bul_sc24_0850			
bul_sc24_0949			
bul_sc24_0989			
bul_sc24_1001			
bul_sc24_1012			

Table 2. continued.

OGLE-name	Other name	Chemical type	Remarks
bul_sc24_1065			
bul_sc24_1202			
bul_sc24_1203			
bul_sc24_1224			
bul_sc24_1230			
bul_sc24_1299			
bul_sc24_1580			
bul_sc24_1684			
bul_sc24_1765			
bul_sc24_1855			
bul_sc24_1915			
bul_sc24_2087			
bul_sc24_2106	IRAS_17500-3250		
bul_sc24_2129			
bul_sc24_2347			
bul_sc24_2421			
bul_sc24_2526			
bul_sc24_2595			
bul_sc24_2610			
bul_sc24_2744			
bul_sc24_2822			
bul_sc24_3033			
bul_sc24_3323			
bul_sc24_3399			
bul_sc24_3455			
bul_sc24_3456			
bul_sc24_3537			
bul_sc24_3547			
bul_sc24_3649			
bul_sc24_3665			
bul_sc24_3768			
bul_sc24_3820			
bul_sc24_4012			
bul_sc24_4119			
bul_sc24_4126			
bul_sc24_4273			
bul_sc25_0010	IRAS_17511-3320		
bul_sc25_0089			
bul_sc25_0093			
bul_sc25_0112			
bul_sc25_0125			
bul_sc25_0218			
bul_sc25_0341			
bul_sc25_0404			
bul_sc25_0409			
bul_sc25_0412			
bul_sc25_0413			
bul_sc25_0421			
bul_sc25_0459			
bul_sc25_0492			
bul_sc25_0527			
bul_sc25_0550			
bul_sc25_0559			
bul_sc25_0561			
bul_sc25_0612			
bul_sc25_0695			
bul_sc25_0733			
bul_sc25_0734			
bul_sc25_0971			

Table 2. continued.

OGLE-name	Other name	Chemical type	Remarks
bul_sc25_1030			
bul_sc25_1238			
bul_sc25_1241			
bul_sc25_1276			
bul_sc25_1502			
bul_sc25_1505			
bul_sc25_1507			
bul_sc25_1557			
bul_sc25_1686			
bul_sc25_1771			
bul_sc25_1839			
bul_sc25_1851			
bul_sc25_1852			
bul_sc25_1909			
bul_sc25_1916			
bul_sc25_1917			
bul_sc25_1962			
bul_sc25_1969			
bul_sc25_1974			
bul_sc25_2019			
bul_sc25_2051			
bul_sc25_2053			
bul_sc25_2059			
bul_sc25_2162			
bul_sc25_2219			
bul_sc25_2472			
bul_sc25_2490			
bul_sc25_2499			
bul_sc25_2508			
bul_sc25_2555			
bul_sc25_2658			
bul_sc25_2659			
bul_sc25_2661			
bul_sc25_2667			
bul_sc25_2679			
bul_sc25_2840			
bul_sc25_3033			
bul_sc25_3046			
bul_sc26_0148			
bul_sc26_0331			
bul_sc26_0332			
bul_sc26_0355			
bul_sc26_0389			
bul_sc26_0390			
bul_sc26_0532			
bul_sc26_0544			
bul_sc26_0565			
bul_sc26_0589			
bul_sc26_0889			
bul_sc26_1225			
bul_sc26_1523			
bul_sc26_1540			
bul_sc26_1856			
bul_sc26_1904			
bul_sc26_1938			
bul_sc26_2023			
bul_sc26_2102			
bul_sc26_2196			
bul_sc26_2198			

Table 2. continued.

OGLE-name	Other name	Chemical type	Remarks
bul_sc26_2264			
bul_sc26_2439			
bul_sc26_2440			
bul_sc26_2441			
bul_sc26_2442			
bul_sc26_2849	V 2063		TO88
bul_sc26_2859			
bul_sc26_2864			
bul_sc26_3038	V 2071		TO88
bul_sc26_3350			
bul_sc26_3354			
bul_sc26_3355			
bul_sc26_3357			
bul_sc26_4174	V 2084		TO88
bul_sc26_4389			
bul_sc26_4435			
bul_sc26_4582			
bul_sc26_4672			
bul_sc27_0038			
bul_sc27_0532			
bul_sc27_0784			
bul_sc27_0893			
bul_sc27_0977	IRAS_17445-3520		
bul_sc27_1070			
bul_sc27_1108			
bul_sc27_1318			
bul_sc27_1335			
bul_sc27_1337			
bul_sc27_1357			
bul_sc27_1703			
bul_sc27_1755			
bul_sc27_1760			
bul_sc27_1950			
bul_sc27_1969			
bul_sc27_1983	IRAS_17446-3506		
bul_sc27_1998			
bul_sc27_2013			
bul_sc27_2080			
bul_sc27_2093			
bul_sc27_2133			
bul_sc27_2150			
bul_sc27_2151			
bul_sc27_2152			
bul_sc27_2404			
bul_sc27_2416			
bul_sc27_2417			
bul_sc27_2418			
bul_sc27_2560	V 2099		TO88
bul_sc27_2693			
bul_sc27_2746			
bul_sc27_2787			
bul_sc27_2857			
bul_sc27_2871			
bul_sc27_3080			
bul_sc27_3094			
bul_sc27_3227			
bul_sc27_3228			
bul_sc27_3245			
bul_sc27_3331			

Table 2. continued.

OGLE-name	Other name	Chemical type	Remarks
bul_sc27_3547			
bul_sc27_3556			
bul_sc27_3567			
bul_sc27_3677			
bul_sc27_3682			
bul_sc28_0235			
bul_sc28_0297			
bul_sc28_0298			
bul_sc28_0328			
bul_sc28_0572			
bul_sc28_0727			
bul_sc28_0738			
bul_sc28_0770			
bul_sc28_0950			
bul_sc28_0991	IRAS_17431-3654		Kwok et al. (1997), te Lintel Hekkert (1991)
bul_sc28_1058			
bul_sc28_1073			
bul_sc28_1201			
bul_sc28_1206			
bul_sc28_1289			
bul_sc28_1449			
bul_sc29_0482	IRAS_17452-3721		
bul_sc29_0489			
bul_sc29_0511			
bul_sc29_0534			
bul_sc29_0536			
bul_sc29_0541			
bul_sc29_0546			
bul_sc29_0817			
bul_sc29_1064			
bul_sc29_1241			
bul_sc29_1268			
bul_sc29_1375			
bul_sc29_1487			
bul_sc29_1490			
bul_sc29_1541			
bul_sc29_1542			
bul_sc29_1561			
bul_sc29_2085			
bul_sc29_2088			
bul_sc29_2098			
bul_sc29_2103			
bul_sc29_2117			
bul_sc29_2147			
bul_sc29_2152			
bul_sc29_2159			
bul_sc29_2161			
bul_sc29_2166			
bul_sc29_2179			
bul_sc29_2184			
bul_sc29_2189			
bul_sc29_2254			
bul_sc29_2256			
bul_sc29_2262			
bul_sc29_2266			
bul_sc29_2317			
bul_sc29_2319			
bul_sc30_0213			

Table 2. continued.

OGLE-name	Other name	Chemical type	Remarks
bul_sc30_0346			
bul_sc30_0630			
bul_sc30_0707			
bul_sc30_0827			
bul_sc30_0868			
bul_sc30_1085			
bul_sc30_1110			
bul_sc30_1156			
bul_sc30_1174			
bul_sc30_1305			
bul_sc30_1341			
bul_sc30_1486			
bul_sc30_1627			
bul_sc30_1821			
bul_sc30_1977			
bul_sc30_2143			
bul_sc30_2377			
bul_sc30_2635			
bul_sc30_2788			
bul_sc30_2943			
bul_sc30_3018			
bul_sc30_3086			
bul_sc30_3209			
bul_sc30_3276	IRAS_17586-2850		
bul_sc30_3484			
bul_sc30_3510			
bul_sc30_3525			
bul_sc30_3585			
bul_sc30_3654			
bul_sc30_3831			
bul_sc30_4185			
bul_sc30_4213			
bul_sc30_4446			
bul_sc30_4589			
bul_sc30_5019			
bul_sc30_5022			
bul_sc30_5063			
bul_sc30_5077			
bul_sc30_5325			
bul_sc30_5413			
bul_sc30_5442			
bul_sc30_5838			
bul_sc30_6043			
bul_sc30_6096			
bul_sc30_6263			
bul_sc30_6264			
bul_sc30_6402			
bul_sc30_6547			
bul_sc30_6861			
bul_sc31_0109			
bul_sc31_0150			
bul_sc31_0155			
bul_sc31_0246			
bul_sc31_0278			
bul_sc31_0329			
bul_sc31_0463			
bul_sc31_0465			
bul_sc31_0476	IRAS_17590-2858		
bul_sc31_0508			

Table 2. continued.

OGLE-name	Other name	Chemical type	Remarks
bul_sc31_0564			
bul_sc31_0696			
bul_sc31_0705			
bul_sc31_0712			
bul_sc31_0788			
bul_sc31_0793			
bul_sc31_0831			
bul_sc31_0856	SCHB 271		Sevenster et al. (1997)
bul_sc31_0866			
bul_sc31_0868			
bul_sc31_1043			
bul_sc31_1138			
bul_sc31_1235			
bul_sc31_1296			
bul_sc31_1308			
bul_sc31_1315			
bul_sc31_1360			
bul_sc31_1407			
bul_sc31_1421			
bul_sc31_1581			
bul_sc31_1797			
bul_sc31_1818			
bul_sc31_1865			
bul_sc31_2002			
bul_sc31_2106			
bul_sc31_2161			
bul_sc31_2187			
bul_sc31_3173			
bul_sc31_3271			
bul_sc31_3478			
bul_sc31_3759			
bul_sc31_3956			
bul_sc31_3976			
bul_sc31_4101			
bul_sc31_4128			
bul_sc31_4159			
bul_sc31_4161			
bul_sc31_4167			
bul_sc31_4193			
bul_sc31_4201			
bul_sc31_4208			
bul_sc31_4257			
bul_sc31_4338			
bul_sc31_4384			
bul_sc31_4403			
bul_sc31_4523			
bul_sc31_4527			
bul_sc31_4542			
bul_sc31_4574			
bul_sc32_0016			
bul_sc32_0062			
bul_sc32_0143			
bul_sc32_0317			
bul_sc32_0324			
bul_sc32_0346			
bul_sc32_0448			
bul_sc32_0455			
bul_sc32_0965			
bul_sc32_0969			

Table 2. continued.

OGLE-name	Other name	Chemical type	Remarks
bul_sc32_0980			
bul_sc32_1148			
bul_sc32_1572			
bul_sc32_1573			
bul_sc32_1634			
bul_sc32_1844			
bul_sc32_1889			
bul_sc32_2140			
bul_sc32_2240			
bul_sc32_2293			
bul_sc32_2351			
bul_sc32_2352			
bul_sc32_2359			
bul_sc32_2397			
bul_sc32_2415			
bul_sc32_2652			
bul_sc32_2653			
bul_sc32_2733			
bul_sc32_2734			
bul_sc32_2811			
bul_sc32_3032			
bul_sc32_3067			
bul_sc32_3194			
bul_sc32_3217			
bul_sc32_3222			
bul_sc32_3225			
bul_sc32_3233			
bul_sc32_3236			
bul_sc32_3518	IRAS_18004-2826		
bul_sc32_3617			
bul_sc32_3618			
bul_sc32_3762			
bul_sc32_3847			
bul_sc32_3907			
bul_sc32_3953			
bul_sc32_4136			
bul_sc32_4258			
bul_sc32_4349			
bul_sc32_4360			
bul_sc32_4384			
bul_sc32_4613			
bul_sc32_4657			
bul_sc32_4815			
bul_sc32_4967			
bul_sc33_0357			
bul_sc33_0445			
bul_sc33_0478			
bul_sc33_0571	IRAS_18018-2912		
bul_sc33_0695			
bul_sc33_0705			
bul_sc33_0743			
bul_sc33_0754			
bul_sc33_0755			
bul_sc33_0979			
bul_sc33_1139			
bul_sc33_1159			
bul_sc33_1178			
bul_sc33_1186			
bul_sc33_1187			

Table 2. continued.

OGLE-name	Other name	Chemical type	Remarks
bul_sc33_1229			
bul_sc33_1308			
bul_sc33_1312			
bul_sc33_1439			
bul_sc33_1525			
bul_sc33_1575			
bul_sc33_1584			
bul_sc33_1603			
bul_sc33_1611			
bul_sc33_1654			
bul_sc33_1795			
bul_sc33_1796			
bul_sc33_1877			
bul_sc33_1882			
bul_sc33_1954	IRAS_18026-2856		
bul_sc33_1998			
bul_sc33_2139			
bul_sc33_2194			
bul_sc33_2208			
bul_sc33_2244			
bul_sc33_2249			
bul_sc33_2334			
bul_sc33_2339			
bul_sc33_2343			
bul_sc33_2357			
bul_sc33_2358			
bul_sc33_2360			
bul_sc33_2361			
bul_sc33_2362			
bul_sc33_2367			
bul_sc33_2496			
bul_sc33_2514			
bul_sc33_2517			
bul_sc33_2608			
bul_sc33_2656			
bul_sc33_2672			
bul_sc33_2678			
bul_sc33_2679			
bul_sc33_2681			
bul_sc33_2682			
bul_sc33_2683			
bul_sc33_2685			
bul_sc33_2767			
bul_sc33_2898			
bul_sc33_2902			
bul_sc33_2907			
bul_sc33_2908			
bul_sc33_3079			
bul_sc33_3080			
bul_sc33_3089			
bul_sc33_3091			
bul_sc33_3095			
bul_sc33_3099			
bul_sc33_3102			
bul_sc33_3104			
bul_sc33_3127			
bul_sc33_3139			
bul_sc33_3140			
bul_sc33_3162			

Table 2. continued.

OGLE-name	Other name	Chemical type	Remarks
bul_sc33_3176			
bul_sc33_3178			
bul_sc33_3179			
bul_sc33_3180			
bul_sc33_3182			
bul_sc33_3240			
bul_sc33_3250			
bul_sc33_3251			
bul_sc33_3266			
bul_sc33_3268			
bul_sc33_3349			
bul_sc33_3350			
bul_sc33_3383			
bul_sc33_3395			
bul_sc33_3398			
bul_sc33_3399			
bul_sc33_3409			
bul_sc33_3414			
bul_sc33_3438			
bul_sc33_3699			
bul_sc33_3737			
bul_sc33_3755			
bul_sc33_3922			
bul_sc33_4149			
bul_sc33_4161			
bul_sc33_4189			
bul_sc33_4268			
bul_sc33_4445			
bul_sc33_4508			
bul_sc33_4566			
bul_sc33_4571			
bul_sc34_0243			
bul_sc34_0816			
bul_sc34_0905			
bul_sc34_0982			
bul_sc34_1635			
bul_sc34_1643			
bul_sc34_1664			
bul_sc34_1677			
bul_sc34_1754			
bul_sc34_1945			
bul_sc34_2181			
bul_sc34_2335			
bul_sc34_2343			
bul_sc34_2647			
bul_sc34_3242	IRAS_17547-2909		
bul_sc34_3269			
bul_sc34_3759	ABC01_113.18155.43, OOS03-PJ175843.9-290711, ISOGAL-PJ175843.9-290711, TLE_Sgr_I_65, V3972 Sgr		Glass et al. (1999), GWCF, LE76
bul_sc34_3854			
bul_sc34_4084			
bul_sc34_4090			
bul_sc34_4100			
bul_sc34_4159			
bul_sc34_4218			
bul_sc34_4327			
bul_sc34_4336			

Table 2. continued.

OGLE-name	Other name	Chemical type	Remarks
bul_sc34_4509			
bul_sc34_4516			
bul_sc34_4552			
bul_sc34_4559			
bul_sc34_4573			
bul_sc34_4586	ISOGAL-PJ175840.2-290122		
bul_sc34_4603			
bul_sc34_5012			
bul_sc34_5028			
bul_sc34_5217			
bul_sc34_5218			
bul_sc34_5343			
bul_sc34_5405	IRAS_17546-2854		
bul_sc34_5448			
bul_sc34_5475			
bul_sc34_5624			
bul_sc34_5863			
bul_sc34_6276			
bul_sc34_6342			
bul_sc34_6360			
bul_sc34_6362			
bul_sc34_6386			
bul_sc34_6747			
bul_sc34_7087			
bul_sc34_7122			
bul_sc34_7153			
bul_sc34_7428			
bul_sc34_7629			
bul_sc34_7639			
bul_sc34_7685			
bul_sc34_7694			
bul_sc34_7708			
bul_sc34_7744			
bul_sc34_7761			
bul_sc34_7879			
bul_sc35_0492			
bul_sc35_0898			
bul_sc35_0967			
bul_sc35_1052			
bul_sc35_1175	IRAS_18008-2810		
bul_sc35_1373			
bul_sc35_1376			
bul_sc35_1395			
bul_sc35_1426			
bul_sc35_1531			
bul_sc35_1620			
bul_sc35_1654			
bul_sc35_1779			
bul_sc35_1782			
bul_sc35_1786			
bul_sc35_2687			
bul_sc35_2842			
bul_sc35_2932			
bul_sc35_2935			
bul_sc35_2965			
bul_sc35_3024			
bul_sc35_3365			
bul_sc35_3388			
bul_sc35_3668			

Table 2. continued.

OGLE-name	Other name	Chemical type	Remarks
bul_sc35_3693			
bul_sc35_3768			
bul_sc35_3797			
bul_sc35_3851			
bul_sc35_3879			
bul_sc35_4087			
bul_sc35_4353			
bul_sc35_4385			
bul_sc35_4475			
bul_sc35_4538			
bul_sc35_4778			
bul_sc35_4952			
bul_sc35_5075			
bul_sc35_5078			
bul_sc35_5091			
bul_sc36_0030			
bul_sc36_0320			
bul_sc36_0812			
bul_sc36_1128			
bul_sc36_1243	IRAS_18028-2817, ESO 456-51	M8.5	Munari & Zwitter (2002), Kohoutek (2002), Medina Tanco & Steiner (1995)
bul_sc36_1254			
bul_sc36_1301			
bul_sc36_1571			
bul_sc36_1654			
bul_sc36_2158			
bul_sc36_2650			
bul_sc36_2764			
bul_sc36_2803			
bul_sc36_3014			
bul_sc36_3646			
bul_sc36_3690			
bul_sc36_3894			
bul_sc36_3908			
bul_sc36_3985			
bul_sc36_3990			
bul_sc36_4282			
bul_sc36_4779			
bul_sc36_4985			
bul_sc36_5032			
bul_sc36_5181			
bul_sc36_5594			
bul_sc36_5774			
bul_sc36_5794			
bul_sc36_5953			
bul_sc36_6354			
bul_sc36_6977			
bul_sc36_7454			
bul_sc36_7668			
bul_sc36_7676			
bul_sc36_7687			
bul_sc36_8151			
bul_sc36_8350			
bul_sc36_8625			
bul_sc37_0066			
bul_sc37_0090			
bul_sc37_0222			
bul_sc37_0617			
bul_sc37_0637			

Table 2. continued.

OGLE-name	Other name	Chemical type	Remarks
bul_sc37_0770			
bul_sc37_0807			
bul_sc37_0812			
bul_sc37_0832			
bul_sc37_0881			
bul_sc37_0914			
bul_sc37_0916			
bul_sc37_0931			
bul_sc37_1102			
bul_sc37_1105			
bul_sc37_1154			
bul_sc37_1176			
bul_sc37_1253			
bul_sc37_1353			
bul_sc37_1452			
bul_sc37_1465			
bul_sc37_1468			
bul_sc37_1508			
bul_sc37_1535			
bul_sc37_1551			
bul_sc37_1656			
bul_sc37_1666			
bul_sc37_1678			
bul_sc37_1779			
bul_sc37_1925			
bul_sc37_1975			
bul_sc37_2000			
bul_sc37_2025			
bul_sc37_2428			
bul_sc37_2433			
bul_sc37_2473			
bul_sc37_2474			
bul_sc37_2676			
bul_sc37_2726			
bul_sc37_2776			
bul_sc37_2787			
bul_sc37_2843			
bul_sc37_2937	IRAS_17497-3004		
bul_sc37_2946			
bul_sc37_2959			
bul_sc37_3015			
bul_sc37_3422			
bul_sc37_3454			
bul_sc37_3575			
bul_sc37_3634	ISOGAL-PJ175247.9-295841		
bul_sc37_3723			
bul_sc37_3761			
bul_sc37_3803			
bul_sc37_3807			
bul_sc37_3843			
bul_sc37_3857			
bul_sc37_3952			
bul_sc37_4220			
bul_sc37_4272			
bul_sc37_4334			
bul_sc37_4519			
bul_sc37_4583			
bul_sc37_4594			
bul_sc37_4613			

Table 2. continued.

OGLE-name	Other name	Chemical type	Remarks
bul_sc37_4614			
bul_sc37_4656			
bul_sc37_4681			
bul_sc37_4701			
bul_sc37_4737			
bul_sc37_4790			
bul_sc37_4860			
bul_sc37_5111			
bul_sc37_5123			
bul_sc37_5173			
bul_sc37_5187			
bul_sc37_5261			
bul_sc37_5276			
bul_sc37_5335			
bul_sc37_5358			
bul_sc37_5466			
bul_sc37_5561			
bul_sc37_5562			
bul_sc37_5569			
bul_sc37_5602			
bul_sc37_5707			
bul_sc37_5816			
bul_sc37_5926			
bul_sc37_6103			
bul_sc37_6185			
bul_sc37_6373			
bul_sc37_6380			
bul_sc37_6467			
bul_sc37_6578			
bul_sc37_7067			
bul_sc37_7089			
bul_sc37_7108			
bul_sc37_7120			
bul_sc37_7122			
bul_sc37_7265			
bul_sc37_7408			
bul_sc37_7553			
bul_sc37_7622			
bul_sc37_7628			
bul_sc37_7637			
bul_sc37_7900			
bul_sc37_7905			
bul_sc37_8065			
bul_sc37_8204			
bul_sc38_0013			
bul_sc38_0489			
bul_sc38_0595			
bul_sc38_0596			
bul_sc38_0665			
bul_sc38_0673			
bul_sc38_0847			
bul_sc38_0953			
bul_sc38_1127			
bul_sc38_1143			
bul_sc38_1155			
bul_sc38_1156			
bul_sc38_1170			
bul_sc38_1208			
bul_sc38_1213			

Table 2. continued.

OGLE-name	Other name	Chemical type	Remarks
bul_sc38_1502			
bul_sc38_1505			
bul_sc38_1738			
bul_sc38_1783			
bul_sc38_1796			
bul_sc38_1815	V4707 Sgr		
bul_sc38_1921			
bul_sc38_1923			
bul_sc38_1933			
bul_sc38_1940			
bul_sc38_1996			
bul_sc38_2018			
bul_sc38_2284			
bul_sc38_2460			
bul_sc38_2464			
bul_sc38_2649			
bul_sc38_2737			
bul_sc38_2739			
bul_sc38_2802			
bul_sc38_2811			
bul_sc38_3090			
bul_sc38_3101			
bul_sc38_3421			
bul_sc38_3450			
bul_sc38_3711			
bul_sc38_4092			
bul_sc38_4234			
bul_sc38_4384			
bul_sc38_4440			
bul_sc38_4460			
bul_sc38_4469			
bul_sc38_4474			
bul_sc38_4481			
bul_sc38_4636			
bul_sc38_4733			
bul_sc38_4793			
bul_sc38_4881			
bul_sc38_4923			
bul_sc38_4955			
bul_sc38_5002			
bul_sc38_5005			
bul_sc38_5060			
bul_sc39_0024			
bul_sc39_0051			
bul_sc39_0076			
bul_sc39_0229			
bul_sc39_0315			
bul_sc39_0342			
bul_sc39_0372			
bul_sc39_0498			
bul_sc39_0513			
bul_sc39_0713			
bul_sc39_1153			
bul_sc39_1166			
bul_sc39_1333			
bul_sc39_1537			
bul_sc39_1593	IRAS_17523-2959		
bul_sc39_1606			

Table 2. continued.

OGLE-name	Other name	Chemical type	Remarks
bul_sc39_1620			
bul_sc39_1773			
bul_sc39_1801			
bul_sc39_1841			
bul_sc39_1908			
bul_sc39_1940			
bul_sc39_2114			
bul_sc39_2183			
bul_sc39_2241			
bul_sc39_2245			
bul_sc39_2252			
bul_sc39_2258			
bul_sc39_2270			
bul_sc39_2279			
bul_sc39_2285			
bul_sc39_2294			
bul_sc39_2312			
bul_sc39_2357			
bul_sc39_2448			
bul_sc39_2542			
bul_sc39_2569			
bul_sc39_2725			
bul_sc39_2739			
bul_sc39_2771			
bul_sc39_2860			
bul_sc39_2901			
bul_sc39_2912			
bul_sc39_3087			
bul_sc39_3260			
bul_sc39_3472			
bul_sc39_3474			
bul_sc39_3577	ISOGAL-PJ175518.2-294358		
bul_sc39_3650			
bul_sc39_3708			
bul_sc39_3751			
bul_sc39_3797			
bul_sc39_3856			
bul_sc39_3890	OOS03-PJ175518.9-294142, ISOGAL-PJ175518.9-294142		
bul_sc39_4272			
bul_sc39_4675			
bul_sc39_4773			
bul_sc39_4790			
bul_sc39_4849			
bul_sc39_4894			
bul_sc39_4901			
bul_sc39_4996			
bul_sc39_5016			
bul_sc39_5058			
bul_sc39_5060			
bul_sc39_5075			
bul_sc39_5130			
bul_sc39_5132			
bul_sc39_5266			
bul_sc39_5267			
bul_sc39_5346			
bul_sc39_5436			
bul_sc39_5679			
bul_sc39_5758			

Table 2. continued.

OGLE-name	Other name	Chemical type	Remarks
bul_sc39_5762			
bul_sc39_5816			
bul_sc39_5851			
bul_sc39_5995			
bul_sc39_6025			
bul_sc39_6108			
bul_sc39_6256			
bul_sc39_6259			
bul_sc39_6294			
bul_sc39_6369			
bul_sc39_6385			
bul_sc39_6392			
bul_sc39_6577			
bul_sc39_6596			
bul_sc39_6679			
bul_sc39_6721			
bul_sc39_6798			
bul_sc39_6816			
bul_sc39_6950			
bul_sc39_7047			
bul_sc39_7050			
bul_sc39_7058			
bul_sc39_7081			
bul_sc39_7086			
bul_sc39_7235			
bul_sc40_0068			
bul_sc40_0148			
bul_sc40_0170			
bul_sc40_0280			
bul_sc40_0281	V2199		TO88
bul_sc40_0292			
bul_sc40_0356			
bul_sc40_0408			
bul_sc40_0425			
bul_sc40_0529	V2177		TO88
bul_sc40_0554			
bul_sc40_0681			
bul_sc40_0704			
bul_sc40_0753			
bul_sc40_0763			
bul_sc40_0846			
bul_sc40_0904			
bul_sc40_1028			
bul_sc40_1155			
bul_sc40_1215			
bul_sc40_1299			
bul_sc40_1408			
bul_sc40_1603			
bul_sc40_1674			
bul_sc40_1720			
bul_sc40_1726			
bul_sc40_1738			
bul_sc40_1785			
bul_sc40_1858			
bul_sc40_1953			
bul_sc40_2086			
bul_sc40_2353			
bul_sc40_2401			
bul_sc40_2423			

Table 2. continued.

OGLE-name	Other name	Chemical type	Remarks
bul_sc40_2086			
bul_sc40_2353			
bul_sc40_2401			
bul_sc40_2423			
bul_sc40_2444			
bul_sc40_2652			
bul_sc40_2653			
bul_sc40_2735	V 2203		TO88
bul_sc40_2750			
bul_sc40_2751			
bul_sc40_2853			
bul_sc40_2936			
bul_sc40_3033	V 2198		TO88
bul_sc40_3035			
bul_sc40_3091	IRAS_17476-3300		
bul_sc40_3098			
bul_sc40_3149			
bul_sc40_3220			
bul_sc40_3524			
bul_sc40_3687			
bul_sc40_3694			
bul_sc40_3795			
bul_sc40_3854			
bul_sc40_3863			
bul_sc40_3962			
bul_sc41_0191			
bul_sc41_0367			
bul_sc41_0551			
bul_sc41_0553			
bul_sc41_0649			
bul_sc41_0837			
bul_sc41_0957			
bul_sc41_1345			
bul_sc41_1357			
bul_sc41_1462			
bul_sc41_1497			
bul_sc41_1569			
bul_sc41_1621			
bul_sc41_1634			
bul_sc41_1636			
bul_sc41_1637			
bul_sc41_1977			
bul_sc41_2039			
bul_sc41_2065			
bul_sc41_2219			
bul_sc41_2384			
bul_sc41_2457			
bul_sc41_2517			
bul_sc41_2648			
bul_sc41_2714			
bul_sc41_2738			
bul_sc41_2756			
bul_sc41_2782			
bul_sc41_2786			
bul_sc41_2870			
bul_sc41_2885			
bul_sc41_2961			
bul_sc41_3028			
bul_sc41_3089			

Table 2. continued.

OGLE-name	Other name	Chemical type	Remarks
bul_sc41_3094			
bul_sc41_3231			
bul_sc41_3279			
bul_sc41_3304			
bul_sc41_3319			
bul_sc41_3366			
bul_sc41_3443			
bul_sc41_3458			
bul_sc41_3512			
bul_sc41_3536			
bul_sc41_3623			
bul_sc41_3672			
bul_sc41_3897			
bul_sc41_3898			
bul_sc41_3911			
bul_sc42_0039	IRAS_18060-2720		
bul_sc42_0046			
bul_sc42_0047			
bul_sc42_0048			
bul_sc42_0084			
bul_sc42_0272			
bul_sc42_0356			
bul_sc42_0362			
bul_sc42_0363			
bul_sc42_0365			
bul_sc42_0391			
bul_sc42_0756			
bul_sc42_0826			
bul_sc42_0945			
bul_sc42_0967			
bul_sc42_0969			
bul_sc42_1312			
bul_sc42_2002			
bul_sc42_2179			
bul_sc42_2190			
bul_sc42_2342			
bul_sc42_2356			
bul_sc42_2357			
bul_sc42_2418			
bul_sc42_2528			
bul_sc42_2600			
bul_sc42_3184			
bul_sc42_3473			
bul_sc42_3485			
bul_sc42_3488			
bul_sc42_4183			
bul_sc42_4185			
bul_sc43_0078			
bul_sc43_0097			
bul_sc43_0105			
bul_sc43_0115			
bul_sc43_0150	V 2603		Terzan & Gosset (1991; TG91)
bul_sc43_0152			
bul_sc43_0153			
bul_sc43_0175			
bul_sc43_0199			
bul_sc43_0243			
bul_sc43_0244	V 2590		TG91
bul_sc43_0313			

Table 2. continued.

OGLE-name	Other name	Chemical type	Remarks
bul_sc43_0358	V 2632		TG91
bul_sc43_0376	V 2662		TG91
bul_sc43_0398			
bul_sc43_0433	V 2655		TG91
bul_sc43_0441			
bul_sc43_0442			
bul_sc43_0513	IRAS_17322-2726		
bul_sc43_0571			
bul_sc43_0575	V 2652		TG91
bul_sc43_0582	V 2665		TG91
bul_sc43_0592			
bul_sc43_0661	IRAS_17322-2724		
bul_sc43_0765	V 2642		TG91
bul_sc43_0769			
bul_sc43_0843	V 2613		TG91
bul_sc43_0865			
bul_sc43_0879			
bul_sc43_0882			
bul_sc43_0896			
bul_sc43_0918			
bul_sc43_1114			
bul_sc43_1115			
bul_sc43_1116			
bul_sc43_1117			
bul_sc43_1120			
bul_sc43_1127			
bul_sc43_1143			
bul_sc43_1149			
bul_sc43_1153			
bul_sc43_1154			
bul_sc43_1156			
bul_sc43_1157			
bul_sc43_1159			
bul_sc43_1168			
bul_sc43_1170			
bul_sc43_1171			
bul_sc43_1172			
bul_sc43_1174			
bul_sc43_1175			
bul_sc43_1176			
bul_sc43_1177			
bul_sc43_1178			
bul_sc43_1213	V 2644		TG91
bul_sc43_1215			
bul_sc43_1216			
bul_sc43_1217			
bul_sc43_1223			
bul_sc43_1246			
bul_sc43_1247			
bul_sc43_1255			
bul_sc43_1257			
bul_sc43_1258			
bul_sc43_1273			
bul_sc43_1274			
bul_sc43_1275			
bul_sc43_1279			
bul_sc43_1281			
bul_sc43_1282			
bul_sc43_1283			

Table 2. continued.

OGLE-name	Other name	Chemical type	Remarks
bul_sc43_1286			
bul_sc43_1300			
bul_sc43_1319			
bul_sc43_1485			
bul_sc43_1492	V 2633		TG91
bul_sc43_1519	V 2598		TG91
bul_sc43_1524			
bul_sc43_1579	V 2588		TG91
bul_sc43_1667	V 2639		TG91
bul_sc43_1676			
bul_sc43_1715	V 2615		TG91
bul_sc43_1919			
bul_sc43_2034			
bul_sc43_2071			
bul_sc43_2098			
bul_sc43_2118			
bul_sc43_2149			
bul_sc43_2173			
bul_sc43_2214			
bul_sc43_2263	V 2659		TG91
bul_sc43_2295	V 2624		TG91
bul_sc43_2333			
bul_sc43_2338			
bul_sc43_2407			
bul_sc43_2423			
bul_sc43_2461	V 2611		TG91
bul_sc43_2627	V 2643		TG91
bul_sc43_2761			
bul_sc43_2782			
bul_sc43_2793			
bul_sc43_2857	V 2596		TG91
bul_sc43_2860			
bul_sc43_2935			
bul_sc43_3001	V 2629		TG91
bul_sc43_3015			
bul_sc43_3029			
bul_sc43_3071			
bul_sc43_3142	V 2595		TG91
bul_sc43_3240			
bul_sc43_3321			
bul_sc43_3348			
bul_sc44_0054	V 2128		TO88
bul_sc44_0237			
bul_sc44_0377			
bul_sc44_0581			
bul_sc44_0606			
bul_sc44_0755			
bul_sc44_0792			
bul_sc44_0795			
bul_sc44_0796			
bul_sc44_0856			
bul_sc44_0913			
bul_sc44_0968			
bul_sc44_0980			
bul_sc44_1144			
bul_sc44_1237			
bul_sc44_1272			
bul_sc44_1352			
bul_sc44_1357			

Table 2. continued.

OGLE-name	Other name	Chemical type	Remarks
bul_sc44_1373			
bul_sc44_1498			
bul_sc44_1568			
bul_sc44_1667			
bul_sc44_1722			
bul_sc44_1727			
bul_sc44_1748	IRAS_17465-3013		
bul_sc44_1893			
bul_sc44_2025			
bul_sc44_2164			
bul_sc44_2189			
bul_sc44_2257			
bul_sc44_2277			
bul_sc44_2288			
bul_sc44_2301			
bul_sc44_2316			
bul_sc44_2317			
bul_sc44_2319			
bul_sc44_2351			
bul_sc44_2361			
bul_sc44_2391			
bul_sc44_2478			
bul_sc44_2493			
bul_sc44_2644			
bul_sc44_2659			
bul_sc44_2665			
bul_sc44_2925			
bul_sc44_2991			
bul_sc44_2999			
bul_sc44_3021			
bul_sc44_3028			
bul_sc44_3053			
bul_sc44_3085			
bul_sc44_3089			
bul_sc44_3128			
bul_sc44_3136			
bul_sc44_3232			
bul_sc44_3268			
bul_sc44_3286			
bul_sc44_3298			
bul_sc44_3393	IRAS_17463-3001		
bul_sc44_3694			
bul_sc44_3721			
bul_sc44_3729			
bul_sc44_3885			
bul_sc44_4178			
bul_sc44_4354			
bul_sc44_4364			
bul_sc44_4436			
bul_sc44_4548			
bul_sc44_4608			
bul_sc44_4689			
bul_sc44_4743			
bul_sc44_4786			
bul_sc44_4898			
bul_sc44_4939			
bul_sc44_4940			
bul_sc44_4942			
bul_sc44_5103			

Table 2. continued.

OGLE-name	Other name	Chemical type	Remarks
bul_sc44_5111			
bul_sc44_5142			
bul_sc44_5290			
bul_sc44_5347			
bul_sc44_5372			
bul_sc44_5391			
bul_sc44_5411			
bul_sc44_5412			
bul_sc44_5460			
bul_sc44_5472			
bul_sc44_5506			
bul_sc44_5534			
bul_sc44_5577			
bul_sc44_5578			
bul_sc44_5596			
bul_sc44_5643			
bul_sc44_5685			
bul_sc44_5726			
bul_sc44_5813			
bul_sc44_5974	IRAS_17463-2946	M8	Raharto et al. (1984)
bul_sc44_5975			
bul_sc44_5993			
bul_sc44_6016			
bul_sc44_6061			
bul_sc44_6153			
bul_sc44_6158			
bul_sc44_6159			
bul_sc44_6160			
bul_sc44_6195			
bul_sc44_6276			
bul_sc44_6279			
bul_sc44_6300			
bul_sc44_6352			
bul_sc44_6484			
bul_sc44_6529			
bul_sc44_6531			
bul_sc44_6554			
bul_sc44_6641			
bul_sc44_6644			
bul_sc44_6708			
bul_sc44_6859			
bul_sc44_7060			
bul_sc44_7107			
bul_sc44_7301			
bul_sc44_7317			
bul_sc44_7324			
bul_sc44_7450			
bul_sc44_7473			
bul_sc44_7551			
bul_sc44_7626			
bul_sc44_7649			
bul_sc44_7690			
bul_sc44_7738			
bul_sc44_7777			
bul_sc44_7828			
bul_sc45_0148			
bul_sc45_0164			
bul_sc45_0170			
bul_sc45_0179			

Table 2. continued.

OGLE-name	Other name	Chemical type	Remarks
bul_sc45_0226			
bul_sc45_0230			
bul_sc45_0275			
bul_sc45_0360			
bul_sc45_0369			
bul_sc45_0373			
bul_sc45_0418			
bul_sc45_0546			
bul_sc45_0704	BW6_V4_MISC, TLE_NGC_6522_644, BMB_87, IRAS_18001-3012, MACHO 119.20088.3574	M8	GS03, Frogel & Whitford (1987; hereafter FW87), G86, GF82, LE76
bul_sc45_0799			
bul_sc45_0842			
bul_sc45_0961			
bul_sc45_0962			
bul_sc45_0972			
bul_sc45_1068	OOS03-PJ180313.8-300306, ISOGAL-PJ180313.8-300306, TLE_NGC_6522_395, BMB_68, MACHO 119.20091.28, V1414 Sgr	M6	GS03, LE76
bul_sc45_1316	OOS03-PJ180311.5-295747, ISOGAL-PJ180311.5-295747		
bul_sc45_1323			
bul_sc45_1374			
bul_sc45_1490			
bul_sc45_1586	TLE_NGC_6522_721, BMB_220, V1471 Sgr, BMB_220, V1471 Sgr, MACHO 119.20353.109	M6	GS03, GF82, LE76
bul_sc45_1589	IRAS_18007-2951, BMB_250	M7	FW87
bul_sc45_1713	BMB_238	M6.5	
bul_sc45_1725			
bul_sc45_1941			
bul_sc45_1980			
bul_sc45_1998			
bul_sc45_2020			
bul_sc45_2055			
bul_sc46_0025			
bul_sc46_0125			
bul_sc46_0214			
bul_sc46_0225			
bul_sc46_0242			
bul_sc46_0254			
bul_sc46_0347			
bul_sc46_0355			
bul_sc46_0427			
bul_sc46_0490			
bul_sc46_0866	TLE_NGC_6522_786, BMB_285, V 1502 Sgr, MACHO 119.20610.46		GS03, LE76
bul_sc46_0950			
bul_sc46_0996	ISOGAL-PJ180448.4-300400		
bul_sc46_1026			
bul_sc46_1048	ISOGAL-PJ180446.3-300318		
bul_sc46_1115			
bul_sc46_1117			
bul_sc46_1163	ISOGAL-PJ180441.9-295958, BW7_V2_MISC		

Table 2. continued.

OGLE-name	Other name	Chemical type	Remarks
bul_sc46_1245			
bul_sc46_1378			
bul_sc46_1419			
bul_sc46_1467			
bul_sc46_1474			
bul_sc46_1583			
bul_sc46_1735			
bul_sc46_2021			
bul_sc47_0024			
bul_sc47_0125			
bul_sc47_0180			
bul_sc47_0303			
bul_sc47_0456			
bul_sc47_0489			
bul_sc47_0655			
bul_sc47_0758			
bul_sc47_0816			
bul_sc47_0964			
bul_sc47_1000			
bul_sc47_1090			
bul_sc48_0186			
bul_sc48_0230			
bul_sc48_0280			
bul_sc48_0306	IRAS_17248-3953		
bul_sc48_0316			
bul_sc48_0340			
bul_sc48_0438			
bul_sc48_0465			
bul_sc48_0568			
bul_sc48_0573			
bul_sc48_0773			
bul_sc48_0914			
bul_sc49_0157			
bul_sc49_0249			
bul_sc49_0251			
bul_sc49_0262			
bul_sc49_0280			
bul_sc49_0463			
bul_sc49_0477			
bul_sc49_0526			
bul_sc49_0575			
bul_sc49_0744			
bul_sc49_0754			
bul_sc49_0756			
bul_sc49_0757			
bul_sc49_0759			
bul_sc49_0770			
bul_sc49_0778			
bul_sc49_0779			
bul_sc49_0782			